US Army Corps of Engineers

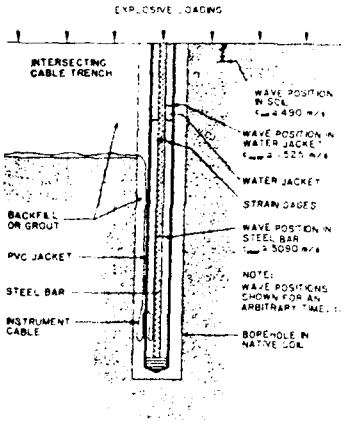

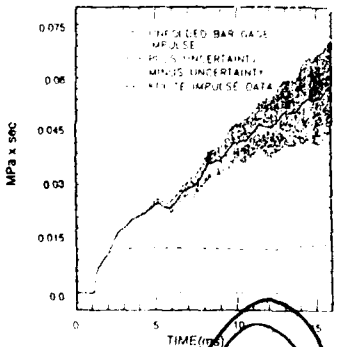

TECHNICAL REPORT SL-92-12

ANALYSIS OF D'ALEMBERT UNFOLDING TECHNIQUE FOR HOPKINSON BAR GAGE RECORDS

by

Alan Paul Ohrt

Structures Laboratory

DEPARTMENT OF THE ARMY
Waterways Experiment Station, Corps of Engineers
3909 Halls Ferry Road, Vicksburg, Mississippi 39180-6199

June 1992
Final Report

Prepared for Defense Nuclear Agency
Washington, DC 20305-1000

Under MIPR No. 90-652

STRUCTURES LABORATORY

The findings in this report are not to be construed as an official Department of the Army position unless so designated by other authorized documents.

The contents of this report are not to be used for advertising, publication, or promotional purposes. Citation of trade names does not constitute an official endorsement or approval of the use of such commercial products.

REPORT DOCUMENTATION PAGE

Form Approved
OMB No. 0704-0188

1. AGENCY USE ONLY (Leave blank)	2. REPORT DATE	3. REPORT TYPE AND DATES COVERED
	June 1992	Final report

4. TITLE AND SUBTITLE

Analysis of D'Alembert Unfolding Technique for Hopkinson Bar Gage Records

5. FUNDING NUMBERS

DNA MIPR No. 90-652

6. AUTHOR(S)

Alan Paul Ohrt

7. PERFORMING ORGANIZATION NAME(S) AND ADDRESS(ES)

US Army Engineer Waterways Experiment Station
Structures Laboratory
3909 Halls Ferry Road, Vicksburg, MS 39180-6199

8. PERFORMING ORGANIZATION REPORT NUMBER

Technical Report SL-92-12

9. SPONSORING/MONITORING AGENCY NAME(S) AND ADDRESS(ES)

Defense Nuclear Agency
Washington, DC 20305-1000

10. SPONSORING/MONITORING AGENCY REPORT NUMBER

11. SUPPLEMENTARY NOTES

Available from National Technical Information Service, 5285 Port Royal Road, Springfield, VA 22161.

12a. DISTRIBUTION/AVAILABILITY STATEMENT

Approved for public release; distribution is unlimited.

12b. DISTRIBUTION CODE

13. ABSTRACT *(Maximum 200 words)*

The bar gage is an instrument frequently used to make measurements of airblast pressures produced by explosive charges. The blast pressure to be measured is applied to the end of a strain-gaged steel bar. Unfortunately, reflections from the ends of the bar will be superposed upon the pressure input, limiting the useful record length. In 1983, a method of numerically removing these reflections was proposed. This method, based upon the D'Alembert solution to the thin rod wave equation, "unfolds" the reflections, thereby creating a record of original pressure input.

In this thesis, the uncertainty of the results from the D'Alembert unfolding method are studied. These error sources are considered: wave speed, reflection coefficients, and dispersion. Numerical and analytical techniques are applied to obtain the uncertainty for an arbitrary pressure wave form. Specific wave forms are unfolded and evaluated to draw general conclusions regarding the uncertainties inherent to the unfolding technique.

14. SUBJECT TERMS

Airblast measurement	Reflections
Bar gages	Stress wave transmission
D'Alembert unfolding	Unfolding

15. NUMBER OF PAGES
136

16. PRICE CODE

17. SECURITY CLASSIFICATION OF REPORT	18. SECURITY CLASSIFICATION OF THIS PAGE	19. SECURITY CLASSIFICATION OF ABSTRACT	20. LIMITATION OF ABSTRACT
UNCLASSIFIED	UNCLASSIFIED		

PREFACE

This error analysis of numerically unfolded bar gage records was sponsored by the Defense Nuclear Agency (DNA) in support of ongoing Test Instrumentation Development programs. Dr. Kent Peterson was the technical monitor of this work performed under Defense Nuclear Agency MIPR No. 90-652.

This research was conducted by the Explosion Effects Division (EED), Structures Laboratory (SL), U.S. Army Engineer Waterways Experiment Station (WES). During this investigation, Mr. L. K. Davis was Director, EED, and Mr. Bryant Mather was Director, SL. Mr. Charles R. Welch provided overall direction for this work. Mr. Alan P. Ohrt was the Principal Investigator throughout the study. This research effort and report also served as a master's thesis, in partial fulfillment of the requirements for a Master of Science degree in Engineering Mechanics through the Department of Aerospace Engineering at Mississippi State University at Starkville, MS.

This study was performed using data from bar gage calibrations performed in the laboratory and also explosive test data that already existed from previous field tests. Mr. Bruce Barker from the Instrumentation Services Division, WES, performed the bar gage calibrations.

At the time of publication of this report, the Director of WES was Dr. Robert W. Whalin. Commander and Deputy Director was COL Leonard G. Hassell, EN.

TABLE OF CONTENTS

LIST OF TABLES

LIST OF FIGURES

LIST OF FIGURES

NOMENCLATURE

a	any variable in F(t) which contains uncertainty
A	reflection coefficient for the dump end of the bar gage
B	reflection coefficient for the measurement end of the bar gage
c_o	low frequency wave speed
C_n	magnitude of the "n_{th}" compressive reflection
E	modulus of elasticity
$f(t)$	time-varying output from the bar gage, containing reflections
$F(t)$	time-varying input to the bar gage
L	length of the bar gage
n	summation index identifying a particular reflection
t	time
TOA	time of arrival of stress pulse on the bar gage record
x	distance from the top of the bar to the strain gages
$u(z,t)$	particle displacement in a thin rod or bar
U_a	uncertainty in the variable "a"
U_A	uncertainty in the reflection coefficient A
U_B	uncertainty in the reflection coefficient B
U_{c_o}	uncertainty in the wave speed c_o
$U_{F(t)}$	uncertainty in the unfolded waveform
z	position along longitudinal axis of the bar (customarily called "x" but changed to avoid conflict with strain gage position "x")

CONVERSION FACTORS, METRIC (SI) TO NON-SI UNITS OF MEASUREMENT

SI (Metric) units of measurement used in this report can be converted to Non-SI units as follows:

Divide	By	To Obtain
metres	0.3048	feet
metres/second	0.3048	feet/second
square metres	0.09290304	square feet
cubic metres	0.02831685	cubic feet
kilograms	0.45359237	pound (mass)
radians	0.1745329	degrees (angle)
megapascals	0.006894757	pounds (force) per square inch
kilograms per cubic metre	16.01846	pounds (mass) per cubic foot

CHAPTER I

INTRODUCTION

Background and Objective

In the last few decades, the Department of Defense has developed a keen interest in the measurement of explosive phenomena. With recent advances in strain gage technology, signal recording, and other related fields, it has become possible to measure the loads and stresses produced by a wide variety of weapons. Previously, it was known that Bomb X produced a certain amount of damage to a particular target. If any of the parameters were to change, however, such as using different bombs or hardening the target, only an educated guess could be made regarding the change in the vulnerability of the target. Obtaining a better answer normally meant constructing more targets and conducting more tests. Such a procedure is dangerously slow and painfully expensive in this age of rapid technological advances. It was eventually realized, and correctly so, that test results must be analyzed sufficiently not only to indicate how much damage Bomb X produces, but how and why it produced the damage that it did. With this knowledge, better judgements can be made regarding the target's vulnerability under different conditions, with fewer tests and less risk required.

Numerous examples of this approach can be given. Airblast measurements are obtained at various distances from developmental munitions to define their effectiveness in imparting blast pressure. Hardened structures, such as fighting bunkers or missile silos, are instrumented with blast pressure gages and motion transducers to characterize their response when subjected to explosive loadings. Specially-configured charges, referred to as high explosive simulators, are used to subject such structures to loadings that are characteristic of those produced by nuclear explosions. These simulators are heavily instrumented with airblast, ground motion, and ground shock transducers, to evaluate the simulator's performance against the desired load conditions. The pressures and stresses that must be measured from high explosive tests such as these are very severe. The blast pressure wave form displayed in Figure 1 is a representative example. The peak pressure is approximately 173 MPa[1], the specific impulse is 0.57 MPa-sec, and the pressure has not completely returned to zero at the end of the plot. The severity of the environment, coupled with the transient nature of the measurement, places extremely difficult demands on the instruments used to obtain these measurements.

One instrument often used for making high-pressure airblast measurements is the strain-gaged Hopkinson bar, or bar gage. The bar gage is a simple device, consisting of a strain-gaged, high-strength steel bar surrounded by a protective PVC jacket. One end of the steel bar is placed at the desired measurement location, where the pressure

---

[1]A table of factors for converting SI (metric) units of measurement to Non-SI units is presented on page viii.

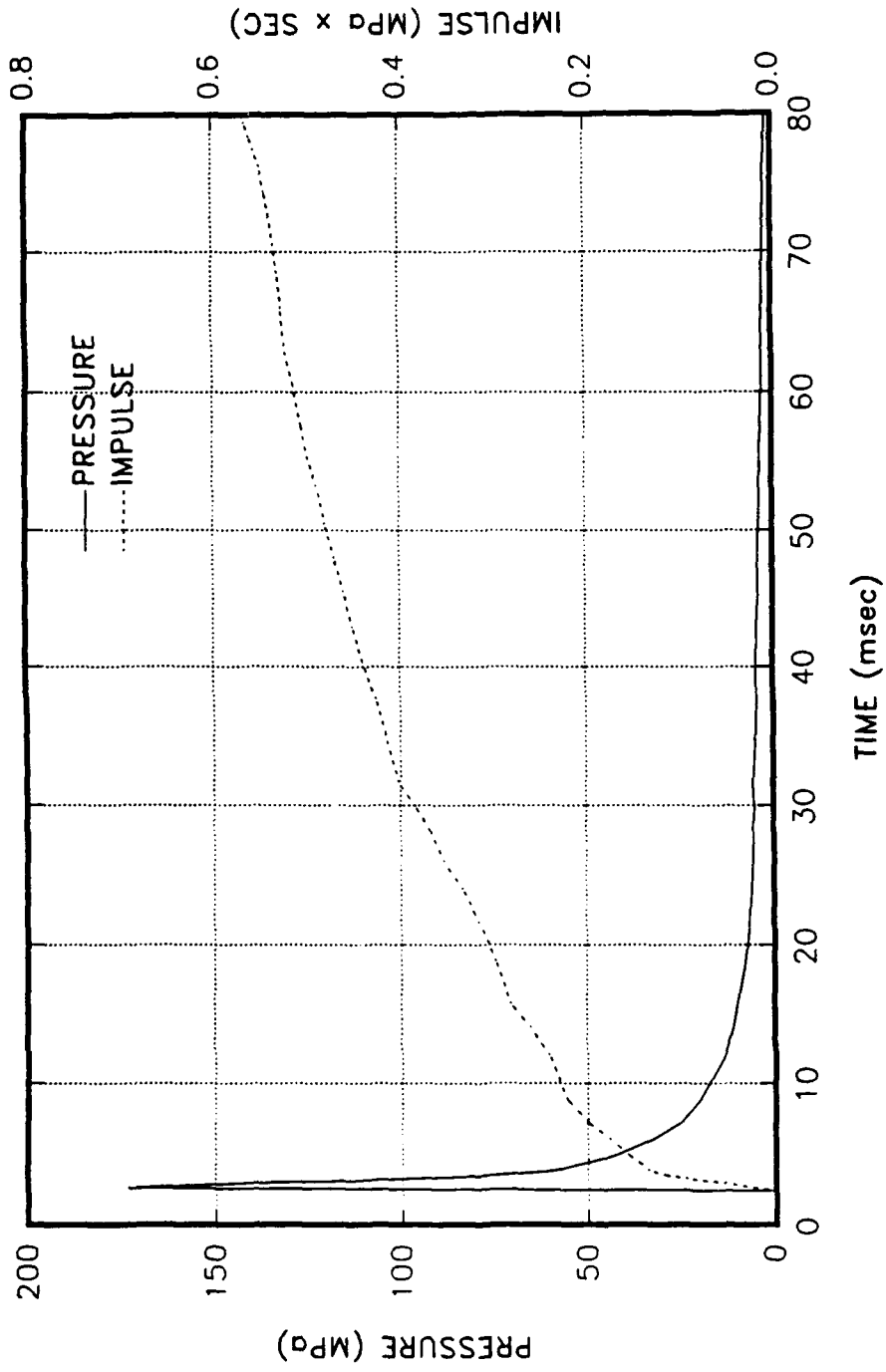

Figure 1. Blast pressure wave form from an explosive test.

pulse is applied. This pressure pulse propagates down the length of the bar as a stress wave with very little change of form. Figure 2 describes the propagation of the stress wave and the corresponding strain gage output. When the stress wave is at position "A" in Figure 2, there is no strain gage output, since the stress wave has yet to reach the strain gages. Once the stress pulse reaches them, however, the strain gages produce a voltage which is linearly related to the pressure input through a calibration factor. Eventually, the stress pulse reaches the opposite end of the bar, where most of the pulse is reflected back into the bar as a tensile stress wave. If the duration of the stress pulse is sufficiently short, the strain gages will completely record it before the tensile reflection arrives at the strain gage position. For most problems of interest however, the duration of the stress wave is long enough that the tensile reflection arrives before the strain gages have completely recorded the stress pulse. Consequently, the tensile stress wave travels from the bottom towards the top of the bar while the "tail" of the initial pressure pulse is still propagating downward from the top of the bar (Position "B", Figure 2).

When the tensile reflection reaches the strain gage location, it masks the "tail" of the pressure wave form, effectively hiding the useful data. Such is the situation when the reflected stress wave is at Position "C", Figure 2. The reflected tensile stress wave will propagate up to the top of the bar and reflect a second time, but now as a compressive wave. When the compressive reflection reaches the strain gages, two reflections are superposed upon the data, as evident

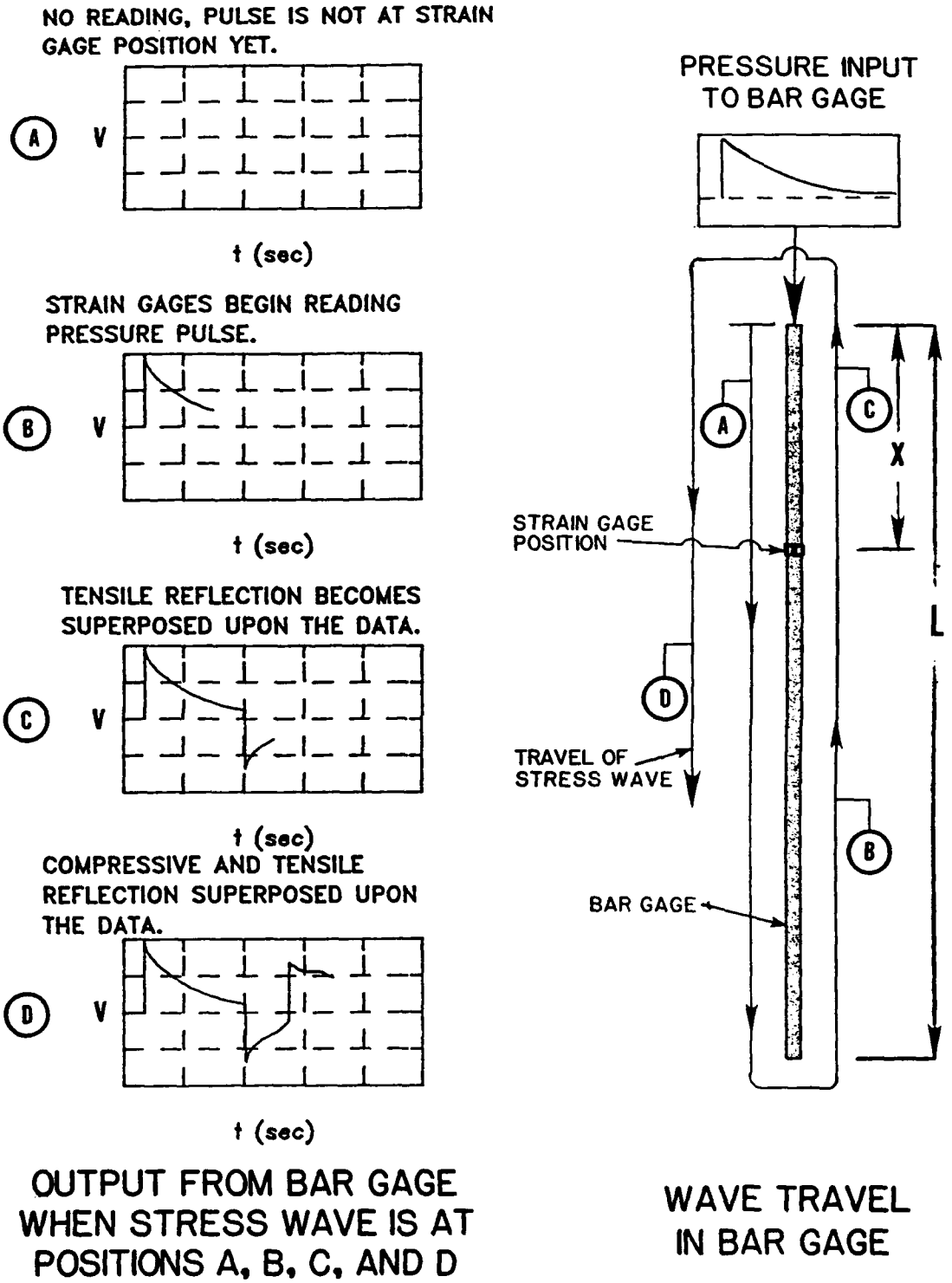

Figure 2. Description of wave propagation and strain gage output in a bar gage.

at Position "D", Figure 2. Reflections will continue to propagate up and down the bar long after the initial pressure pulse is over, assuming the cables and strain gages remain undamaged. Due to the limitations of current data reduction techniques, only the data prior to the first tensile reflection is considered to be valid, and the subsequent reflections are discarded.

A technique of numerically "unfolding" the reflections to extend the valid record length was proposed by Welch in 1983 (Reference 1). A computer routine, based upon the D'Alembert solution to the basic wave equation governing wave propagation in a thin rod, was used by White (1985) to unfold several bar gage records (Reference 2). While the technique appeared promising, no opportunities for comparing unfolded bar gage records of a known input wave form occurred to establish the method's credibility. Meanwhile, critics pointed out potential flaws in the unfolding technique. In this thesis, an error analysis is performed on the D'Alembert unfolding technique. The objective is to ascertain the overall credibility of D'Alembert unfolding as a data reduction technique for bar gage measurements.

Brief Historical Account

Bar gages are not new arrivals to the field of dynamic measurement. As early as 1914, Hopkinson (Reference 3) reported the first use of a cylindrical bar to measure peak pressure, and hence, many bar gages to this date are referred to as Hopkinson bar gages. In Hopkinson's method, the pressure to be measured is applied to one end of the bar, while the magnitude of that pressure is deduced from the

measurement of the momentum of a detachable timepiece at the opposite end of the bar. Pressure as a function of time is not obtainable with this technique (Reference 4).

Later in the century, electrical methods of strain and displacement measurement were applied to the Hopkinson bar gage to obtain pressure measurements as a function of time. Condensers and microphones were used in conjunction with analog recording devices to measure the longitudinal strains in the bar resulting from a dynamic pulse applied at the end. In some instances, the motion of one end of the bar was monitored to deduce the characteristics of the pressure pulse applied to the opposite end. The advent of small, wire strain gages permitted even finer measurements of the strain pulse propagating down the bar. Researchers such as Davies (Reference 4), Fox and Curtis (Reference 5), and Miklowitz (Reference 6) employed condenser and strain gage technology to study the detailed wave mechanics involved with the propagation of pulses in thin cylindrical bars. Their research revealed phenomena such as pulse distortion and vibrational modes of the bar, both of which apply to the use of the bar gage as an airblast measurement device.

Baum, of the University of New Mexico Engineering Research Institute (NMERI), was one of the first to use strain-gaged bars to measure explosion effects. Specifically, he used bar gages to evaluate the performance of high explosive charges designed to simulate the dynamic load environments produced by nuclear explosions. Baum used foil strain gages attached to a high-strength steel bar, which was surrounded completely by a steel sleeve and a short water jacket near

the top of the bar (Reference 7). These added features were designed to contend with the ground shock and high-speed detonation products peculiar to high explosive simulators. Other groups, such as S-Cubed (La Jolla, CA) and the U.S. Army Engineer Waterways Experiment Station (WES), have produced bar gages similar to those of NMERI with good results. However, since some simulators and munitions have pulse durations on the order of many milliseconds, it has been impractical to design bar gages which measure for a sufficient length of time before the measurement becomes complicated by the arrival of tensile reflections from the bottom end of the bar gage.

Research is currently underway to measure the late-time airblast histories which are masked by the reflections within the bar gage. One approach taken by S-Cubed is to create an end condition for the bar gage which will damp out all reflections (Reference 8). Another approach is to develop other gage types which will capture the late-time airblast data. The data from the bar gage could then be considered in tandem with that of the late-time airblast gage to "piece together" the airblast measurement. If numerical unfolding can be used to remove the reflections from the bar gage record, a very simple and direct remedy might be obtained for extending the bar gage record length. Even unfolding just one tensile and compressive reflection would more than double the record length, providing the analyst with valuable data that was previously unavailable. However, the practicality of such notions has been subject to debate, and hence, is addressed in this thesis.

Approach

In order to unfold a bar gage record, the low-frequency wave speed, c_o, and the reflection coefficients for each end of the bar must be identified. The author contends that errors in identifying these parameters lead to considerable error in the unfolded result. Other error sources exist, such as dispersion and material nonlinearities, but these errors are thought to be less significant. Consequently, an effort is made in this thesis to quantify the uncertainties due to incorrect wave speed and reflection coefficients, while the other error sources are merely mentioned. Classical uncertainty analysis, as presented by Coleman and Steele (Reference 9), is adhered to as much as possible throughout the thesis. For the case of c_o, classical uncertainty analysis proves difficult, so a numerical approach is employed to give insight into the errors resulting from incorrect wave speed.

The WES bar gage is described in detail in Chapter 2. Its installation and operation is discussed to aid the reader in understanding how tensile reflections appear and disturb the measurement. In Chapter 3, the mathematics and theory pertaining to wave propagation in a bar gage, and the D'Alembert unfolding method, is presented. The assumptions and limitations of D'Alembert unfolding are also pointed out. An error analysis of the D'Alembert unfolding technique is conducted in Chapter 4. A numerical approach is used to determine the error due to the use of incorrect wave speed. An analytical solution is developed to determine the error caused by the use of incorrect reflection coefficients. These errors are then

combined to give the uncertainty in the unfolded wave form. The error analysis is demonstrated using actual field data in Chapter 5. Bar gage records from an explosive test are analyzed and unfolded. The resulting unfolded wave forms are compared to those acquired by other gage types to draw conclusions about the performance of the bar gages. Lastly, the conclusions and recommendations of the thesis are discussed in Chapter 6.

CHAPTER II

BAR GAGE DESCRIPTION

A detailed cross-section of a typical WES bar gage is shown in Figure 3. The heart of the instrument is a 1-in. diameter, high-strength steel bar with four semiconductor strain gages installed in a full bridge configuration at a prescribed location down the length of the bar. The lengths of typical bar gages vary, depending on the measurements to be obtained, but typical lengths might range from 2 to 7 meters. Correspondingly, strain gage locations typically range from 0.6 to 2 meters from the top end of the bar. The steel bar is placed inside a 3-in. diameter PVC pipe. The pipe serves to temporarily protect the bar from lateral loadings produced by the explosion, whether through airblast or ground shock. Under harsh loadings, the PVC pipe may fail, but generally not until after the measurement has been obtained. Wooden spacers center the bar within the PVC pipe.

The bottom end (or dump end) of the bar gage rests on a stack of alternating disks of styrofoam and wood. This arrangement was chosen to simulate a free end condition at the dump end, causing almost all of the pressure pulse to be reflected back into the bar. This was thought to be the most advantageous situation for the subsequent unfolding of the wave form. It has since been suggested that other dump end support conditions would be better, and these are being considered for future

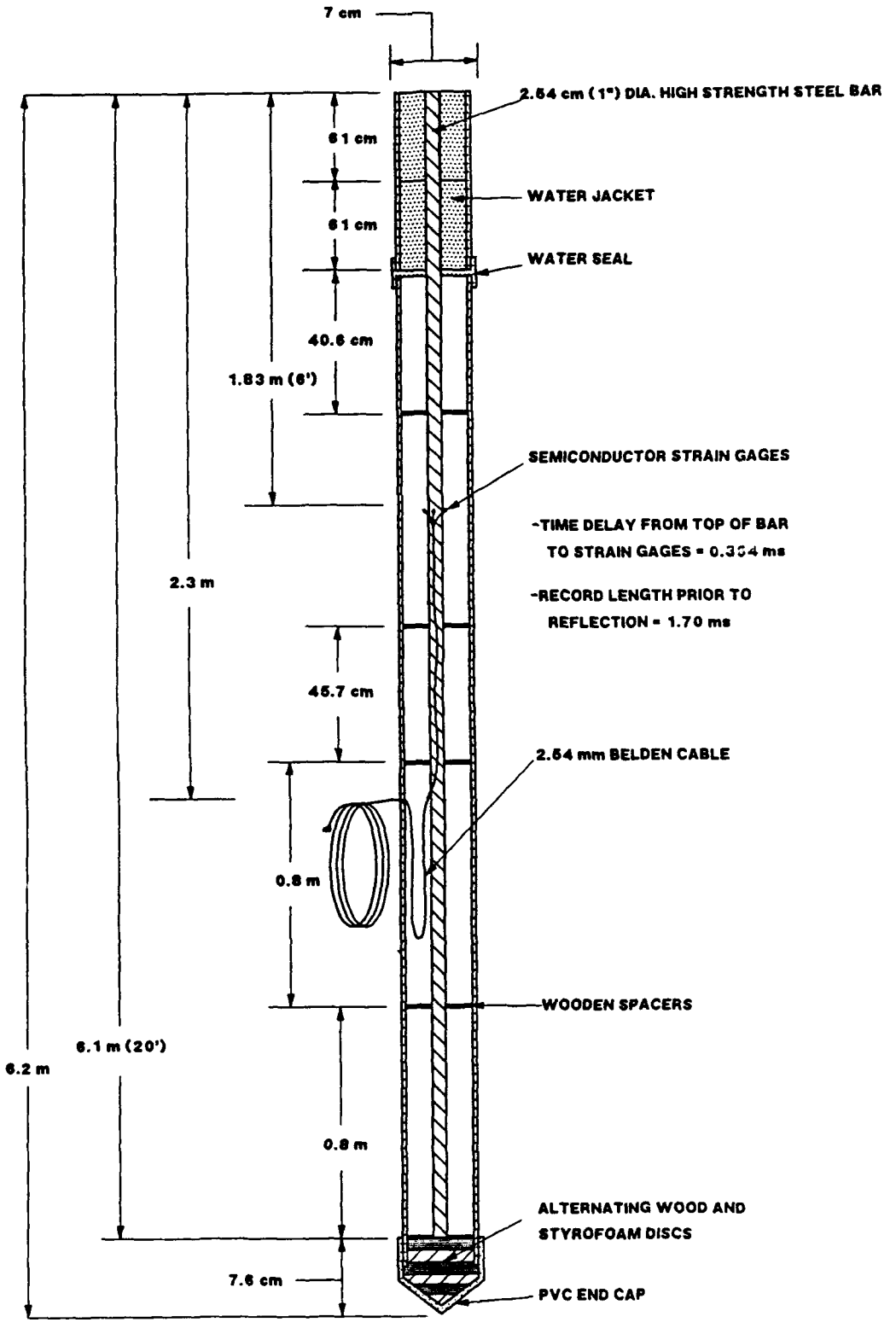

Figure 3. Detailed cross-section of a typical bar gage.

testing. At the top end of the bar gage, the annulus between the steel bar and the PVC pipe is left open, except for a small quantity of water added shortly before conducting the test. This annular column of water, extending from the top end of the bar to a short distance above the strain gages, is called the water jacket.

The water jacket is an important part of the bar gage. Often, the top end (or measurement end) of the bar gage is placed in contact with, or very near, explosive charges. Detonation of the explosive produces very high-pressure, high-temperature gases. Early bar gage designs without water jackets suffered early failures from these high velocity gases propagating along the bar gage, destroying the strain gages and cables. To prevent this, the upper portion of the bar gage was surrounded with water, creating the "water jacket". While the water jacket has been very effective at increasing the survival times of bar gage measurements, its effect on bar gage measurements has not been quantified.

Instrument cables are routed through a hole in the PVC pipe and back to a recording van, with care taken to ensure that they are not damaged by the explosive test. The instrument cables are often buried until they have extended a safe distance from the test area. Cable protection, such as rubber hose or steel tubing, is an option with bar gages, but has usually not been used because the length of the bar allows the attached cable to be buried at a considerable distance from the explosion, and thereby protected.

Installation

Bar gages can be installed in a number of ways to obtain a meaningful measurement. However, the installation technique shown in Figure 4 is used most often, and offers some unique advantages. With this installation, the bar gage is buried in the soil test bed, with just the measurement end exposed to the explosive charge. This technique takes advantage of the differing wave speeds in the bar gage materials and the surrounding media. The blast pressure wave strikes the measurement end of the bar, the water jacket, and the surrounding soil at essentially the same time. The wave travels rapidly down the steel bar, since its low-frequency wave speed, c_o, is about 5090 m/s (16700 ft/s). The pressure pulse travels more slowly through the water jacket (about 1525 m/s), and slower yet through the soil (305 m/s to 1525 m/s). As a result, any lateral inputs to the bar from the water jacket or the ground shock are delayed until after the initial arrival of the stress pulse at the strain gage position. If present, lateral inputs from these sources might then be more noticeable because of their delayed input into the bar. If the bar gage were simply placed in the free air near the charge, the wave speeds in the highly compressed air near the charge could be excessively high, destroying the acoustic delay effect and putting large lateral loads on the steel bar.

Physically, the installation of Figure 4 is usually achieved by drilling a borehole or excavating a trench or pit and backfilling around the bar gages. Cables are usually routed through intersecting horizontal boreholes or cable trenches. This installation technique

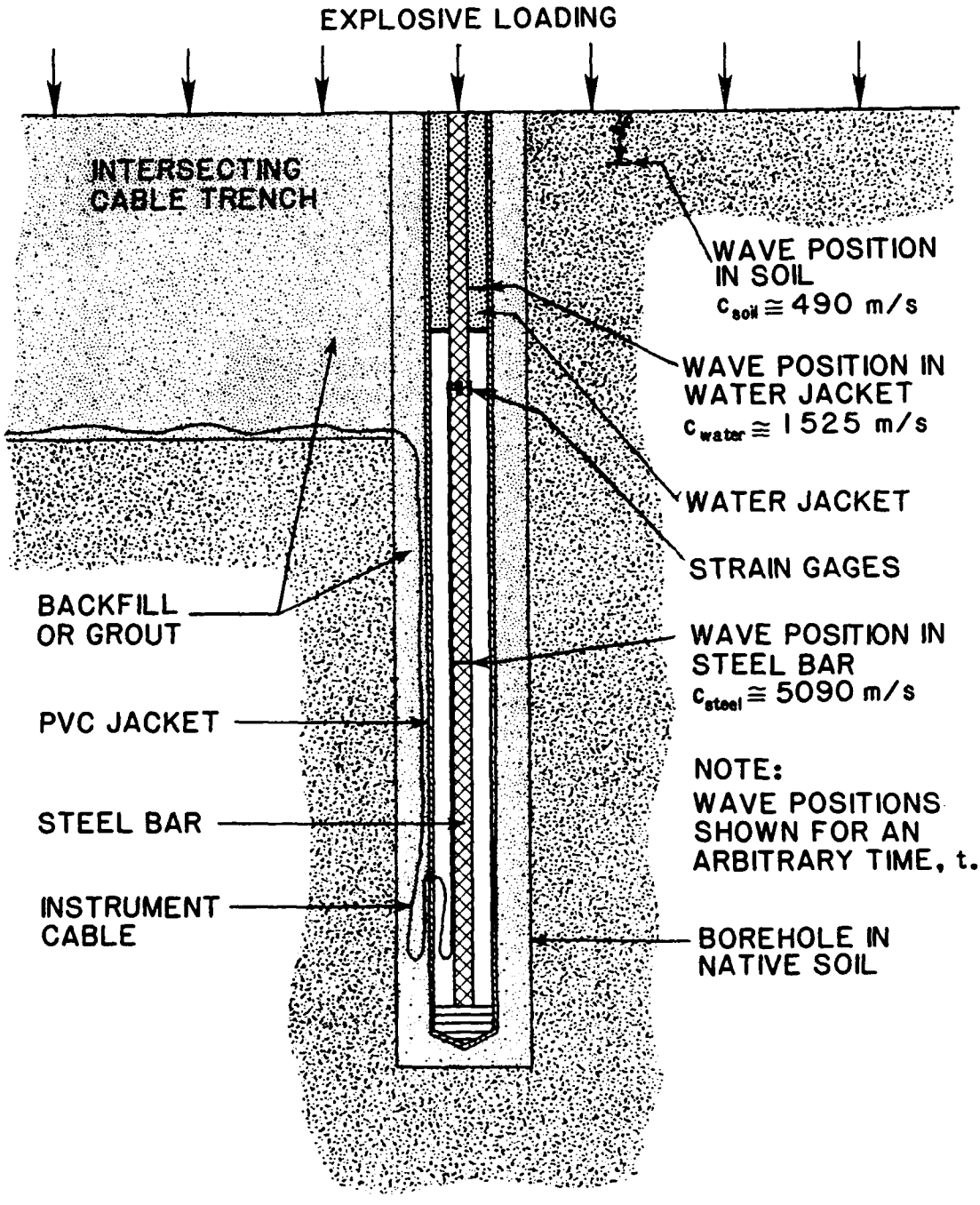

Figure 4. Typical installation techniques for a bar gage.

is tailored for those tests where high pressures and long durations are expected. For other applications, simpler deployments may suffice.

Design

The installation technique depicted in Figure 4 provides some unique contributions toward good bar gage design. The length of the bar gage has been determined by the length of measurement desired. Often, the measurement desired is too long to obtain with a practical length of bar gage, in which case the longest practical bar gage is used (6 to 12 m). The pulse duration recorded prior to the arrival of tensile reflections at the strain gage position is

$$\frac{2(L-x)}{c_o} \qquad 2.1$$

where L is the length of the bar

x is the distance between the top of the bar and the strain gages

c_o is the wave speed in the bar.

As can be seen from Equation 2.1, the record length can be increased only in a limited number of ways:

1. Increase the bar length, L.
2. Decrease the distance x.
3. Eliminate the occurrence of reflections.
4. Unfold the bar gage record, removing the reflections numerically.

As pointed out earlier, there are practical limits pertaining to the length of bar gage that can be successfully constructed and installed. Forty-foot long bar gages have been fielded, but only with limited success. Decreasing the distance from the top of the bar to the strain gages is limited due to the presence of the water jacket. Also, it is undesirable to place the strain gages less than 10 to 20 bar diameters from the measurement end (top) of the bar gage (Reference 5). Unfolding the bar gage record also holds promise, and successful unfolding could serve to relax some of the physical constraints on bar gage design.

Choosing the position of the water jacket with respect to the strain gages is somewhat judgmental. The effects of the water jacket length depend upon the severity of the test and several other factors. In some severe cases, the spalling of the water jacket might damage the cables attached to the strain gages. Some bar gage designs have taken this into account, and have dimensioned the water jacket in such a way that spalled water cannot reach the strain gages until after the first tensile reflection has arrived at the strain gage position. Then, if the strain gages and cabling survive, the subsequent reflections can be unfolded. If the strain gages and cabling do not survive, then at least the portion of the record prior to the first tensile record will be obtained.

Calibration and Recording

Semiconductor strain gages are used on the WES bar gages because of their superior sensitivity, compared to foil strain gages. One

drawback of the semiconductor strain gage is the variability of the gage factors; i.e., manufacturer-stated values of the gage factors are only approximate. This is in contrast to foil strain gages, whose gage factors are known with confidence, permitting the sensitivity of the bar gage to be calculated. WES bar gages are calibrated to overcome this problem.

The preferred method of calibration is the ball-drop calibration technique. A steel ball is dropped from a known height onto the end of the steel bar. Its rebound height is recorded on video tape, and then read from a scale in the field of view. Knowing the height of the ball drop, its rebound height, and the ball's mass, the impulse imparted to the bar can be obtained. The output from the bar gage is also recorded, and then integrated to obtain the impulse seen by the bar gage. When the electrical quantities (gains, excitation voltages, etc.) and the cross-sectional area of the bar gage are properly considered, the quotient of the two impulses defines the sensitivity level of the bar gage. Impulse hammers have also been used in similar fashion, and with good results, to input a known stress pulse to the bar gage.

The electronics necessary to operate and record strain gage readings will, in general, operate bar gages sufficiently well. WES uses specially-designed amplifiers capable of balancing strain gage bridges which, due to installation difficulties, may be considerably out of balance. The amplifiers also allow easy implementation of shunt calibration techniques. In the past, recording of the signals was done with analog tape recorders. Tape recorders are still used, but digital

recorders are now being used whenever possible. Frequency response must be adequate throughout the signal conditioning and recording system to capture the rise times and peak values of the blast pressures anticipated.

CHAPTER III

THE D'ALEMBERT UNFOLDING TECHNIQUE

The D'Alembert Solution to the Wave Equation

Several simple solutions, approximate solutions, and algorithm-based classical wave equations have been used to describe the longitudinal propagation of stress pulses in thin rods. The more complex approximate solutions and algorithms consider factors such as lateral and rotary inertia, in an effort to predict the dispersion of the stress pulse as it travels down the rod. One of the most simple classical solutions is the D'Alembert solution, developed by D'Alembert in 1748. In one dimension, this solution is expressed by the equation

$$u(z,t)=f(z-c_o t) + g(z+c_o t) \tag{3.1}$$

where $u(z,t)$ is the displacement of a particle caused by the propagating wave. The D'Alembert solution treats the stress pulse as a harmonic wave propagating up and down the rod (or bar gage) without change in shape. This allows for easy superposition of pulses as they propagate, and hence is a good choice for an unfolding algorithm. Choosing approximate solutions that attempt to account for dispersion would become exceedingly complex for purposes of numerical unfolding.

Since the D'Alembert solution is the basis of the unfolding routine, leading to the name "D'Alembert unfolding", a brief derivation

is provided. The basic wave equation for longitudinal waves in a thin bar is:

$$\frac{\partial^2 u}{\partial z^2} = \frac{1}{c_o^2} \frac{\partial^2 u}{\partial t^2} \tag{3.2}$$

where

$$c_o = \sqrt{\frac{E}{\rho}}$$

Equation 3.2 is obtained by considering the dynamically varying forces acting on an element of the bar. In these equations, z refers to a cross-section of the rod, while the longitudinal displacement of that cross-section is given by u. E is the modulus of elasticity of the bar material, and ρ is the material's density.

Mathematically, Equation 3.1 is obtained by introducing the following change of variables:

$$\xi = z - c_o t, \quad \eta = z + c_o t \tag{3.3}$$

So, rather than the particle displacement being a function of z and t, u becomes a funtion of ξ and η. The first step is to use chain-rule differentiation to obtain second partial derivatives of u with respect to both z and t. The first differentiation yields

$$\frac{\partial u}{\partial z} = \frac{\partial u}{\partial \xi}\frac{\partial \xi}{\partial z} + \frac{\partial u}{\partial \eta}\frac{\partial \eta}{\partial z} = \frac{\partial u}{\partial \xi} + \frac{\partial u}{\partial \eta}$$

$$\frac{\partial u}{\partial t} = \frac{\partial u}{\partial \xi}\frac{\partial \xi}{\partial t} + \frac{\partial u}{\partial \eta}\frac{\partial \eta}{\partial t} = -c_o\frac{\partial u}{\partial \xi} + c_o\frac{\partial u}{\partial \eta}$$

And the second differentiation yields

$$\begin{aligned} \frac{\partial^2 u}{\partial z^2} &= \frac{\partial^2 u}{\partial \xi^2} + 2\frac{\partial^2 u}{\partial \xi \partial \eta} + \frac{\partial^2 u}{\partial \eta^2} \\ \frac{\partial^2 u}{\partial t^2} &= c_o^2\left(\frac{\partial^2 u}{\partial \xi^2} - 2\frac{\partial^2 u}{\partial \xi \partial \eta} + \frac{\partial^2 u}{\partial \eta^2}\right) \end{aligned} \tag{3.4}$$

When substituting Equations 3.4 into the wave equation (3.2), many terms cancel out, leaving

$$\frac{\partial^2 u(\xi,\eta)}{\partial \xi \partial \eta} = 0 \tag{3.5}$$

Equation 3.5 must be integrated to obtain the expression for $u(\xi,\eta)$. First, the integration is performed with respect to η, and then with respect to ξ. Realize that, since u is only a function of ξ and η, its partial with respect to one of those variables is simply some function of that variable (by the definition of partial differentiation). This integration process is:

$$\int_\eta \frac{\partial^2 u}{\partial \xi \partial \eta}\, d\eta = \frac{\partial u}{\partial \xi} = f(\xi)$$

$$\int_\xi \frac{\partial^2 u}{\partial \xi \partial \eta}\, d\xi = \frac{\partial u}{\partial \eta} = g(\eta)$$

So, the most general expression satisfying Equation 3.5 is

$$u(z,t) = f(\xi) + g(\eta)$$

and by changing variables back according to Equation 3.3, the D'Alembert solution to the wave equation is obtained (Reference 10).

Two characteristics of the D'Alembert solution are particularly noteworthy. First, it is easy to see how the arbitrary functions f and g represent propagating disturbances in the bar. In order for the arguments of the functions to remain constant, z must increase as t increases. This corresponds to a propagating wave. As the solution is written in Equation 3.1, the function f represents a wave propagating in the positive z direction, and the function g represents a wave propagating in the negative z direction. Secondly, realize that there is no mechanism in the D'Alembert solution for the shape of the functions f and g to change as they propagate up and down the bar. The functions will remain the same as they were initially, with only the position of the waves changing as they are propagating up and down the bar. These attributes prove useful in assembling the framework upon which numerical unfolding can be based.

Derivation of Unfolding Equations

The D'Alembert solution illustrates how the general wave equation allows for the propagation of a pulse up and down the length of a bar. D'Alembert unfolding uses that concept to unravel the tensile and compressive reflections that are superposed upon the airblast input to the bar gage. For the sake of brevity, D'Alembert unfolding will be

referred to simply as "unfolding" or "numerical unfolding" throughout the remainder of this thesis.

To begin the derivation of the unfolding equations, it is prudent to first discuss some of the basic phenomena taking place. After a length of time, L/c_o, the stress wave has advanced to the dump end of the bar gage. Because this end is in direct contact with some other material (usually wood), some of the pulse is transmitted into the contact material, and the remainder of the stress pulse is reflected back into the bar. Since the acoustic impedance of the steel bar is much greater than that of wood and other contact materials, the majority of the stress pulse reflects as a tensile wave and travels upward in the bar. The percentage of the incident stress wave reflected back into the bar is called the reflection coefficient. For the dump end of the bar, this coefficient is assigned the variable *A*.

The tensile wave continues to travel back up the bar and, as mentioned earlier, when it reaches the strain gage position, begins to mask the late time portion of the incoming airblast signal that is still being applied to the top of the bar. The tensile wave reaches the measurement end of the bar at time $2L/c_o$. Here again, some of the tensile wave transmits into the material in contact with the measurement end of the bar (usually air or detonation products), and some of the tensile wave reflects back into the bar as a compressive wave. The percentage of the tensile wave reflecting back into the bar as a compressive wave is defined as the reflection coefficient *B*. This wave reflection process continues indefinitely at each end of the bar,

with the reflection coefficients reducing the wave form at each reflection by their prescribed percentages.

The actual values of the reflection coefficients for a particular bar gage are determined empirically from the data record. Figure 5 describes this technique. The reflection coefficient, *A*, is the ratio between the magnitude of the peak reflected stress and the magnitude of the initial peak stress that strikes the end of the bar. Both magnitudes are read from the data record, as shown in Figure 5. The record shows the peak reflected stress riding upon the tail end of the original incoming wave. The sharp rise times associated with the peak stress and the peak reflected stress make it possible to judge when the reflection begins and what its magnitude is. Attempting to judge reflection coefficients at times other than initial arrivals of reflections is not recommended, since a sharp, recognizable departure from incoming data to a reflection is not assured. The same approach is used in determining the reflection coefficient *B*. The reflection coefficient *B* is the ratio of the magnitude of the reflected compressive peak stress to the magnitude of the reflected tensile peak stress. Since the measurement end of the bar is in contact with air or detonation products (nearly a free-end condition), *B* usually has a value of approximately one. These reflection coefficients are assumed to be constant throughout the entire measurement.

In Figure 6, an example wave form is used to illustrate the unfolding process. The input and output wave forms are shown for a bar gage having a length of 6.1 m and a distance of 1.8 m between the strain gages and the measurement end of the bar. The peak stress is

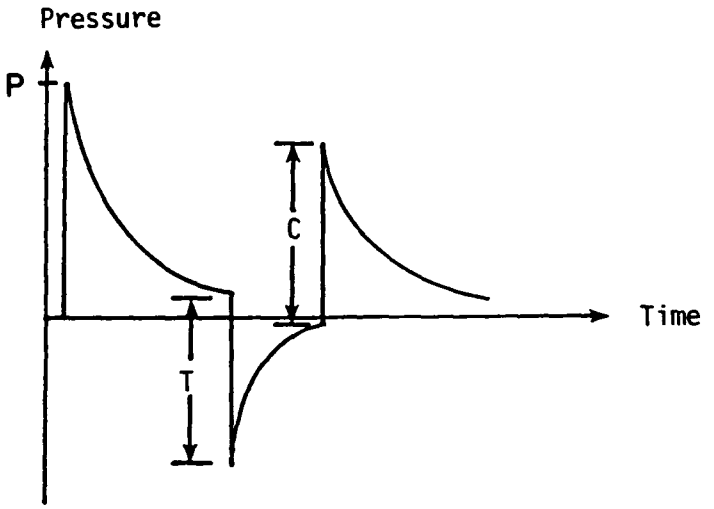

$$A = \frac{T}{P} \qquad B = \frac{C}{T}$$

P = peak input stress
T = peak stress of tensile reflection
C = peak stress of compressive reflection
A = reflection coefficient for dump end of bar
B = reflection coefficient for measurement end of bar

Figure 5. Technique for determining reflection coefficients from a bar gage record.

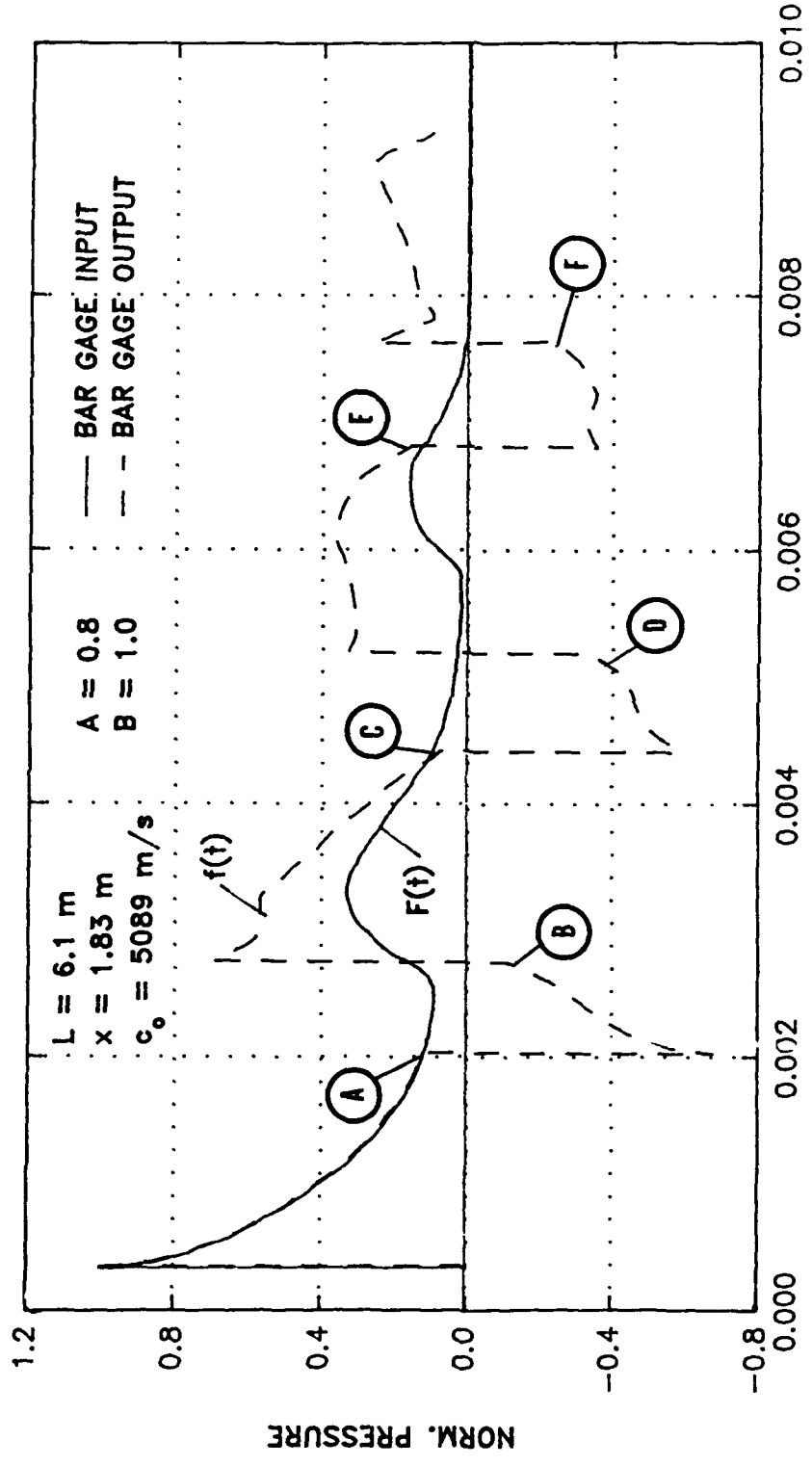

Figure 6. Arbitrary pressure input wave form and corresponding bar gage output for a typical bar gage.

normalized to a value of one for this example. The input airblast wave form applied to the measurement end of the bar gage is referred to as $F(t)$, while the actual output recorded from the bar gage is called $f(t)$. The arrival time and magnitude of reflections are correctly computed by using the values for A, B, and c_o shown on the figure. The input wave form has been shifted in time, x/c_o, to lie directly over the bar gage output for comparison.

Markers A through F are placed on the wave form, labelling each reflection. Let us begin at the front of the wave form and work through to the end, stopping at each marker to account for all the pulses (both incoming and reflected waves) that pass the strain gage position (Note: Compressive stresses are positive and tensile stresses are negative in sign). Figure 7 shows all of the waves at the instant before they pass the strain gage position for Markers A through F. After a time interval of $2(L-x)/c_o$, measured from the arrival of the stress pulse, the input and output wave forms are the same, since no reflections have arrived at the strain gage position. Marker A, however, denotes the arrival of the first tensile reflection. This reflection is the original pressure pulse that arrived at a time $2(L-x)/c_o$ earlier in the wave form, but after being influenced by reflection coefficient A. Simply adding all of the stress waves shown in Figure 7a yields the following equation for the output of the strain gages.

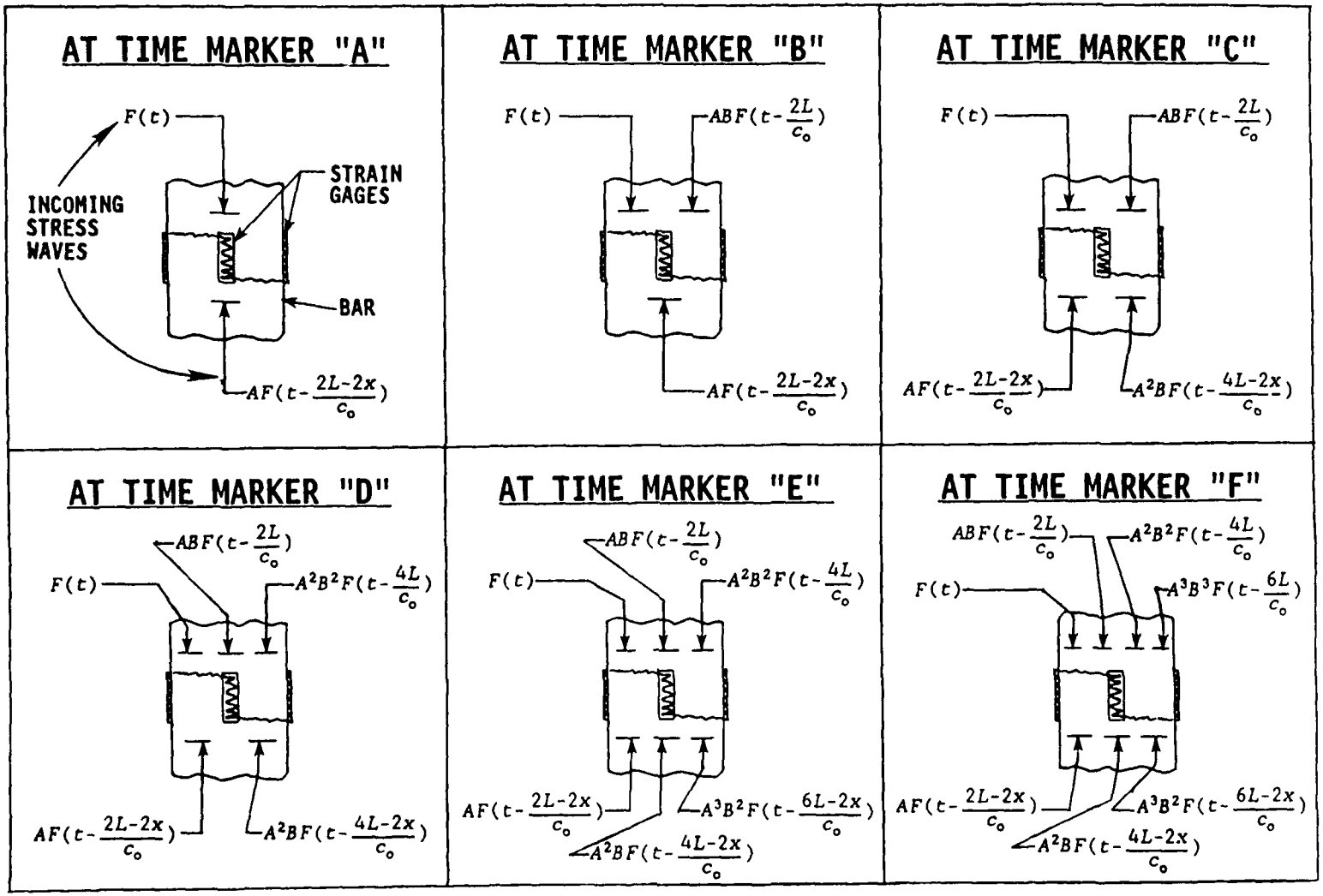

Figure 7. Schematic diagram of stress waves and reflections influencing strain gage output in a bar gage for time markers A through F.

$$f(t) = F(t) - AF(t - \frac{2(L-x)}{c_o}) \tag{3.6}$$

Marker B indicates the arrival of the first compressive pulse at time $2L/c_o$. Hence, another compressive input is influencing the strain gage output, as depicted in Figure 7b. Keep in mind that the stress waves being measured by the strain gages are the original inputs to the bar, $F(t)$, but after being diminished successively by reflection coefficients. Observing Figure 7b, three inputs are influencing the strain gage output: the incoming data, $F(t)$; incoming data from the first tensile reflection, $AF(t-2(L-x)/c_o)$; and the data from the first compressive reflection. The first compressive reflection has been influenced by both reflection coefficients A and B. The input wave becomes a compressive reflection when it has traversed the distance:

$$(L-x) + (L-x) + x + x = 2L$$

The strain gage output for the first set of reflections (one tensile and one compressive); i.e., n = 1, is the sum of these three waves, or

$$f(t) = F(t) - AF(t - \frac{2(L-x)}{c_o}) + ABF(t - \frac{2L}{c_o}) \tag{3.7}$$

At Marker C, we have all of the inputs shown in Equation 3.7, but also the arrival of the second tensile reflection. This second tensile reflection has been influenced by three reflection coefficients; A twice, and B once. The second tensile reflection is recorded by the strain gages after the input wave has traversed the distance

$$(L-x)+(L-x)+x+x+(L-x)+(L-x) = 4L-2x$$

after initial contact with the strain gages. So, observing Figure 7c, the input waves are summed together to obtain the strain gage output:

$$f(t) = F(t) - AF(t-\frac{2L-2x}{c_o}) + ABF(t-\frac{2L}{c_o}) - A^2BF(t-\frac{4L-2x}{c_o}) \tag{3.8}$$

At Marker D, all of the inputs from Equation 3.8 are present, plus the second compressive reflection. The second compressive reflection has been influenced by four reflection coefficients; *A* twice, and *B* twice. The second compressive reflection is recorded when the input wave has traversed the distance

$$(L-x)+(L-x)+x+x+(L-x)+(L-x)+x+x = 4L$$

after initial contact with the strain gages. Accordingly, the inputs shown on Figure 7d can be summed as before to obtain the strain gage output through the second set of reflections; i.e., n = 2:

$$f(t) = F(t) - AF(t-\frac{2L-2x}{c_o}) + ABF(t-\frac{2L}{c_o}) - A^2BF(t-\frac{4L-2x}{c_o}) + A^2B^2F(t-\frac{4L}{c_o}) \tag{3.9}$$

At Marker E, all of the inputs of Equation 3.9 are present, but the third tensile reflection also comes into play. This reflection has been influenced by five reflection coefficients; *A* three times, and *B*

twice. The third tensile reflection is recorded when the input wave has traveled

$$(L-x)+(L-x)+x+x+(L-x)+(L-x)+x+x$$
$$+(L-x)+(L-x) = 6L-2x$$

after initial contact with the strain gages. Summing all of the stress wave inputs indicated by Figure 7e gives the strain gage output:

$$f(t) = F(t) - AF(t-\frac{2L-2x}{c_o}) + ABF(t-\frac{2L}{c_o}) - A^2BF(t-\frac{4L-2x}{c_o}) + A^2B^2F(t-\frac{4L}{c_o}) - A^3B^2F(t-\frac{6L-2x}{c_o}) \quad (3.10)$$

At Marker F, the third compressive reflection is added to the inputs of Equation 3.10 are present. This reflection has been influenced by six reflection coefficients; A three times, and B three times. The third compressive reflection is recorded when the input wave has traveled

$$(L-x)+(L-x)+x+x+(L-x)+(L-x)+x+x$$
$$+(L-x)+(L-x)+x+x = 6L$$

after initial contact with the strain gages. As before, summing all of the stress wave inputs displayed on Figure 7f yields the strain gage output for the third set of reflections, i.e.,

n = 3:

$$f(t) = F(t) - AF(t-\frac{2L-2x}{c_o}) + ABF(t-\frac{2L}{c_o}) - A^2BF(t-\frac{4L-2x}{c_o}) + A^2B^2F(t-\frac{4L}{c_o}) - A^3B^2F(t-\frac{6L-2x}{c_o}) + A^3B^3F(t-\frac{6L}{c_o}) \quad (3.11)$$

After this laborious exercise, a pattern becomes obvious. Observe Equation 3.7 for the case of n = 1, Equation 3.9 for the case of n = 2, and Equation 3.11 for the case of n = 3. Several of the terms are similar, and can be simplified into the series expression shown below

$$f(t) = F(t) - \sum_{n=1}^{\infty} A^n B^{n-1} F(t-\frac{2(nL-x)}{c_o}) + \sum_{n=1}^{\infty} A^n B^n F(t-\frac{2nL}{c_o}) \quad (3.12)$$

This shows that the total strain gage output is the original input to the bar, $F(t)$, with tensile and compressive reflections superposed on $F(t)$. However, in the practical situation, the data analyst has the bar gage record, $f(t)$, and desires to know the true input to the bar gage, $F(t)$. This is accomplished by rearranging Equation 3.12 to solve for $F(t)$.

$$F(t) = f(t) + \sum_{n=1}^{\infty} A^n B^{n-1} F(t-\frac{2(nL-x)}{c_o}) - \sum_{n=1}^{\infty} A^n B^n F(t-\frac{2nL}{c_o}) \quad (3.13)$$

Equation 3.13 is referred to as the general unfolding equation. Notice that the series terms in Equation 3.13 always operate upon data that has already been recorded by the strain gages, facilitating

reconstruction of the original input wave form by working from the beginning to the end of the bar gage record.

The Unfolding Computer Program

Equation 3.13 lends itself well to implementation in a computer program. Welch (1983) wrote an initial computer program to run on a Tektronics 4051 computer. Since the limited memory of these early computers did not allow processing of many data points, the unfolding computer program was rewritten in FORTRAN to run on a VAX 11/750 computer. The program was named UNFOLD, and is used when unfolding wave forms with a large number of data points (more than 16,000). The unfolding program has been updated to run on IBM personal computers (or other compatible PC's) as part of this thesis. The PC-based unfolding program, still written in FORTRAN code, works well for wave forms having less than 16,000 points. This size of data file allows for acceptable speed and memory size, and also permits the use of several off-of-the-shelf plotting programs to display the results.

Since the unfolding program is used (and modified) so often in this thesis, a brief explanation of its operation is given in this section. A flow chart of the unfolding program is shown in Figure 8 and a program listing is given in the Appendix. The analyst must input the bar gage dimensions and wave speed, time of arrival, reflection coefficients, and file names for the input bar gage record and the unfolded output. The input file must be of a certain format, namely,

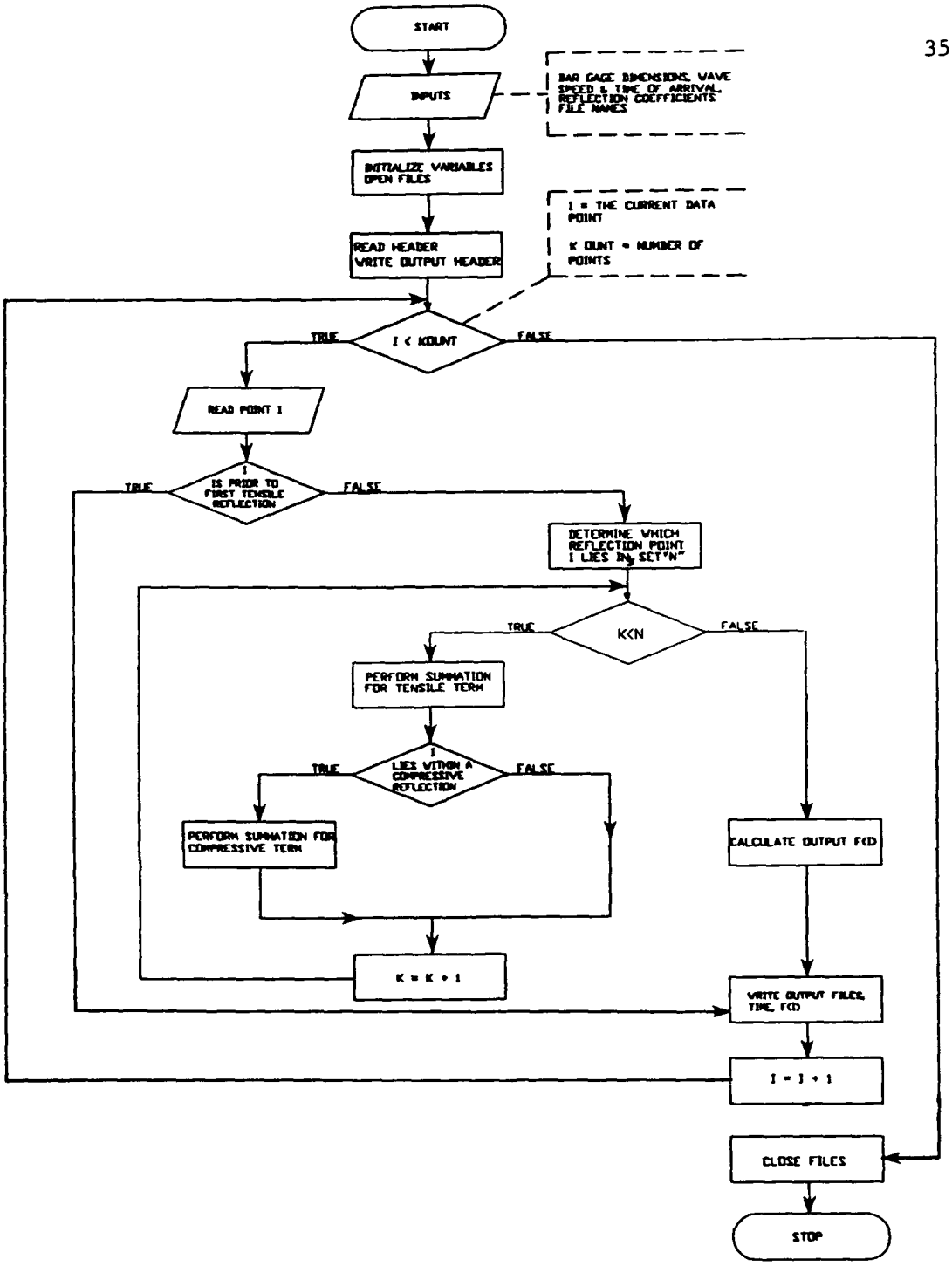

Figure 8. Flow chart of the unfolding computer program.

LINE 1: TIME VALUE OF FIRST POINT

LINE 2: TIME INCREMENT

LINE 3: NUMBER OF DATA POINTS

LINE 4: X(1), Y(1)

LINE 5: X(2), Y(2)

" " "

" " "

ETC.

Two arrays are established; A(I) is the input bar gage data, and F(I) is the unfolded output of the program. The calculational kernel begins by reading the first data points from the input file and deciding if they occur before the arrival of the first tensile reflection. If they do, the data points are simply copied to the output file because no unfolding is necessary. Once beyond the first tensile reflection, the program determines which set of reflections contains the point "I". This is analogous to the index *n* in Equation 3.13 and also sets the counter on the first DO loop. Once within the inner DO loop, the summing operation is performed. The calculational kernel determines if point "I" lies within a tensile or compressive reflection and applies the summation process indicated in the second and third terms of Equation 3.13. The summations indicated in the second term of Equation 3.13 are the variable G1, and the summations indicated in the third term of Equation 3.13 are the variable G2. When the summation has been performed "*n*" times, the inner loop is exited. The value of the unfolded wave form at point "I" is then:

$$F(I) = A(I) + G1 - G2 \tag{3.14}$$

The value of the time interval at point "I" and F(I) are written to the output file and the whole process is continued for the next point "I". When "I" has reached the last point in the file, as specified in line 3 of the input file, execution is terminated.

The output of the program is a two-column ASCII file. This file can be plotted using various plotting routines. Such routines are not included in the unfolding program. Since the data files are written in an ASCII format, the files can become quite large.

Demonstration of the Unfolding Technique

To illustrate the effect of the unfolding computer program, a wave form from a high explosive test will be unfolded. The bar gage record and its integrated impulse are shown in Figure 9a. The low-frequency wave speed, c_o, is customarily determined by measuring the time between the arrival of the initial pressure pulse and the first tensile reflection. The wave speed is then obtained by

$$c_o = \frac{2(L-x)}{t}$$

The reflection coefficients are determined using the procedure indicated earlier in this section. The time of arrival of the initial pressure pulse is obtained by observation. The bar dimensions are, of course, known prior to the test. Besides specifying file names, this

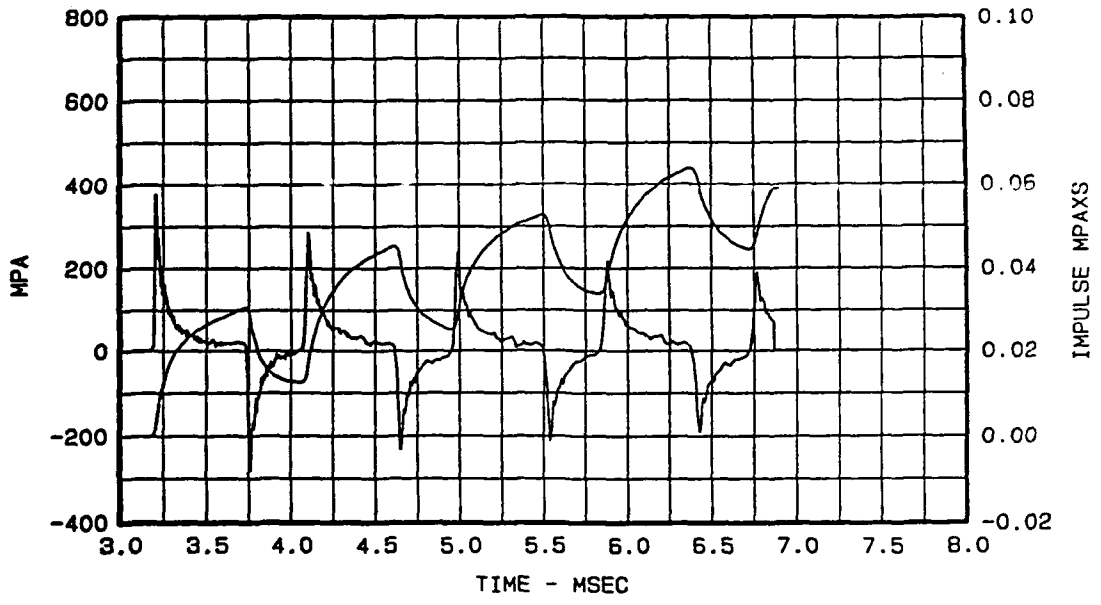

a. Bar gage wave form prior to unfolding.

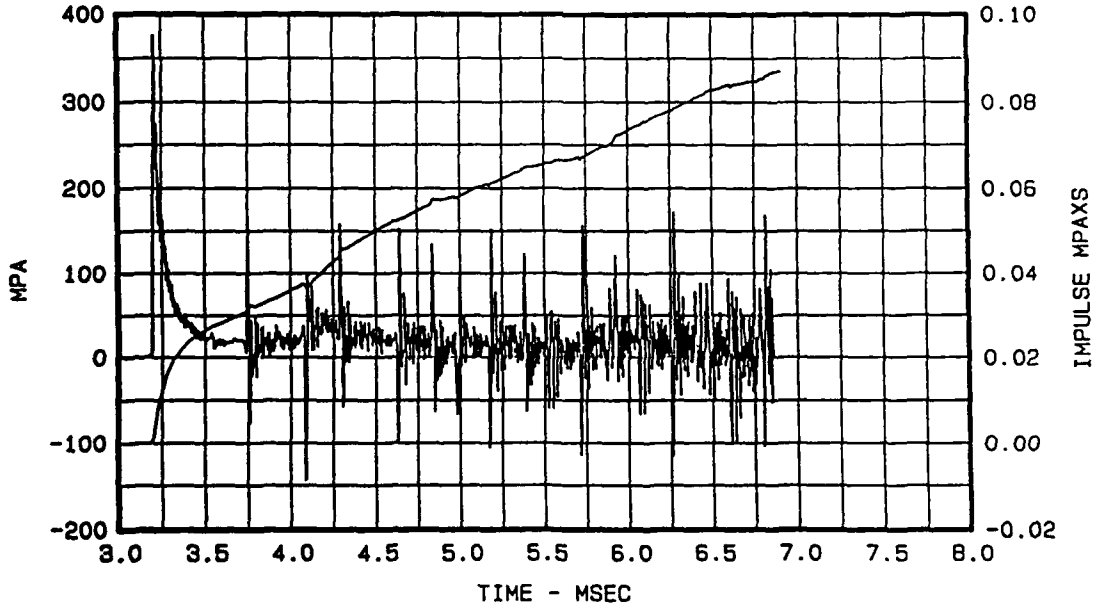

b. Unfolded wave form.

Figure 9. Demonstration of the unfolding technique on a typical bar gage wave form.

constitutes all of the information needed to unfold the wave form of Figure 9a. The values used for this particular wave form were:

c_o = 5089 m/s TOA = 0.00323 s A = 0.92

x = 0.86 m L = 2.25 m B = 0.97

The result of the unfolding procedure is shown in Figure 9b. As expected, the reflections have been removed from the record, producing a reasonable restoration of the original pressure pulse entering the bar. The drastic fluctuations in the impulse wave form have also been removed, resulting in an impulse wave form of classical appearance. The process did not provide a perfect unfolding of the high-amplitude portions of the wave form (peak values of the input waveform and also the reflections), as evidenced by the spikes occurring at positions where reflections had previously existed. This produces corresponding anomalies in the impulse wave form, although not severely so. If the spiky behavior is ignored, the unfolded result is a reasonable pressure wave form.

Criticism of the Unfolding Technique

From a mathematical prospective, the D'Alembert unfolding method is difficult to refute. If indeed the pulse is not changing shape significantly as it propagates down the bar, then the unfolding technique should accurately remove the reflections. However, potential shortcomings do exist. The shortcomings arise primarily from the inability of the analyst to provide exactly correct input to the unfolding routine.

Consider the spiky behavior present on the unfolded wave form of Figure 9b. The spikes result from using a slightly incorrect value of wave speed, c_o. If the analyst specifies a value of c_o that is too large, the unfolding routine will anticipate the arrival of the first tensile reflection too soon. While the routine should be summing the high-amplitude portion of the initial pulse with the high-amplitude, negative portions of the first tensile reflection, it actually is adding a high-amplitude positive value to a low-amplitude positive value. A high-frequency spike results from this sort of superposition. Since the unfolding routine uses these values over again later in the wave form, the error repeats itself, sometimes even growing with additional recurrences. While it is felt that this behavior will not cause large errors in the impulse measurement, the propagation of this error through the unfolded wave form has not been sufficiently studied.

Another concern lies with the choice of values for the reflection coefficients. Theory suggests that there is one precise reflection coefficient for each end of the bar gage, and the method described earlier in this section should reveal the value of these coefficients. However, observation of subsequent reflections often shows a change in the value of the reflection coefficients. Figure 10 illustrates such a bar gage record, recorded on a high explosive test. Notice how the reflection coefficients change throughout the record. This forces the analyst to make a judgement regarding which value of the reflection coefficient to use for unfolding purposes. Inspection of the unfolding equation (Equation 3.13) indicates that the reflection coefficients *A* and *B* influence the value of each point after the first tensile

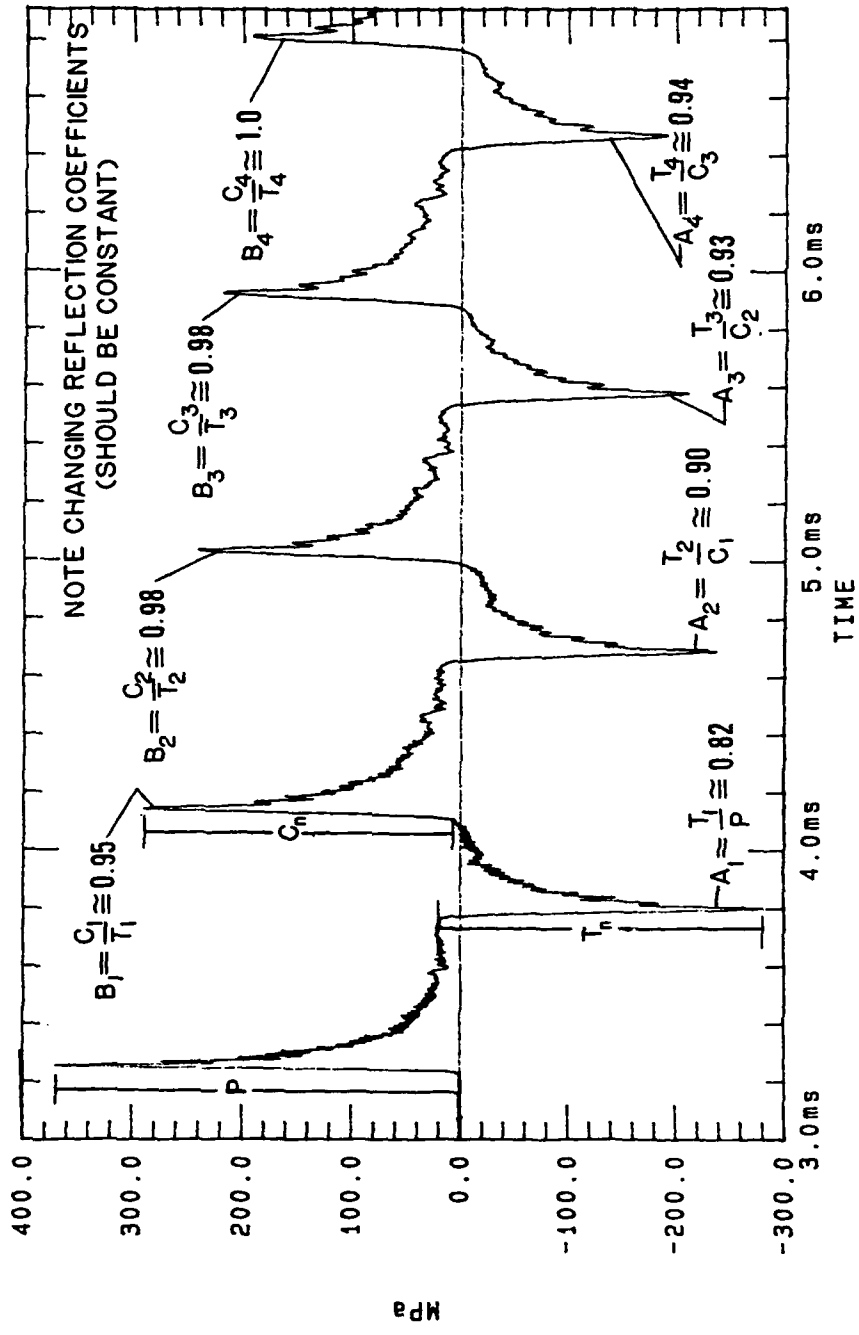

Figure 10. Illustration of reflection coefficients changing during a typical high explosion test record.

reflection. The net effect that varying values of reflection coefficients may have on the unfolded pressure and impulse wave form has not been studied.

In summary, while the unfolding technique will indeed remove reflections from the bar gage wave form, the significance of errors induced by the technique are subject to question. The value of unfolding is substantial, for if even one set of reflections are unfolded, the length of the measurement is more than doubled. But questions surrounding the errors induced by the use incorrect wave speeds and reflection coefficients lead to controversy in using the unfolding technique. Accordingly, this thesis seeks to quantify the errors inherent to the D'Alembert unfolding method, defining situations where unfolding is appropriate.

CHAPTER IV

ERROR ANALYSIS OF THE UNFOLDING TECHNIQUE

Bar gage records from high explosive tests can be influenced by phenomena that is not fully understood. For instance, ground shock may put lateral loads on the bar through the water jacket. If so, then that part of the wave form we observe, and treat as data, may in fact be a measure of lateral loading. The reflection coefficient at the dump end of the bar can change during the high explosive test because of bar translation, which causes the bar to push into the material at the end of the bar. This "rigid-body" motion of the bar can occur after two wave transit times. Also dispersion of the stress pulse may complicate the analyst's selection of reflection coefficients.

When unfolding bar gage records from high explosive tests, it may be difficult to sort out which discrepancies are do to the numerical aspects of unfolding and which are due to the "limitations" of bar gages as currently designed. With this in mind, the next study will investigate the merits of bar gage unfolding through the use of analytical and numerical means. This will minimize the confusion imparted by the response of the bar gage to high-frequency inputs from explosive tests, and permit us to concentrate on the errors strictly due to the unfolding process.

In this section three sources of error in the D'Alembert unfolding techniqueare identified and analyzed. The three error sources addressed are:

1. Errors due to using an incorrect, low-frequency wave speed.
2. Errors due to specifying incorrect reflection coefficients, or assigning constant values to reflection coefficients that, in reality, are changing.
3. Other errors, such as incorrect bar gage dimensions and dispersion. Errors which apply to bar gages, though not necessarily numerical unfolding errors, are also included in this section.

The first error is addressed by modifying the unfolding computer program in such a way that it calculates not only the unfolded wave form based upon the best estimate of the wave speed, c_o, but also based upon user-specified upper and lower bounds of c_o. The second error source is addressed by applying classical uncertainty analysis to the unfolding equation presented in Chapter 3. An analytical expression is obtained which relates the uncertainty of an unfolded wave form to an uncertainty in the reflection coefficients. The errors due to both of these primary sources are then combined in a manner consistent with uncertainty analysis, to arrive at upper and lower bounds of where the "true" unfolded wave form must lie.

The last error source is addressed only qualitatively, as no analytical or concise experimental technique could be devised to isolate those unfolding errors that are due to subtleties such as

dispersion. The manner in which such errors manifest themselves on typical wave forms is discussed, and shown to be relatively insignificant when impulse is the desired quantity.

Errors Due To Incorrect Wave Speed

The low-frequency wave speed, c_o, must be known accurately in order for the timing to be correct during the unfolding process. If the wave speed is incorrect, the unfolding routine will sum incorrect terms while reconstructing the wave form. For instance, summing terms from the high-amplitude front end of the wave form with those representing low-amplitude parts of the wave form (rather than the high-amplitude portions which are opposite in sign), will result in noise-like or spiky output from the unfolding routine. This procedure is illustrated in Figure 11.

The analyst must measure the time between reflections, and calculate the wave speed based upon the known dimensions of the bar gage. Choosing places to measure the time between reflections is somewhat judgmental, resulting in slightly different values of wave speed. Since we tend to measure the time differences between peaks or arrival times (i.e., high-frequency content), dispersion can cause the analyst to choose an incorrect value of wave speed. As will be discussed later, dispersion itself results from the wave speed changing as a function of the frequency of the input. Consequently, high-frequency portions of the wave form are prone to being unfolded incorrectly. Such shortcomings make it almost impossible to perfectly unfold a wave form. The wave form of Figure 12a was unfolded using

A. Suppose that c_o is too small. Then the computer routine begins unfolding the first tensile reflection too late, leaving a negative spike. When the computer routine does begin unfolding the first reflection, it adds the high amplitude initial peak (times reflection coefficient A) to negative values which are too small. This results in a positive "recovery" spike.

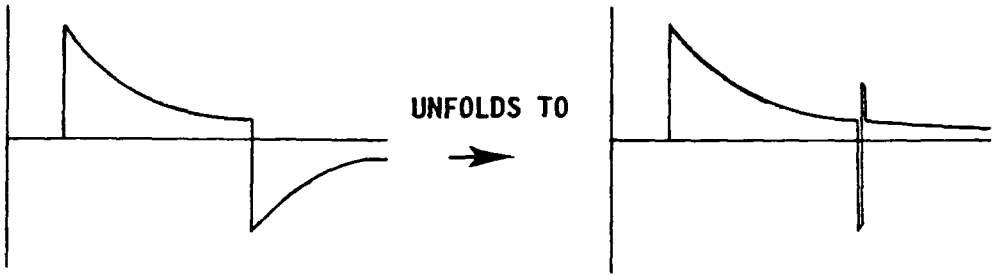

B. Suppose that c_o is too large. Then the computer routine begins unfolding the first tensile reflection too soon, leaving a positive spike. When the unfolding process reaches the true time of the first reflection, it adds the lower amplitude positive values (times reflection coefficient A) to larger negative values. This results in a negative "recovery" spike.

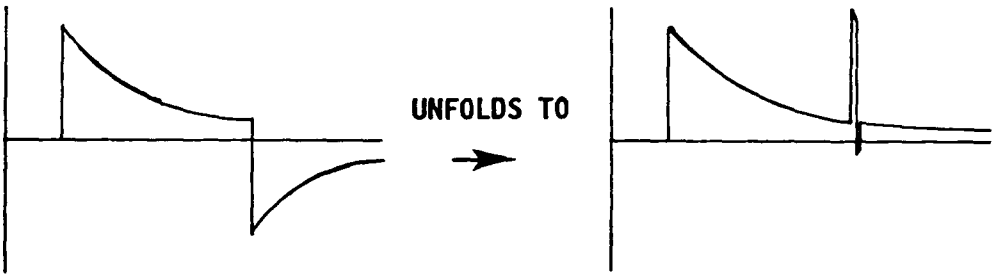

C. This unfolding program propagates these spikes throughout the rest of the waveform.

Figure 11. Mechanism by which the unfolding method produces spikes in unfolded wave forms.

common textbook value for the wave speed of steel (5030 m/s), and the output displayed in Figure 12b. The input wave form to the bar gage in Figure 12a was a 100-μs pulse, with no subsequent inputs to the bar. Consequently, all of the noise-like inputs later in the wave form are due to the data reduction process and the incorrect wave speed used in the unfolding routine. This illustrates the necessity of choosing an accurate value of c_o for the steel bar.

The proper wave speed value to choose is the low-frequency wave speed, c_o. Wave speeds determined from the time differences between peak values, or between times-of-arrival of reflections, tend to be different than the true low-frequency wave speed. This is because these features of the wave form are comprised of wave speed high-frequency content, which is being dispersed, or distorted, as it propagates down the bar. Choosing a wave speed based upon unfolding high-frequency data with the best performance might cause substantial errors in the unfolding of low-frequency data. Errors in unfolding low-frequency data might lead to large errors in impulse, which is particularly undesirable for many applications.

Two recommendations are given to minimize the error imparted by use of an incorrect wave speed. First, whenever possible, choose the wave speed for a particular bar gage from the gage calibration record, rather than the actual data record. A ball drop calibration, for instance, generates frequencies up to roughly 7000 Hz. This frequency content is too low for dispersion to be prevalent, so the wave speed is more easily discerned. Secondly, measure the time required to shift the wave form $2L/c_o$ by determining the time shift which causes

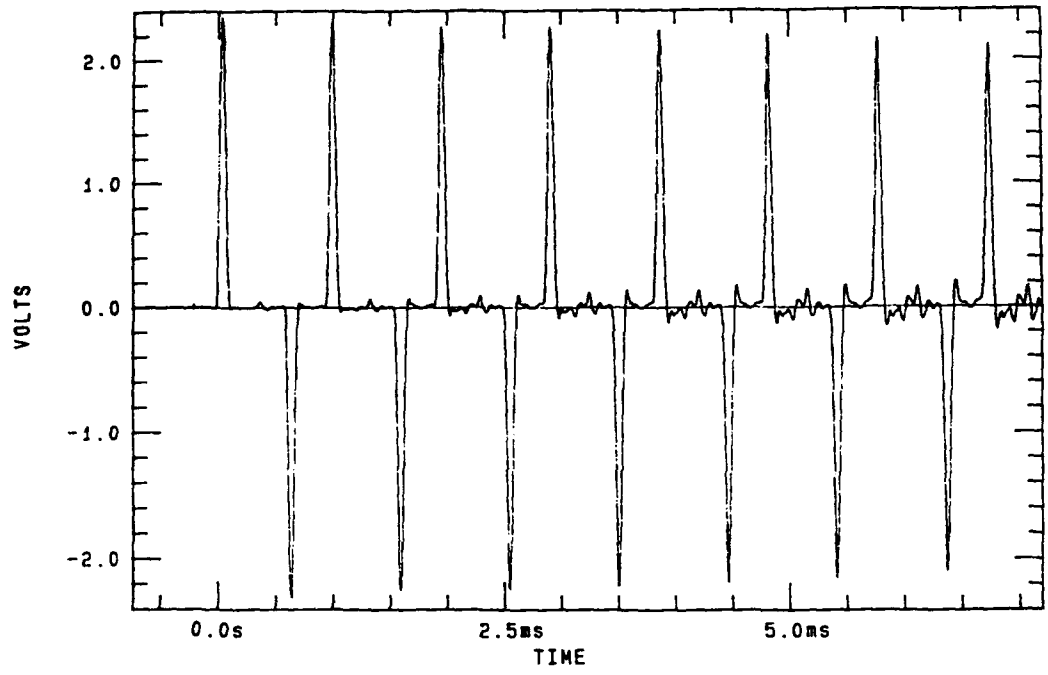

a. Precision bar gage wave formprior to unfolding.

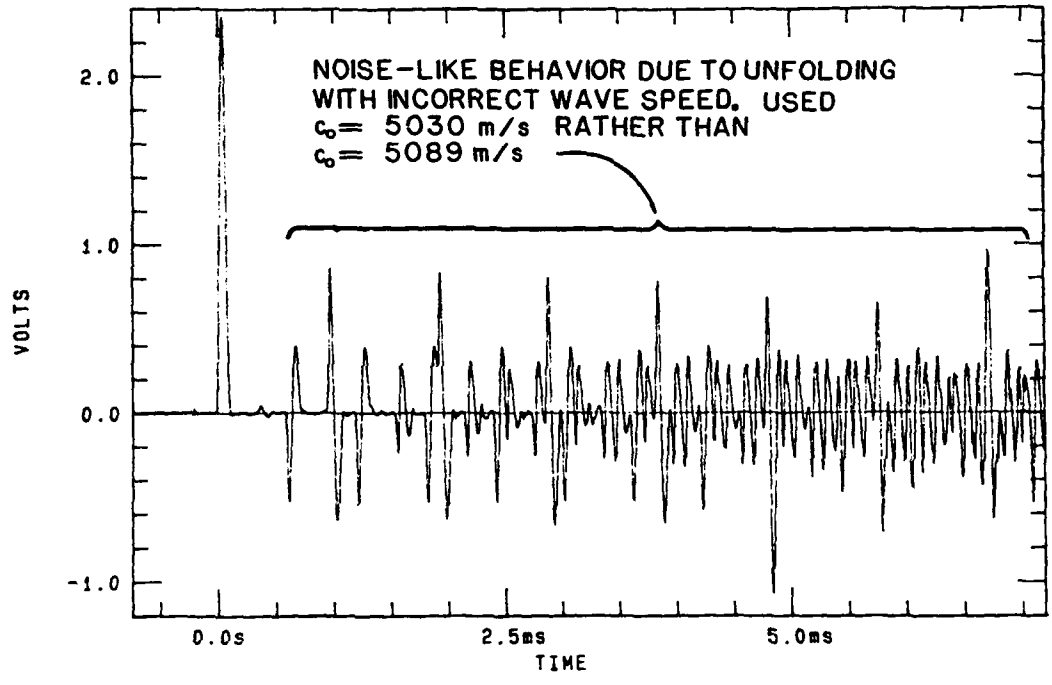

b. Unfolded wave form using incorrect wave speed.

Figure 12. Typical results produced by the unfolding technique when incorrect values of wave speed are used.

subsequent compressive (or tensile) pulses to best over-lay each other. This technique measures the time expired between low-frequency events in the wave form (i.e., the whole compressive pulse rather than just peaks) and produces more consistent results.

Since we wish to combine two or more errors (wave speed and reflection coefficients) to arrive at the total error present in an unfolded wave form, classical uncertainty analysis will be used. Classical uncertainty analysis provides an accepted and concise technique for calculating uncertainties and combining them to give the total uncertainty in an experimental or numerical result. The general expression for the uncertainty in the unfolded wave form, $U_{\underline{F(t)}}$, is

$$U^2_{\underline{F(t)}} = \left[\frac{\partial F(t)}{\partial a_1} U_{a_1}\right]^2 + \left[\frac{\partial F(t)}{\partial a_2} U_{a_2}\right]^2 + \ldots + \left[\frac{\partial F(t)}{\partial a_n} U_{a_n}\right]^2 \qquad (4.1)$$

where

F(t) = the unfolded wave form at any time t

$a_{1,2,..n}$ = variable upon which F(t) depends and which contains uncertainty

U_{a_n} = uncertainty associated with each variable

$U_{\underline{F(t)}}$ = total uncertainty in the unfolded wave form due to all of the variable uncertainties

Recall the analytical expression for the unfolded wave form from Chapter 3:

$$F(t) = f(t) + \sum_{n=1}^{\infty} A^n B^{n-1} F\left[t - \frac{2}{c_o}(nL - x)\right] - \sum_{N=1}^{\infty} A^n B^n F\left[t - 2\frac{nL}{c_o}\right]$$

It is not practical to utilize uncertainty analysis directly to arrive at a general expression for $U_{\underline{F(t)}}$ as a function of the uncertainty in c_o. This requires taking the partial derivative of $F(t)$ with respect to c_o, which in turn requires $F(t)$ to be a differentiable (in closed-form) function of its argument.

Accordingly, an indirect method will be devised for obtaining $U_{\underline{F(t)}}$ as a function of specified uncertainty in c_o. The unfolding computer program will be adjusted to so calculate $F(t)$ for an upper and lower bound of c_o. The uncertainty in c_o will be specified, i.e., U_{c_o}, and the computer program will be used to unfold the wave forms for the additional cases where:

$$c = c_o + U_{c_o}$$
$$c = c_o - U_{c_o}$$

In this way, the error present in $F(t)$ due to the uncertainty in c_o will be obtained for a particular wave form by comparing the resultant wave forms. $U_{\underline{F(t)}}$ will thus be the difference of the two wave forms at each point, or

$$U_{F(t)}|_{c_o} = F(c_o, t) - F(c_o + U_{c_o}, t)$$

The above mathematical nomenclature is used frequently in this chapter. The vertical bar following $U_{\underline{F(t)}}$ indicates the variables contributing to the uncertainty of $F(t)$. It is read, "The uncertainty of $F(t)$ due to uncertainty in c_o, is equal to...". The values in the arguments of F are those which are being considered in the particular equation. The nomenclature identifies the value of the function, F, when the specific

arguments are used. It does not imply that the function F is only a function of the arguments listed; obviously the unfolded bar gage record, $F(t)$, is a function of many variables. Only those variables being changed in the particular equation are listed, along with t, to indicate the dynamic nature of these equations.

The unfolding computer program was modified to incorporate these changes and named "UNFOLD1". A program listing is included in the Appendix. UNFOLD1 computes three unfolded wave forms, one each for c_o, $c_o + U_{c_o}$, and $c_o - U_{c_o}$. This computer program was applied to two wave forms; one from a ball drop calibration on a precision bar gage (i.e., a bar gage where the dimensions were precisely known), and a pressure record denoted a high explosive experiment. After careful study of many bar gage records, the uncertainty associated with c_o was chosen to be plus or minus 15 m/sec, i.e., the three wave speeds used were 5074, 5088, and 5104 m/sec.

In Figure 13a, each of the three unfolded wave forms from the ball drop calibration of the precision bar gage are plotted on the same plot. The records from the precision bar gage were used because the bar length and strain gage positions were known to within 0.03 inches. The ball drop calibration also produces wave forms which consist of low-frequency content, therefore minimizing the effects of dispersion. The impulse records from the wave forms were obtained by integrating the pressure records, and are plotted in Figure 13b. Consider the pressure wave forms. The errors in c_o produced spikes at the times where reflections occur in the wave form. This is reasonable, since high-amplitude values are being summed upon one another at these points

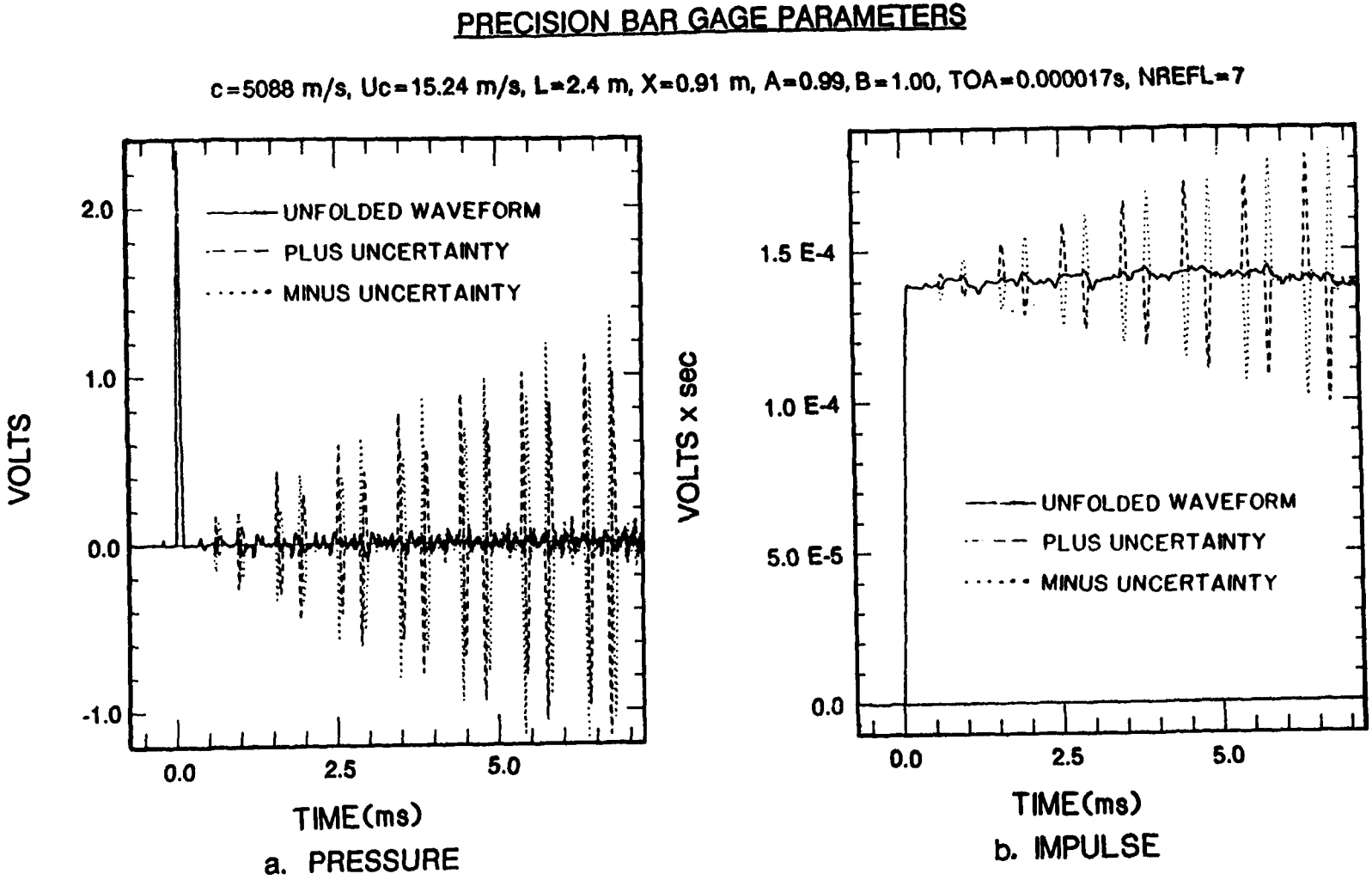

Figure 13. Uncertainty in a ball drop calibration wave form due to uncertainty in wave speed.

in the wave form. The error in c_o causes the unfolding routine to sum the wrong values, and high-amplitude spikes result. Note that these spikes grow with time as the errors accumulate. The wave forms are nearly identical except for these spikes, regardless of the wave speed used. This is evident from the impulse wave forms. Since no other data is being recorded by the bar gage in the ball drop calibration, the spikes produce large fluctuations in impulse. But the periodic nature of the spikes cause the impulse to return to the mean value, regardless of the wave speed used.

The unfolded pressure wave forms for the WLB1 record are given in Figure 14a and the corresponding impulse wave forms in Figure 14b. The same trends are noted on these records as were noted on the unfolded precision bar gage records. The pressure plots show that the only significant errors produced by the uncertainty in wave speed are the spikes occurring at the times when reflections had occurred. Since this is a record from a high explosive test, the frequency content is much higher than that of the ball drop calibration test on the precision bar gage. The unfolded wave forms exhibit erratic, spiky behavior in the region where reflections occurred. Because the reflections are characterized by high-frequency content, it is believed that the poor performance of the unfolding routine in these regions is due to dispersion. If dispersion is indeed the cause of the spikes, no value of wave speed will eliminate them.

The unfolded wave forms using the higher and lower wave speeds do not exhibit clear, symmetric trends as was the case with the precision bar gage example. In general, such trends should not be expected from

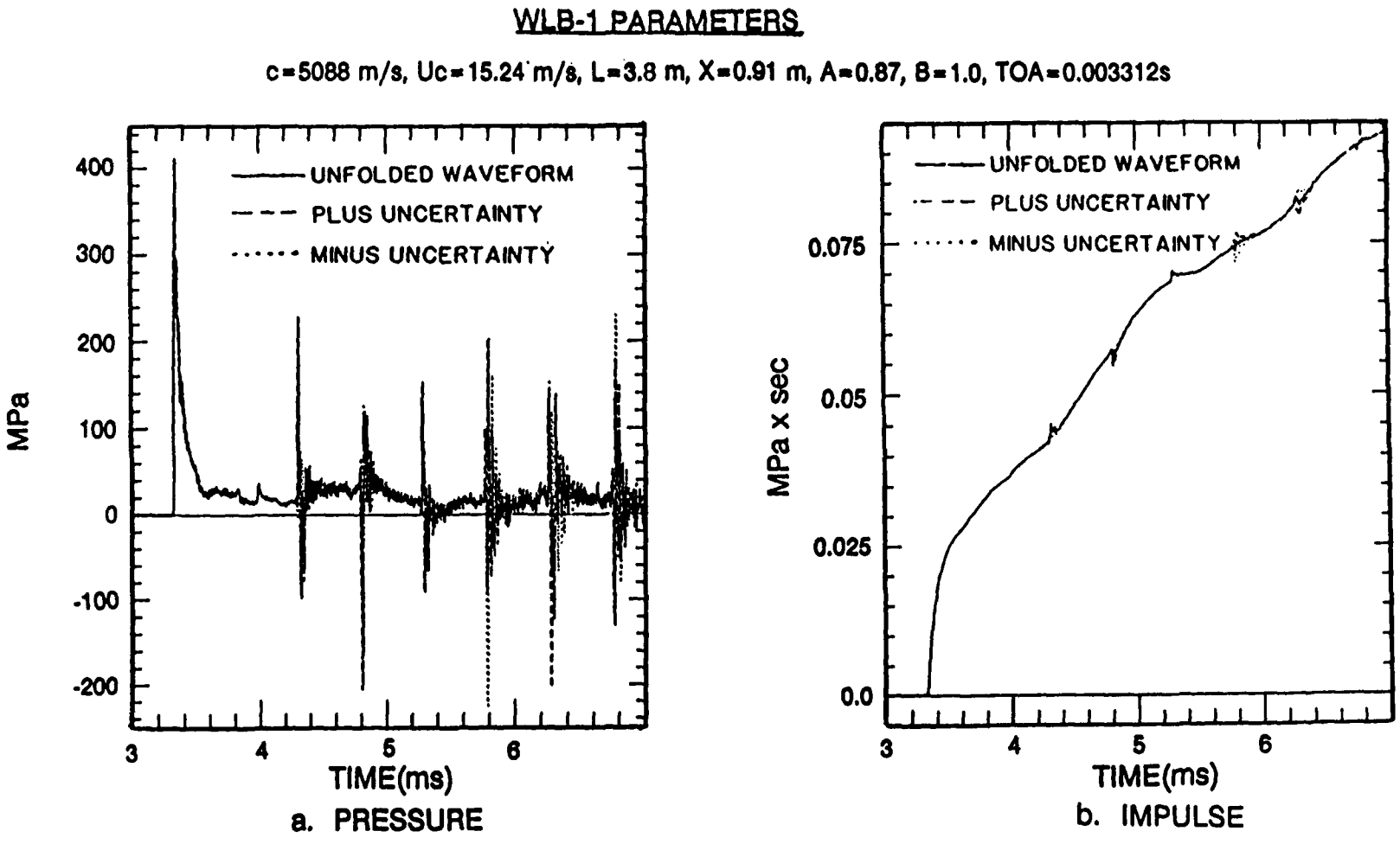

Figure 14. Uncertainty in the WLB1 high explosive test wave form due to uncertainty in wave speed.

explosive test records that contain a considerable amount of high frequency content. Once again, however, it is clear from the impulse wave forms that the error in wave speed causes very little error in impulse.

Two conclusions are drawn from these examples of the use of an incorrect wave speed when unfolding bar gage records. First, spikes are to be expected in the portions of the wave form where reflections had previously occurred. Although spikes are likely to occur even when the correct value of c_o is used, they will be even more prevalent and erratic when incorrect values of c_o are used. Also, spikes become more obvious (and unavoidable) as the frequency content of the wave form increases. Wave forms containing only low-frequency data can be unfolded with little or no high-amplitude spikes, provided the correct value of c_o is chosen.

Secondly, it can be concluded that errors in wave speed tend to produce little change in the mean value of the impulse wave form. Consequently, if impulse is the parameter to be derived, errors due to wave speed may be insignificant. However, the uncertainty in wave speed in our examples was small (15 m/sec). If a reckless choice of wave speed were made, resulting in a large value of U_{c_o}, then impulse might be affected substantially. In general, the errors produced by incorrect wave speed are easily discerned by the experienced analyst, and can be easily ignored, or even removed, if the need exists.

Errors Due To Incorrect Reflection Coefficients

Errors due to incorrect reflection coefficients can be quantified more precisely than errors due to incorrect wave speeds. This is accomplished by exploiting classical uncertainty analysis, as presented by Coleman and Steele (Reference 9). The analytical expression for the unfolded wave form is (Equation 3.13):

$$F(t) = f(t) + \sum_{n=1}^{\infty} A^n B^{n-1} F\left(t - \frac{2(nL-x)}{c_o}\right) - \sum_{n=1}^{\infty} A^n B^n F\left(t - \frac{2nL}{c_o}\right)$$

The classical uncertainty equations are well suited for such an equation. Applying Equation 4.1 and limiting our uncertainty analysis to errors in the reflection coefficients, A and B, the uncertainty of the unfolded wave form, F(t), is

$$U_{F(t)}\big|_{A,B} = \sqrt{\left[\frac{\partial F(t)}{\partial A} U_A\right]^2 + \left[\frac{\partial F(t)}{\partial B} U_B\right]^2} \qquad (4.2)$$

where U_A and U_B are the uncertainties of the reflection coefficients A and B.

A technique is not obvious for taking partial derivatives with respect to A and B when these reflection coefficients are preceded by the summation signs. This difficulty was overcome by taking the partial derivative for successive values of "n" until a pattern became obvious. To illustrate, consider the root of the first term under the radical of Equation 4.2:

$$\frac{\partial F(t)}{\partial A} U_A$$

This term is written out below for n=1, n=2, and n=3 below:

for n=1:

$$[F(t - \frac{2L}{c_o} + \frac{2x}{c_o}) - BF(t - \frac{2L}{c_o})]\ [U_A]$$

for n=2:

$$\left[F(t - \frac{2L}{c_o} + \frac{2x}{c_o}) - BF(t - \frac{2L}{c_o}) + 2AB[F(t - \frac{4L}{c_o} + \frac{2x}{c_o}) - BF(t - \frac{4L}{c_o})\right]\ [U_A]$$

for n=3:

$$\left[F(t - \frac{2L}{c_o} + \frac{2x}{c_o}) - BF(t - \frac{2L}{c_o}) + 2AB[F(t - \frac{4L}{c_o} + \frac{2x}{c_o}) - BF(t - \frac{4L}{c_o}] + 3A^2B^2[F(t - \frac{6L}{c_o} + \frac{2x}{c_o}) - BF(t - \frac{6L}{c_o})]\right]\ [U_A]$$

The series thus becomes:

$$U_{F(t)}|_A = \left\{\sum_{n=1}^{\infty} nA^{n-1}B^{n-1}\left[F(t-\frac{2nl}{c_o}+\frac{2x}{c_o}) - BF(t-\frac{2nL}{c_o})\right]\right\}[U_A] \qquad (4.3)$$

The second term is derived similarly. The complete solution for the uncertainty in the unfolded wave form due to the uncertainty in the reflection coefficients is:

$$U_F(t)|_{A,B} = \left\{\left[\left(\sum_{n=1}^{\infty} nA^{n-1}B^{n-1}[F(t-\frac{2nL}{c_o}+\frac{2x}{c_o}) - BF(t-\frac{2nl}{c_o})]\right)[U_A]\right]^2 + \left[\left(\sum_{n-1}^{\infty} A^nB^{n-2}[(n-1)F(t-\frac{2nL}{c_o}+\frac{2x}{c_o}) - nBF(t-\frac{2nL}{c_o})]\right)[U_B]\right]^2\right\}^{1/2} \qquad (4.4)$$

A computer routine, called UNFOLD2 (see Appendix), was developed to solve Equation 4.4 and assemble the plus and minus uncertainties of the unfolded wave form. The portion of the code which considered the effect of incorrect wave speed is not included in UNFOLD2; hence, it looks at errors due to reflection coefficients alone. This useful modification to the unfolding routine generates the error bounds for a specific wave form with specific uncertainties in reflection coefficients.

The same two wave forms studied earlier are used here again as examples. The output from the ball drop calibration test of the precision bar gage is unfolded using UNFOLD2 to comprise the first example. The uncertainties in the reflection coefficients (*UA* and *UB*) were each taken to be plus or minus two percent for this case. The unfolded wave form, and the plus and minus uncertainties, are displayed in Figure 15. The errors in the unfolded wave form tend to increase with time. This is reasonable since the errors are raised to higher powers with increasing "n". Substantial uncertainty occurs only when the high-amplitude portions of the wave form are being operated upon by the unfolding routine. The features between the spikes of the uncertainty wave forms are essentially identical to comparable features of the unfolded wave form. Some insight into this behavior can be obtained by observing Equation 3.13. The uncertainty at each point is comprised of the sum of reflection coefficients raised to powers, multiplied by the amplitude of the reflecting pulse at the particular time. If the amplitude of the reflecting pulse at the particular time is very low, the uncertainty must also be low. If the amplitude of the

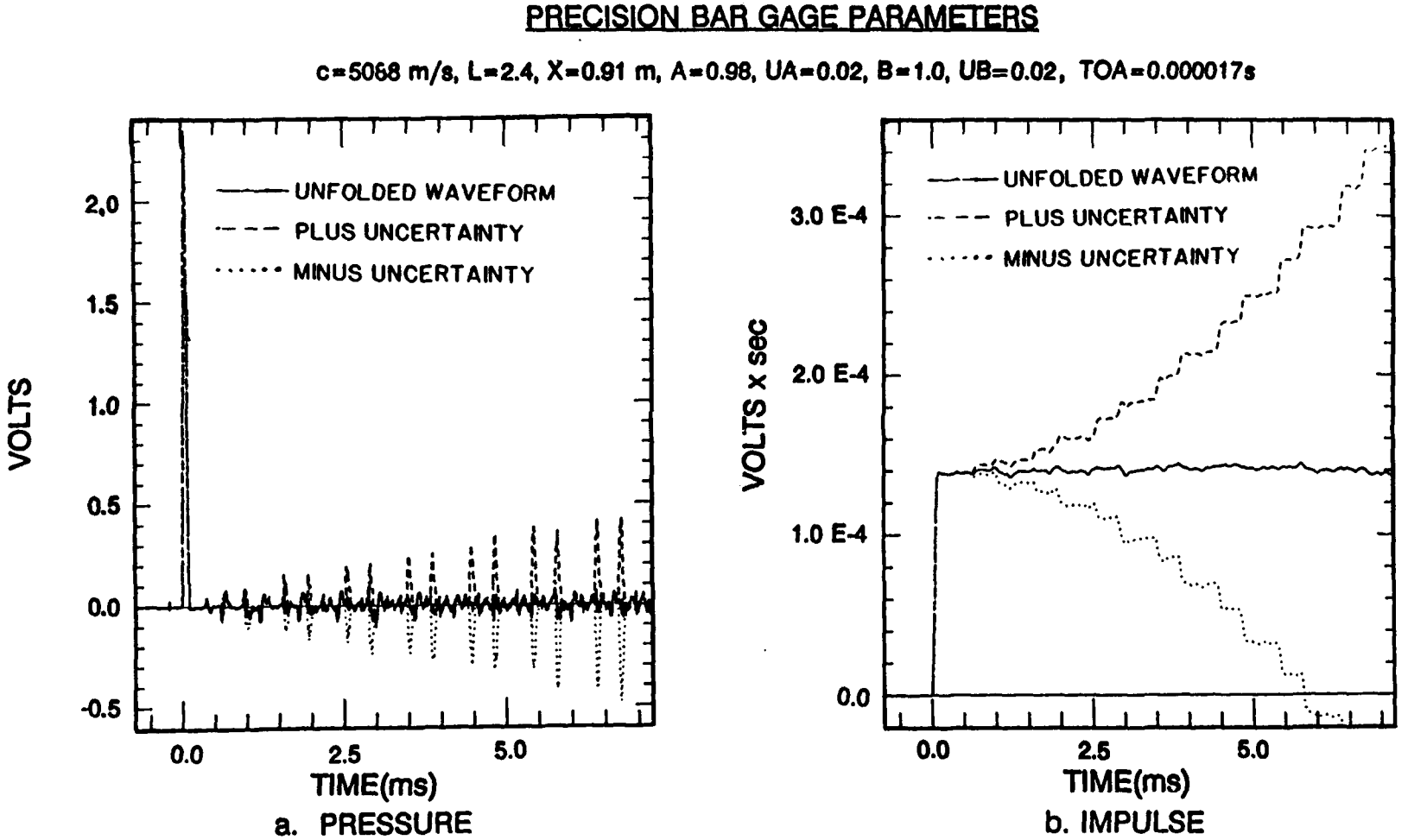

Figure 15. Uncertainty in a ball drop calibration wave form due to uncertainty in reflection coefficients.

reflecting pulse is high, the uncertainty can be more obvious, as demonstrated by this example. It can be concluded from this observation that the uncertainty of an unfolded wave form is dependent upon the character of the input wave form.

The WLB-1 record was unfolded using the program UNFOLD2. The reflection coefficients for this wave form were more difficult to choose than those of the ball drop calibration record. The uncertainty values for the dump end and input end coefficients were taken to be ±5% and ±3%, respectively. The unfolding routine calculated the plus and minus extremes of the unfolded wave form due to these uncertainties in reflection coefficients. These bounds are plotted on Figure 16a, along with the unfolded wave form. The three wave forms are barely distinguishable, requiring careful inspection of the spikes to tell them apart. While the bounds on the pressure record are quite tight, the errors become much more prominent on the impulse wave forms. Even though the uncertainties in the pressure records may be slight the errors become significant when integrated over several reflections. This may be observed in Figure 16b, a plot showing the impulse wave form of the unfolded data and its plus and minus uncertainties. It can be seen that the unfolded impulse wave form is only accurate within about ±10.8 percent during the second reflection due to the uncertainty in reflection coefficients.

This ability to calculate the uncertainty of a wave form due to reflection coefficients comprises a useful tool for determining the length of record that can be unfolded without incurring too much error. In other words, if an error greater than ±10% is unacceptable, the

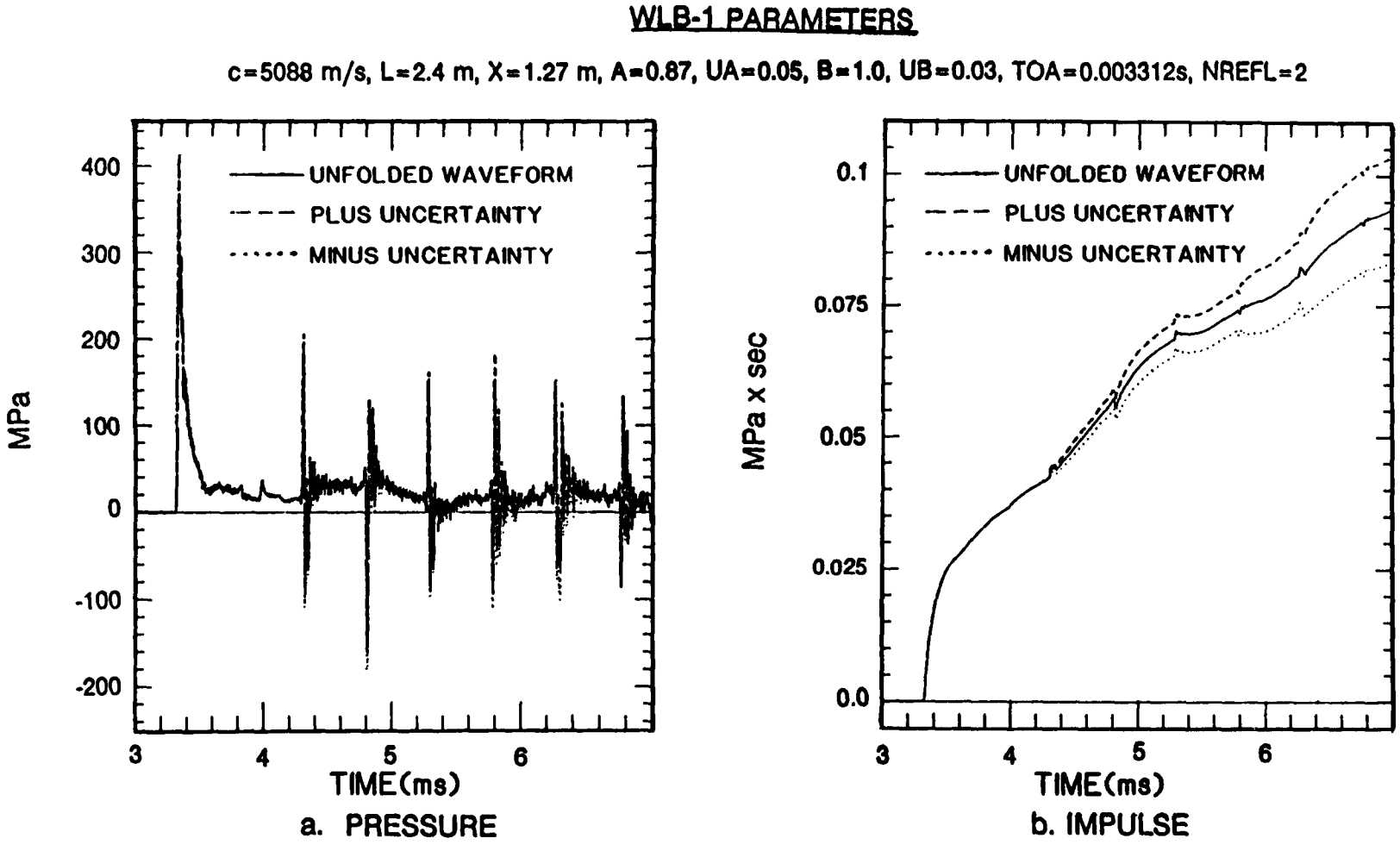

Figure 16. Uncertainty in the WLB1 high explosive test wave form due to uncertainty in the reflection coefficients.

analyst can choose to only consider the first one or two reflections of a specific wave form.

Combining Errors Due To Wave Speed and Reflection Coefficients

The error due to uncertainty in the values of reflection coefficients must be combined with the error due to using an incorrect wave speed to determine the total uncertainty in the unfolded result. The proper method of combining these errors is subject to debate, but the most widely accepted method of combining uncertainties is the Root-Sum-Square (RSS) method, as illustrated earlier in Equation 4.1. The RSS method is ordinarily preferred over a linear combination of the errors (adding them all together) since the probability is low that the most extreme values of all the uncertainties will occur in a given event. Furthermore, it is even less likely that all of the variables will suffer errors in the same direction (or same sign). It is much more likely that some variables will be subject to error near their largest uncertainty, while some variables will be subject to less error. In turn, some variables will be higher than their mean value, and some lower, for a particular experiment. The RSS method removes the sign dependency and gives an overall uncertainty that is somewhat less than the most extreme values would suggest with a linear combination, thus providing a more statistically valid combination of errors.

The RSS method is used here to combine the error due to wave speed with the errors due to incorrect reflection coefficients. The computer program was modified to square the error due to uncertainty in c_o, and

add it to the square of the error due to incorrect reflection coefficients, and then take the square root of the sum. This simple calculation was performed at each point to obtain the plus and minus bounds of the unfolded wave form. This computer program is called UNFOLD3.

Before applying this program to an example, consider what the output should look like. The differences in the pressure wave forms should be slight, since neither error source produced noticeable changes in the pressure values. The impulse was largely unaffected by the error in c_o, but errors due to reflection coefficients generated substantial errors in the impulses of the unfolded wave forms. Consequently, the combined error should be similar to that caused by the error due to reflection coefficients, being only slightly larger.

Now consider the result of this combination of errors for the example of the WLB-1 wave form, shown in Figure 17. Notice that the combination of errors produces plus and minus uncertainties much larger than those produced by erroneous reflection coefficients, which seems contrary to logic. Simple inspection of the wave forms did not help to explain this phenomena. Numerous checks were made on the modified computer program, no errors were found in the coding. The anomaly is attributed to the RSS method as applied to wave forms such as these.

In the general case, it is considered advantageous to square the errors, because the true signs of the errors are not known. With the error analysis method used here, however, the signs for the errors in wave speed are known precisely. After all, they were calculated at each point for both upper and lower bounds of the unfolded result. By

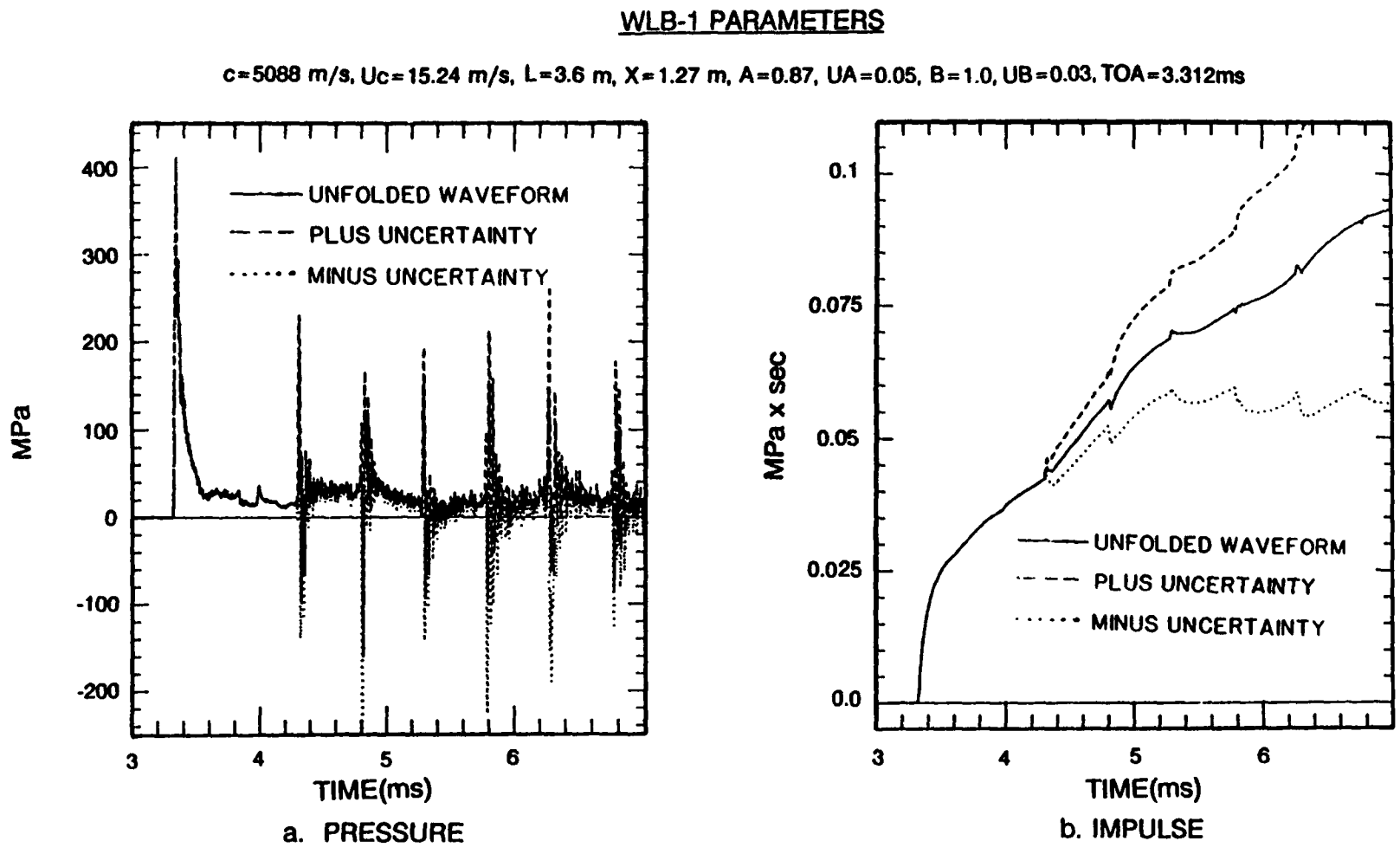

Figure 17. Uncertainty in the WLB1 wave form due to the combination of uncertanties in wave speed and reflection coefficents when using the RSS method of combination.

squaring the errors due to c_o, and then taking the square root of the sum of the errors, all of the errors due to c_o are forced to be positive, even when some were actually calculated to be negative. To see the resulting error, consider the expanded plot in Figure 18. The unfolding routine was modified to calculate the unfolded wave form and the plus and minus values of uncertainty due to an error in c_o only (as in UNFOLD1). This removed the added complexity of the uncertainty due to errors in reflection coefficients. This modified unfolding program outputted:

1. The unfolded wave form, $F(I)$.
2. The plus uncertainty, short-dashed trace, via:

$$U_p = F(c_o) + (F(c_o) - F(c_o + U_{c_o}))$$

3. The minus uncertainty, long-dashed trace, via:

$$U_m = F(c_o) - (F(c_o) - F(c_o - U_{c_o}))$$

4. The minus uncertainty, dotted trace, via:

$$U_m = F(c_o) - \sqrt{(F(c_o) - F(c_o - U_{c_o}))^2}$$

Figure 18 is plotted to an expanded time scale to show the specific differences between the RSS method and direct linear combination, with proper signs associated with the errors. The dashed traces represent uncertainty calculated with linear combination of the error due to incorrect c_o. The dashed traces are identical to the output from UNFOLD1, the program used earlier to calculate the uncertainty due to incorrect c_o. Notice that these traces tend to

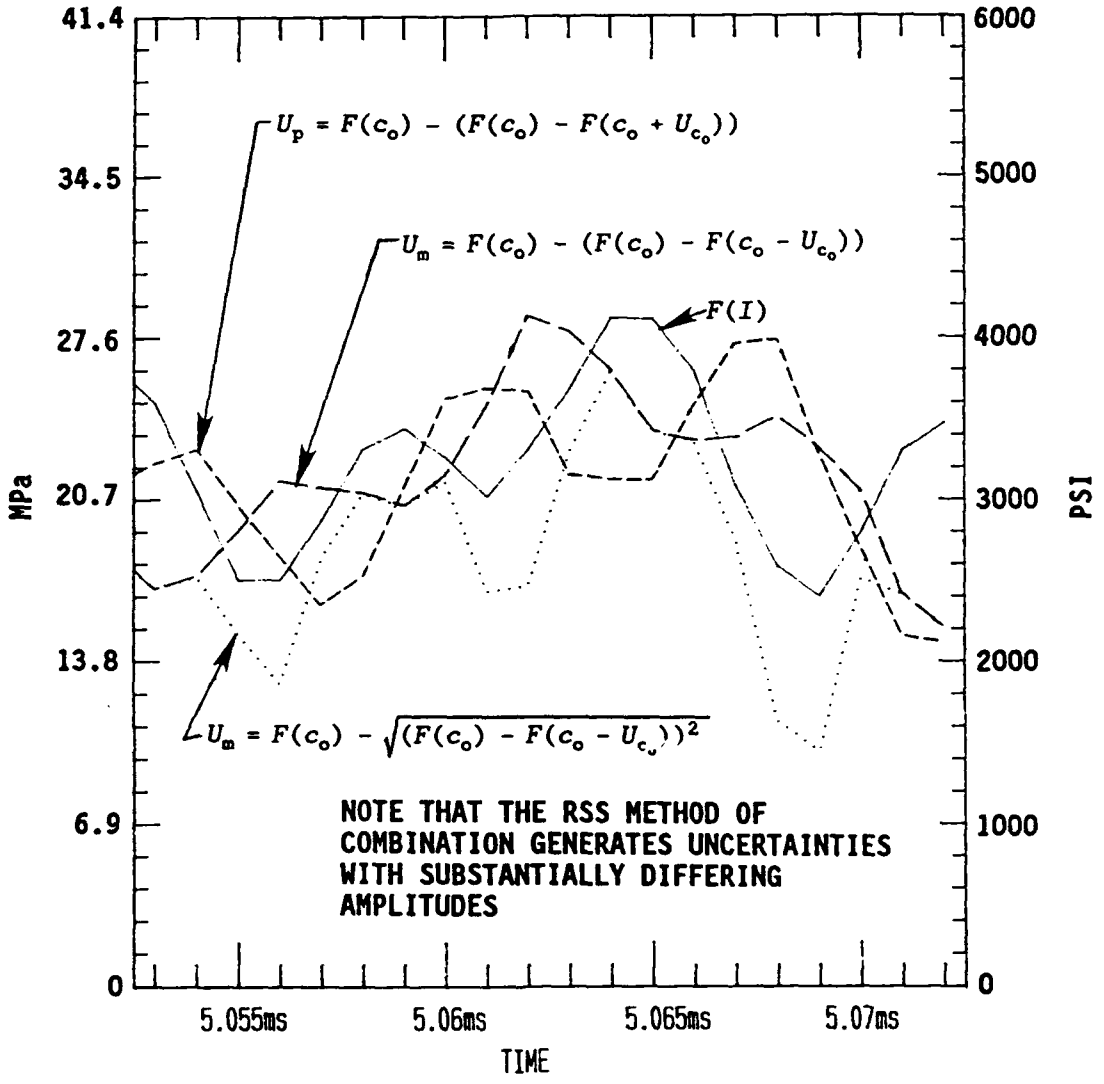

Figure 18. Expanded time plot of the WLB1 wave form showing the effect of the RSS method of combination.

exhibit more error in "phase" than error in amplitude, which is consistent with the earlier findings. Errors in phase produce little error in impulse, which was one of the conclusions regarding uncertainty due to incorrect c_o. The RSS method however, as shown in the dotted trace, produces error in amplitude and is in phase with $F(I)$. The second term in the equations above represent the error due to the incorrect c_o. While the unfolding routine may accurately calculate its direction to be negative, the squaring/square root process forces it to be positive. Hence, a positive error is always subtracted from the unfolded wave form to generate the minus uncertainty. Accordingly, the minus uncertainty depicted by the dotted trace (RSS method) is always lower than the unfolded wave form. This causes the gross error in impulse with the RSS technique.

For combining errors due to uncertainty in wave speed and reflection coefficients while unfolding bar gage records, the author suggests using linear combination for the errors due to wave speed and RSS combination for the errors due to the reflection coefficients. With this approach, the technique can no longer be labeled "classical" uncertainty analysis, as it has become specialized for this application. Mathematically, the plus and minus uncertainties would be expressed as:

$$U_p|_{c_o,A,B} = U_{F(t)}|_{c_o+U_{c_o}} + \sqrt{[U_{F(t)}|_A]^2 + [U_{F(t)}|_B]^2}$$

$$U_m|_{c_o,A,B} = U_{F(t)}|_{c_o-U_{c_o}} - \sqrt{[U_{F(t)}|_A]^2 + [U_{F(t)}|_B]^2}$$

This technique of combining errors was incorporated into the unfolding routine and labeled UNFOLD4 (see Appendix). It is considered to be the

best of the unfolding routines, since it combines the errors in the most reasonable manner. UNFOLD4 was used to unfold the wave forms studied earlier in this section. Figure 19 shows the unfolded pressure wave forms for the WLB1 record. The only significant difference between the combination of both error types and that including error only due to reflection coefficients is a slight increase in the impulse uncertainties. This is as expected since the uncertainty in impulse due to incorrect c_o was slight.

Dispersion and Other Errors

While errors due to uncertainty in low-frequency wave speed and reflection coefficients can be addressed analytically or numerically, errors due to dispersion and other more subtle sources are difficult to quantify. Dispersion leads to errors in an unfolded wave form in a manner similar to that of unfolding with an incorrect wave speed. Dispersion in the bar gage causes the high-frequency portion of the stress pulse to change shape as it propagates down the bar gage. Specifically, the high frequency content propagates more slowly down the bar than the low frequency content. As a result, the rise to peak is "rolled off", as the low-frequency components outrun the high frequency peak information and superimpose themselves upon the high frequency data. As the stress wave travels up and down the bar, the peak continues to roll off.

To include uncertainty due to dispersion in the unfolding technique, the variance of wave speed with frequency would have to be defined and incorporated into the calculational portion of the

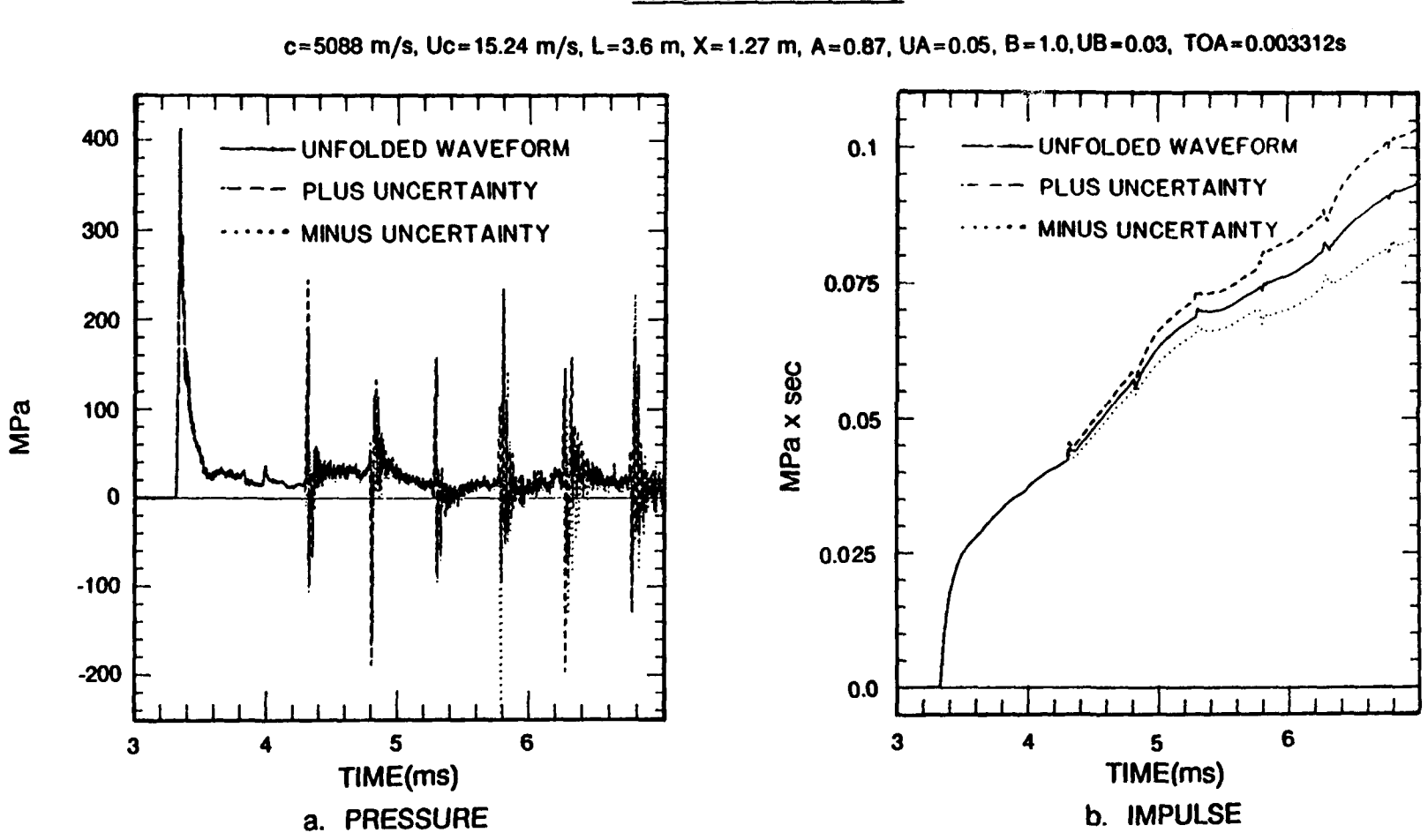

Figure 19. Uncertainty in the WLB1 wave form due to the combination of uncertainties in wave speed and reflection coefficients when both linear and RSS methods of combination are used.

unfolding routine. In turn, the unfolding routine would have to keep track of the frequency of data which was being handled at each point in time. This would be a difficult task and is beyond the scope of this thesis.

If the wave form contains limited high frequency data, dispersion will not cause significant errors. Also, errors due to dispersion will manifest themselves much the same way as errors due to incorrect c_o. When the routine unfolds the high frequency data, which in most all cases is limited to the high amplitude initial peak and the subsequent reflections, it will sum together improper portions of the wave form. As a result, a noise-like or spiky character would be expected at those places in the wave form where high amplitude reflections were present. Such errors are not expected to produce much error in impulse. In the unusual case where a bar gage was used to measure a pulse which contains a great deal of high frequency content, more error may be inherent to the unfolded wave form. However, the use of a bar gage for such a high frequency measurement is questionable, even before considering the validity of unfolded data obtained by the bar gage.

Sometimes the analyst does not know the length of the bar and position of the strain gages along the bar with precision. Such precision is unnecessary if the bar gage records are not to be unfolded, and consequently such precision has often not been applied to the manufacture of bar gages. The only time that the unfolding routine uses the bar gage dimensions is in the argument of the functions, just as was the case with c_o. Consequently, errors due to incorrect bar gage dimensions lead to the same sort of errors as c_o, causing the

unfolding routine to sum the improper sequence of amplitudes. Gross errors in bar gage dimensions can be troublesome. For instance, a 6-mm discrepancy in bar length has the same effect as a 10 m/s error in wave speed.

The most correct way of handling errors due to bar gage dimensions would be to perform a separate uncertainty analysis on the arguments of the functions before using the unfolding program. With the arguments being composed of simple expressions, this uncertainty analysis would be easy compared to the analysis performed in this chapter. The resulting uncertainty for the whole argument, due to the uncertainty in c_o, x, and L, could be input to the unfolding program as the uncertainty in c_o. Even this thorough of approach has problems though. Uncertainties in c_o, L, and x are not independent of one another, i.e., x and L are used to determine c_o. This makes for a more complex and judgmental uncertainty analysis, and hence it is only mentioned here. Generally though, if care has been taken in the manufacture of the bar gages, errors due to incorrect bar gage dimensions should be relatively insignificant.

Other error sources can be conceived that would effect the accuracy of the unfolding process. Things such as material variations throughout the length of the bar gage, material nonlinearities, etc., cannot be considered by the unfolding technique, and hence lead to errors. Such errors are thought to be quite small. Accordingly, they are not considered in this thesis.

The intent of this chapter is not to suggest that the error sources discussed here are the only sources of error associated with

measurements made by bar gages. Indeed, calibration errors, ground shock effects, frequency response limitations, etc., lead to errors in bar gage measurements. Some of these errors will be evident in the next chapter, where actual field data is examined. However, these errors are not caused by the numerical unfolding process, which is the concern of this thesis.

CHAPTER V

APPLICATION OF BAR GAGE UNFOLDING TO FIELD DATA

Test Description

The uncertainty analysis will be applied to an actual high explosive test in this chapter. In this experiment, bar gage data was obtained at regions where other types of blast pressure gages made measurements as well. This is an unusual situation because bar gages are typically used in regions where very few types of airblast gages can function reliably, due to the high peak pressure levels. On this test, however, bar gages were intentionally placed at pressure levels low enough to compare to other airblast gages. The other airblast gages in this case were Kulite HKS series airblast gages (Reference 11). HKS airblast gages are quite reputable in the peak pressure range from 3.45 to 345 MPa (500 to 5,000 psi) and, being a diaphragm-type gage, yield a long term pressure measurement with no interruption from tensile reflections. Hence, with the Kulite airblast gages being placed at the same distance as the bar gages from an axisymmetric charge, the Kulite gage records can be compared to the unfolded bar gage records.

The experiment of interest involved the detonation of an explosive charge that was suspended at a certain height above the ground surface.

Airblast gages were placed on the ground surface to measure the blast pressure on the ground surface at different radial positions. Figure 20 is a plan view of the instrument layout. The explosive charge is suspended above the origin depicted on this plan view. The bar gages are denoted by B1, B2, etc., at the pressure ranges close to the charge. The Kulite pressure gages are denoted by AB15, AB16, etc. They are located at the same radial distance, and also close to the bar gages. Bar gage B3 was located at the center of the instrument array. Bar gages B2, B4, and B6 were located at the same radial distance from the charge center, arbitrarily referred to as radial "A". Bar gages B1 and B5 were placed at another radial distance arbitrarily referred to as radial "B". It is the data from these instruments that is of interest to us in this thesis. Comparisons will be made between these bar gages and their corresponding Kulite airblast gages. The appropriate gage comparisons and their radial positions are presented in Table 1.

In this chapter, we will compare the records from those combinations listed in the previous table. The bar gage records will be unfolded to the best capability and the uncertainties calculated using the UNFOLD4 program explained in Chapter 4. The impulses from the unfolded bar gage records will then be plotted on the same scales as the Kulite airblast gage impulses. If the gage performance were similar, then the Kulite airblast impulses would lie within the upper and lower bounds of the unfolded bar gage impulses. If the Kulite airblast gage impulses lie outside of these bounds, it means that either the gages are performing (or measuring) differently, or else

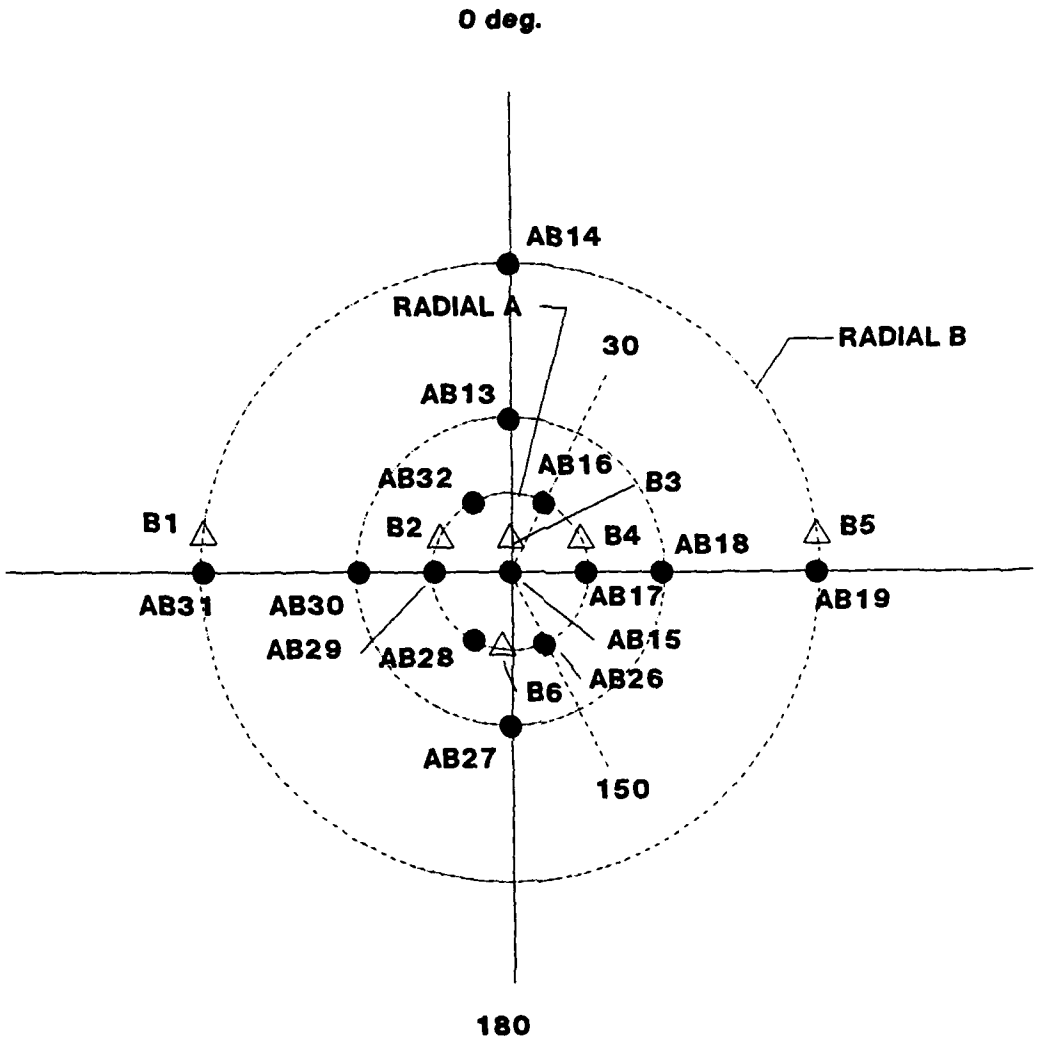

Figure 20. Plan view of the pertinent instruments for the subject explosive test.

TABLE 1

BAR GAGES AND KULITE AIRBLAST GAGES AT COMPARABLE TEST BED POSITIONS.

COMPARISON NO.	RADIAL POSITION	BAR GAGE DESIGNATION	KULITE AIRBLAST GAGE DESIGNATION
1	CENTER	B3	AB15
2	RADIAL A	B2	AB29
3	RADIAL A	B4	AB16
4	RADIAL A	B6	AB28
5	RADIAL B	B1	AB31
6	RADIAL B	B5	AB19

the charge is not producing a uniformly axisymmetric airblast environment. An analysis will be performed along these lines to see if any interesting conclusion can be drawn about the accuracy or utility of bar gage unfolding.

Analysis

The bar gages used on this test were 5.8 m long with the strain gages placed 1.83 m from the top of the bar. This is a standard bar gage design used on high explosive tests which have no special measurement requirements, e.g., spatial constraints, long measurement times, etc. The bar gage records were unfolded using the computer program UNFOLD4 to calculate both the unfolded wave form, and the uncertainties due to incorrect wave speed and reflection coefficients. A low frequency wave speed of 5089 m/sec was found to be the best choice for these bar gage records (as it was for the other bar gage types investigated). This value of low-frequency wave speed will

likely apply to all bar gages made from the same lot of high-strength steel. Reflection coefficients and all of the uncertainties were chosen in a manner consistent with that described earlier.

The results of the unfolding are given in Figures 21 through 26. The unfolded pressure wave forms, with the plus and minus uncertainties, are shown in the left-hand plot, while the corresponding integrated impulses are displayed in the right-hand plot. Two points are noteworthy from these plots. First, B1 and B5 are peculiar looking unfolded pressure wave forms when compared to the other unfolded wave forms. B1 has a repeating pulse, which judging from the timing, is propagating up and down the bar. This record was unfolded several times with carefully chosen parameters. The same results were always achieved. Therefore, it is presumed that B1 was unfolded correctly, and the oscillations represent a mechanical pulse not due to the pressure applied to the measurement end of the bar gage.

B5 displays late-time pulses different than that of B1. The late-time inputs evident on B5 are not as periodic in nature. These are above the baseline indicating positive pressure. B5 may be responding to a mechanical input, perhaps from the explosive or some anomalous behavior in the bar. The other unfolded bar gage records appear to be reasonable. The uncertainties in the pressure wave form reveal themselves in the high-frequency spikes at times when the reflections are being unfolded, as was observed in the previous chapter.

Note that had the records not been unfolded, it is possible that B1 and B5 would not have been singled out as suspect. Since their initial pulses looked reasonable, and the rest of the records looked

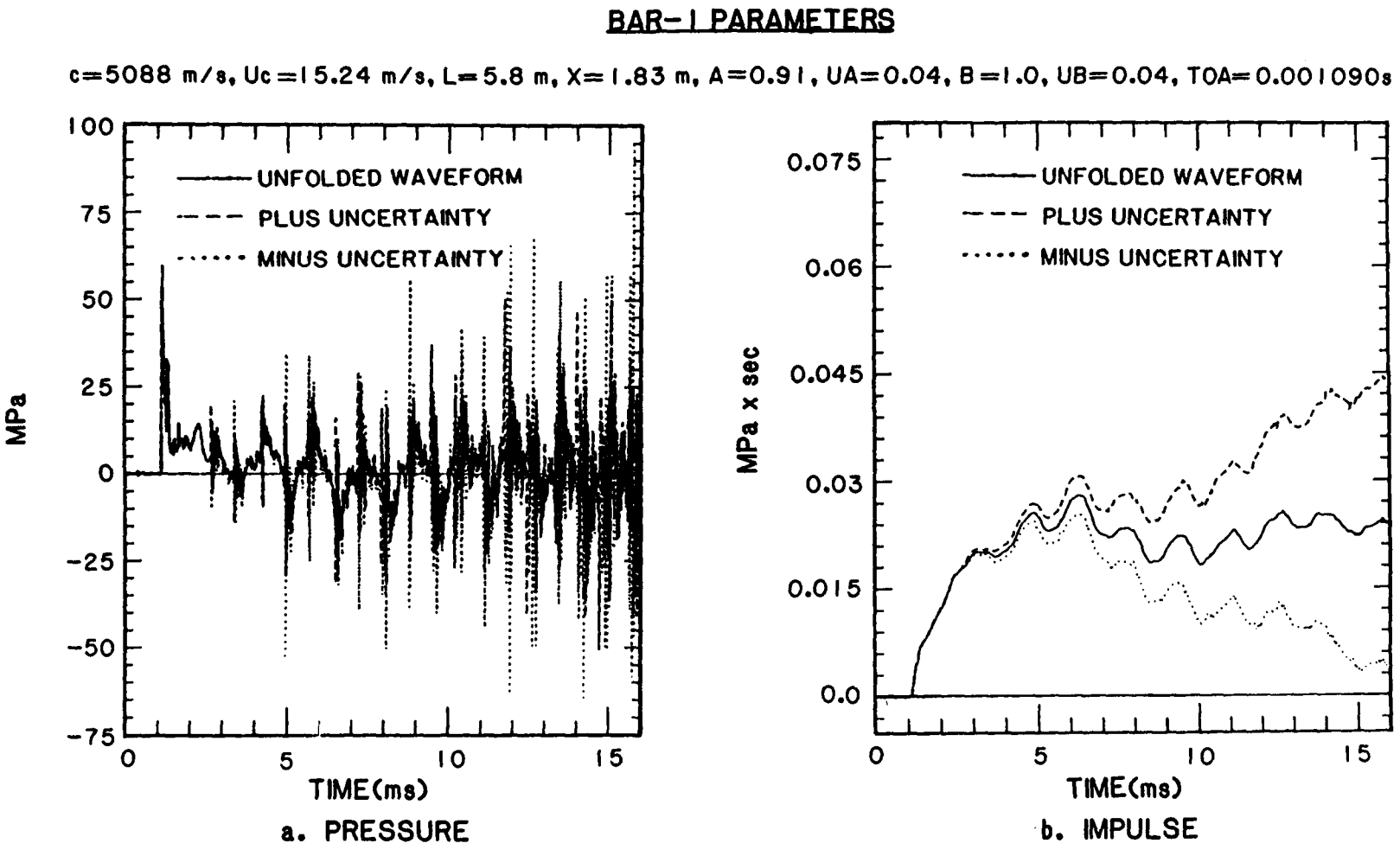

Figure 21. Unfolded wave form from Bar-1, including plus and minus uncertainties.

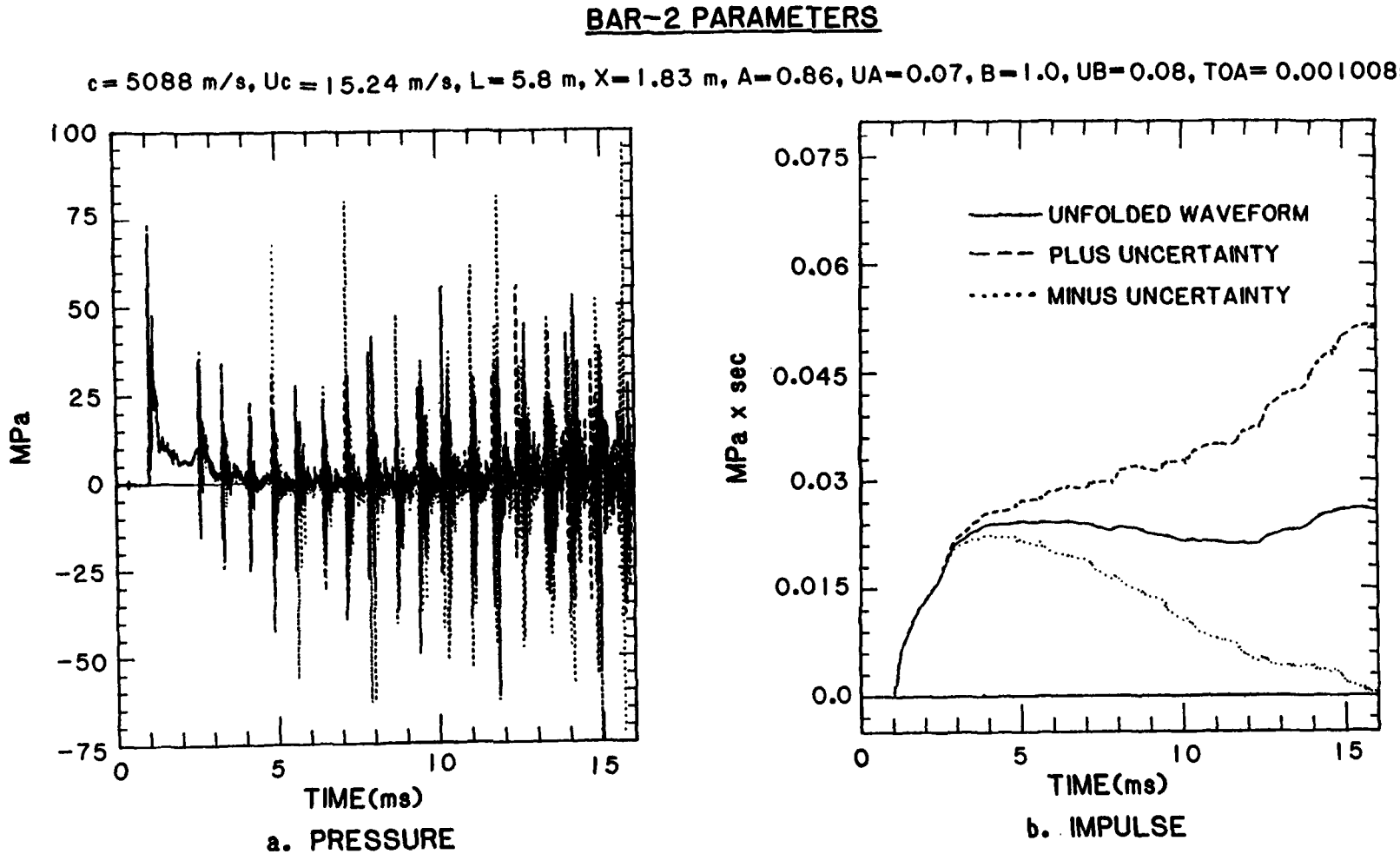

Figure 22. Unfolded wave form from Bar-2, including plus and minus uncertainties.

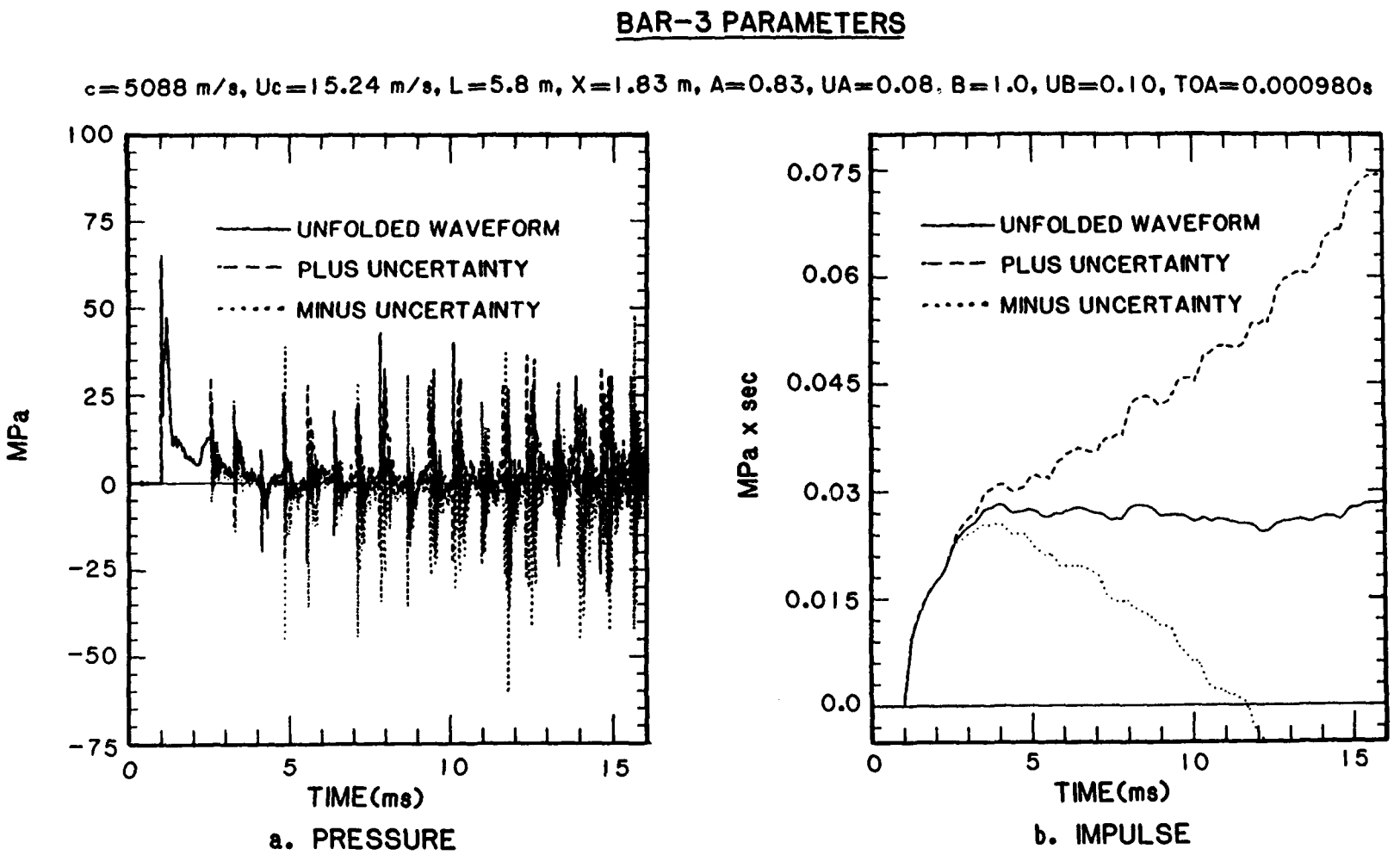

Figure 23. Unfolded wave form from Bar-3, including plus and minus uncertainties.

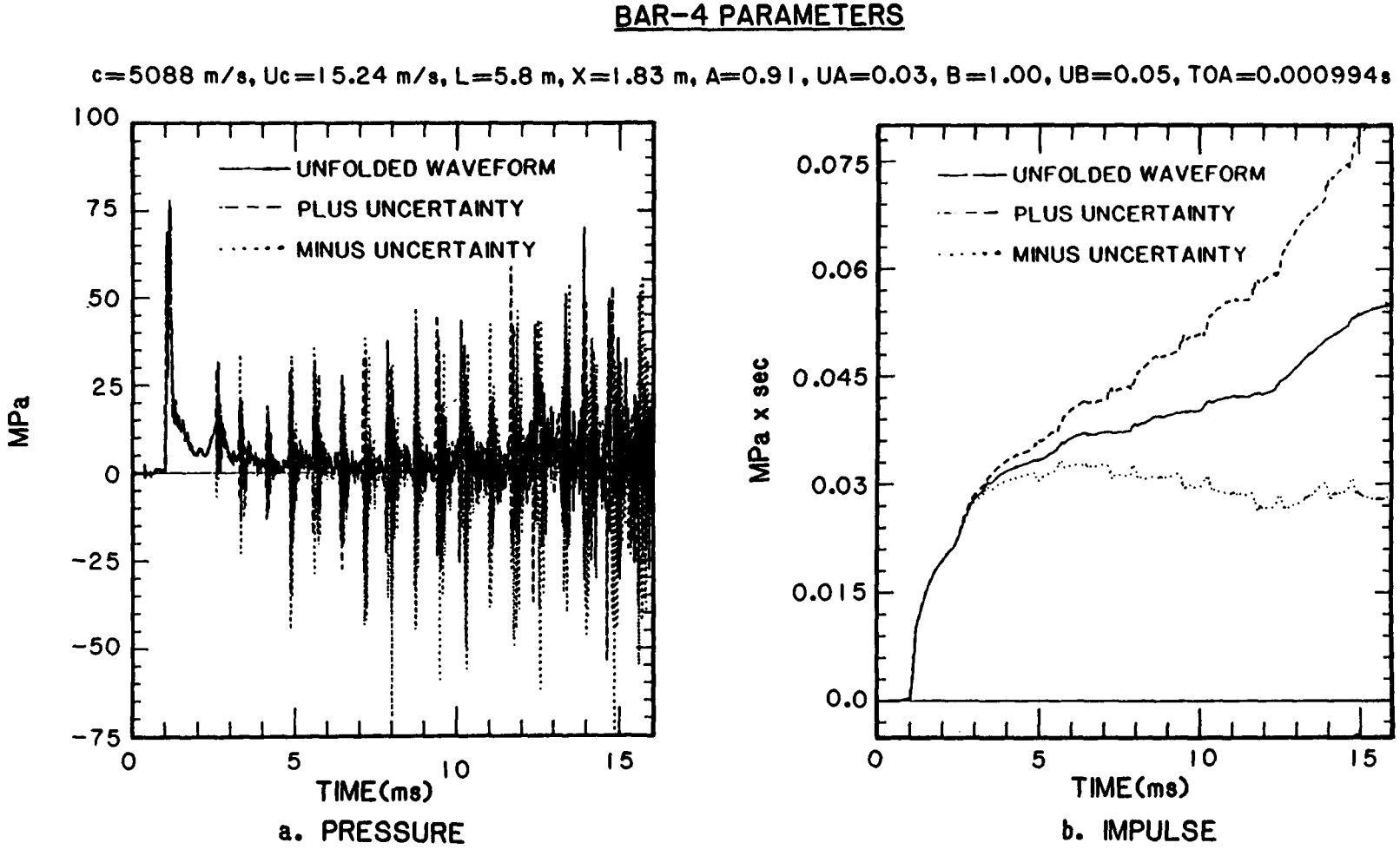

Figure 24. Unfolded wave form from Bar-4, including plus and minus uncertainties.

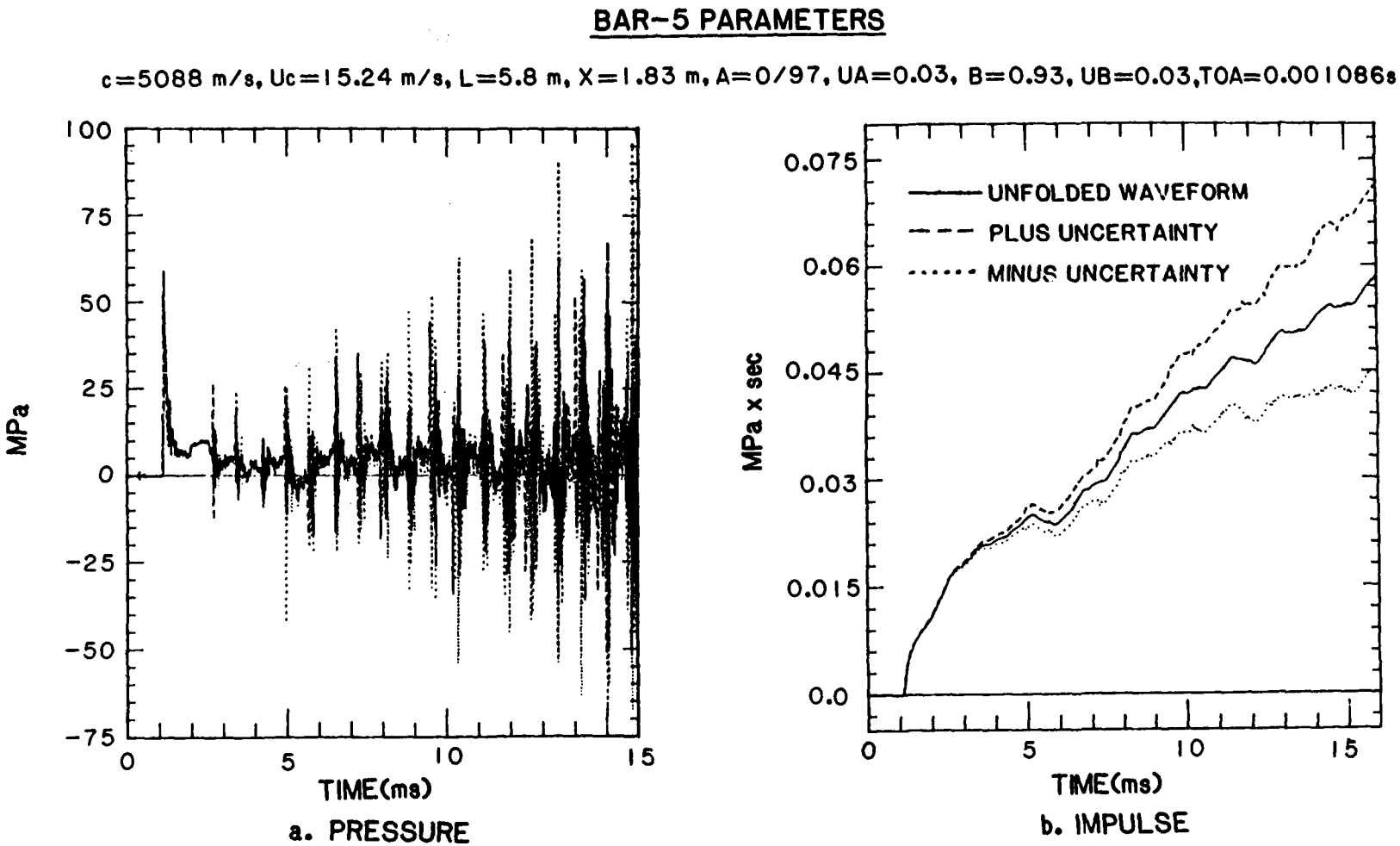

Figure 25. Unfolded wave form from Bar-5, including plus and minus uncertainties.

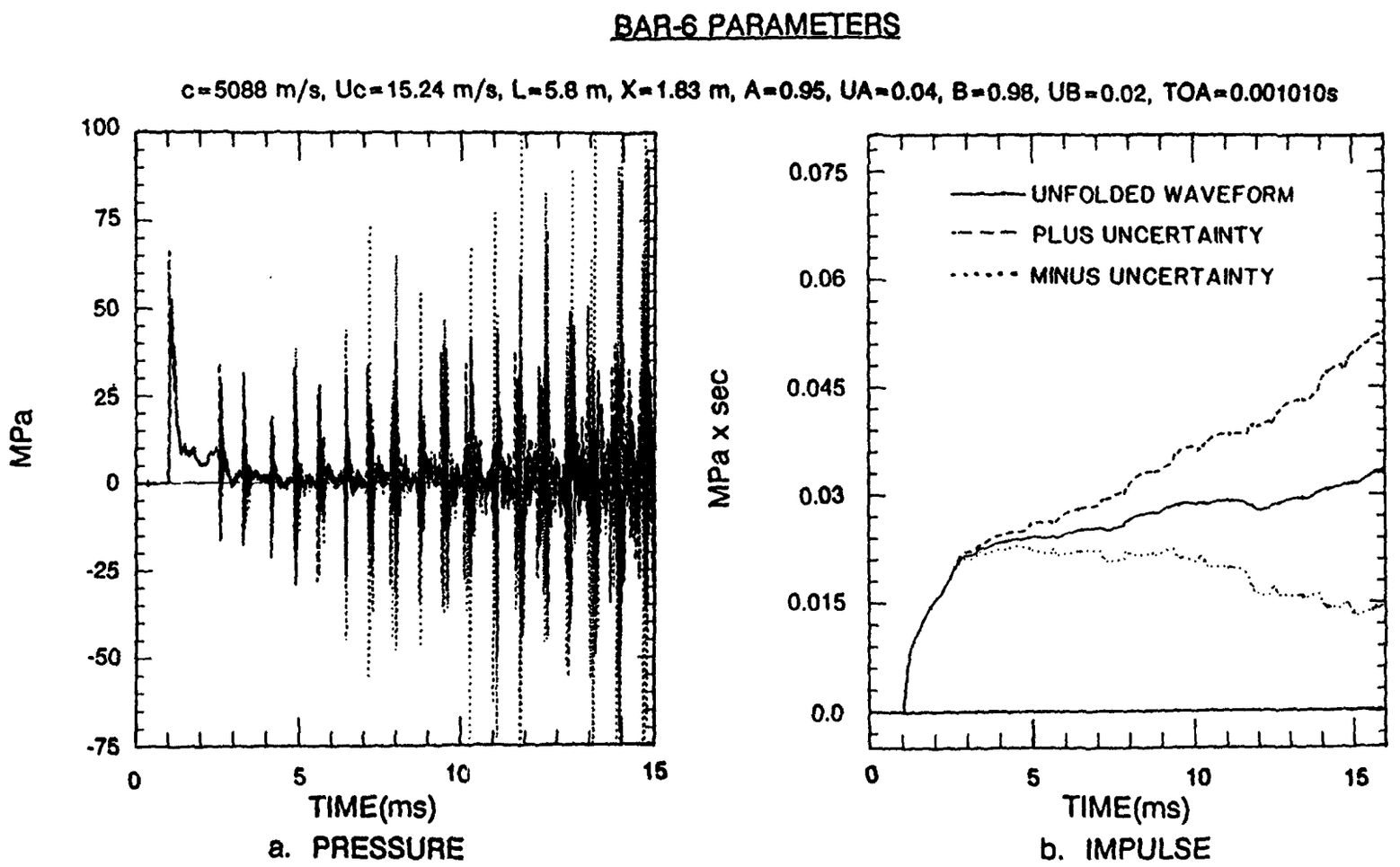

Figure 26. Unfolded wave form from Bar-6, including plus and minus uncertainties.

"bar gage-like", it would be easy to conclude that records were valid. By unfolding the records, the differences became obvious. With regard to this example, it is concluded that unfolding the bar gage records can be useful in evaluating the quality of the bar gage measurement.

The uncertainties due to the reflection coefficients yield large uncertainties in the unfolded impulses. This is a second noteworthy point regarding the unfolding of these bar gage records. Even the most careful examination of the bar gage records could not yield a constant reflection coefficient. The reflection coefficient varied as much as eight percent, requiring that amount of uncertainty to be input to the unfolding program. As can be seen in Figure 23, these sorts of uncertainties in reflection coefficients cause gross errors in the unfolded impulse. An analyst could only use one or two reflections of an unfolded impulse wave form with uncertainties that large. Some of the records had less uncertainty in their reflection coefficients and the unfolded impulse waveforms are more reasonable. B5 and B6 in Figures 25 and 26 are good examples of this.

Each unfolded bar gage record is plotted along with its corresponding Kulite airblast gage record in Figures 27 through 32. As before, the pressure wave forms are grouped together on one plot and the integrated impulses on another. The plus and minus uncertainties of the unfolded pressure wave form are left off of these plots for clarity. The airblast data from the Kulite airblast gages required little or no data manipulation. Prior to making these plots, 100-ms plots of the Kulite airblast data were studied to determine the maximum

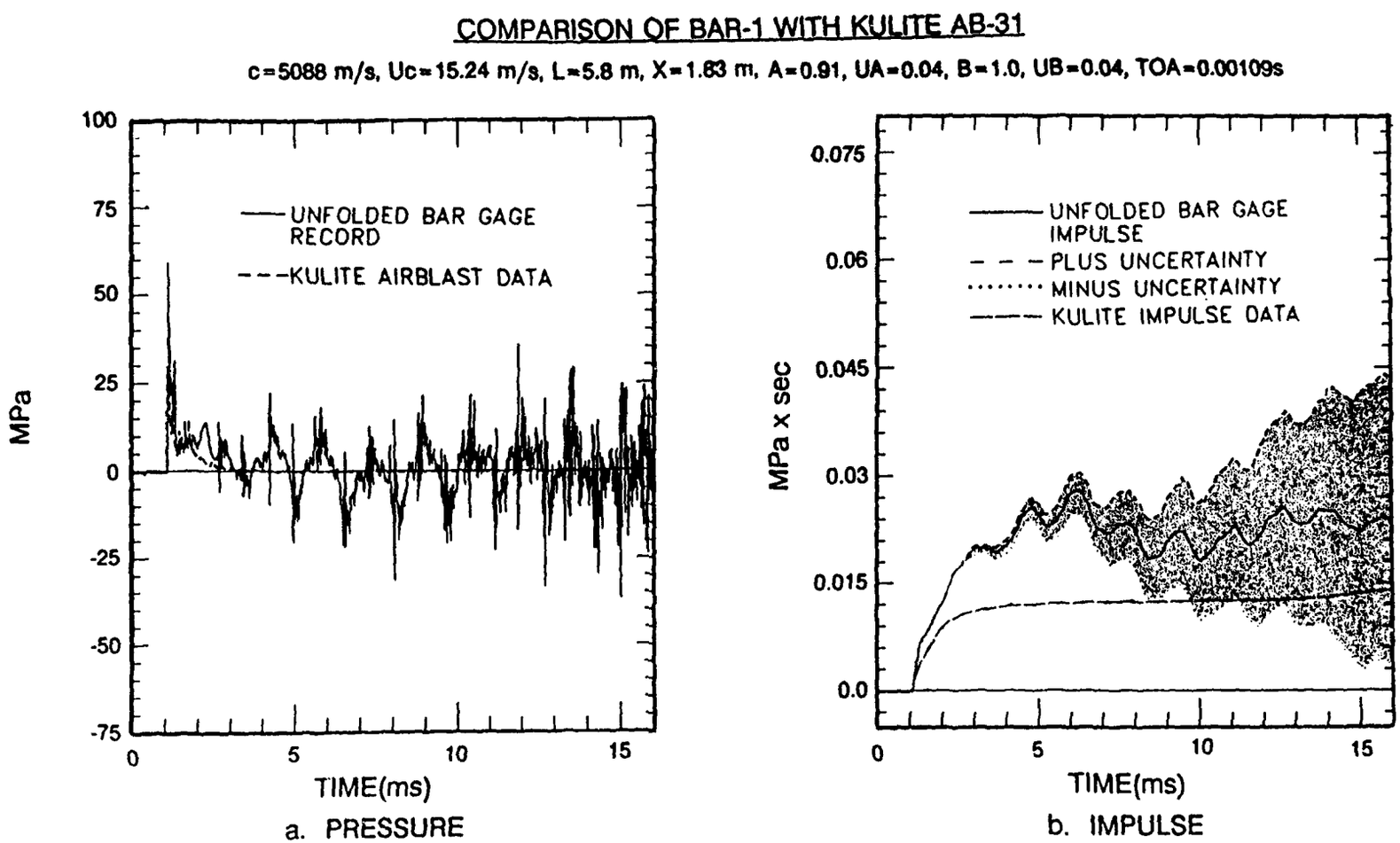

Figure 27. Comparison of the unfolded wave form of Bar-1 to the wave form recorded by the Kulite airblast gage AB-31.

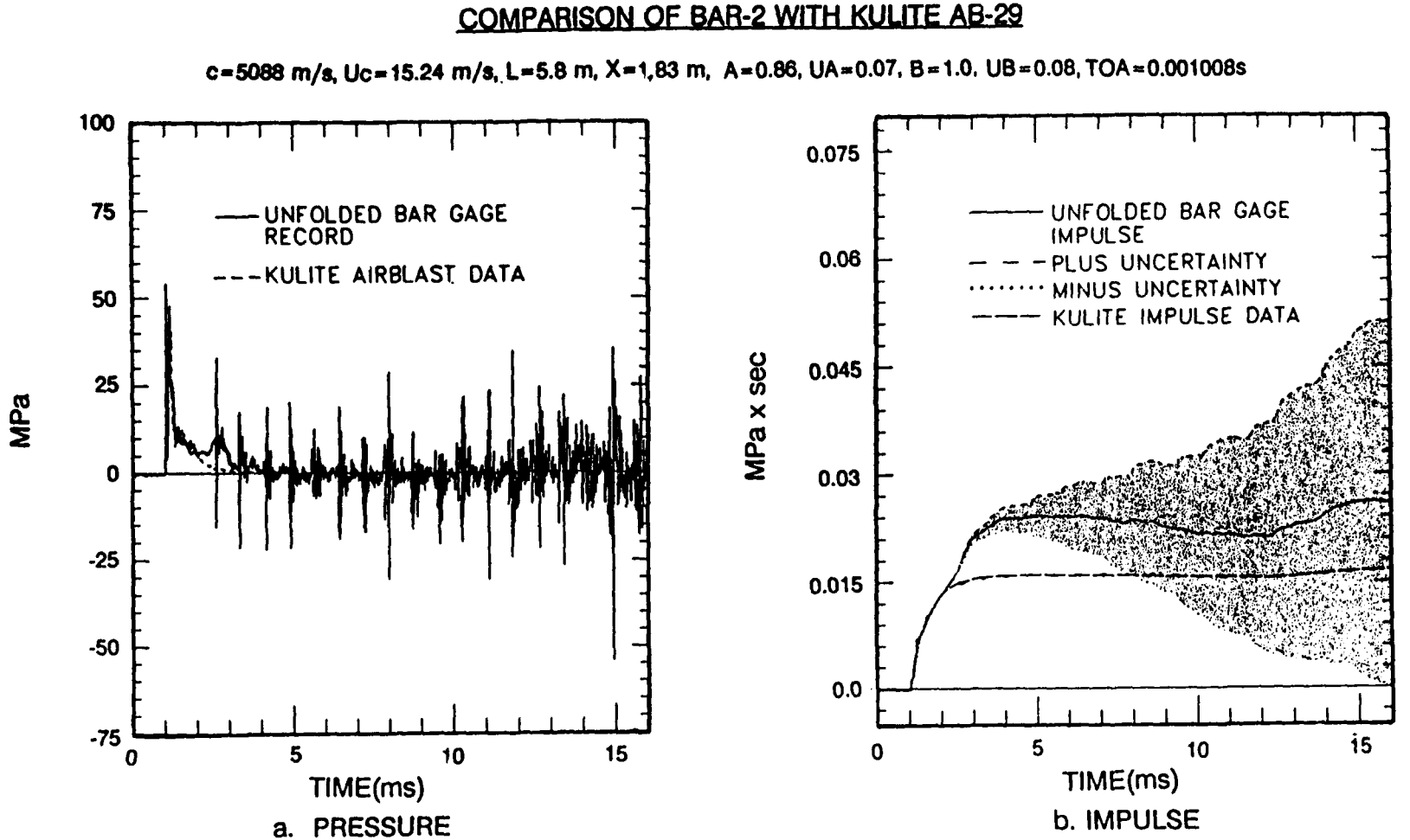

Figure 28. Comparison of the unfolded wave form of Bar-2 with the wave form recorded by the Kulite airblast gage AB-29.

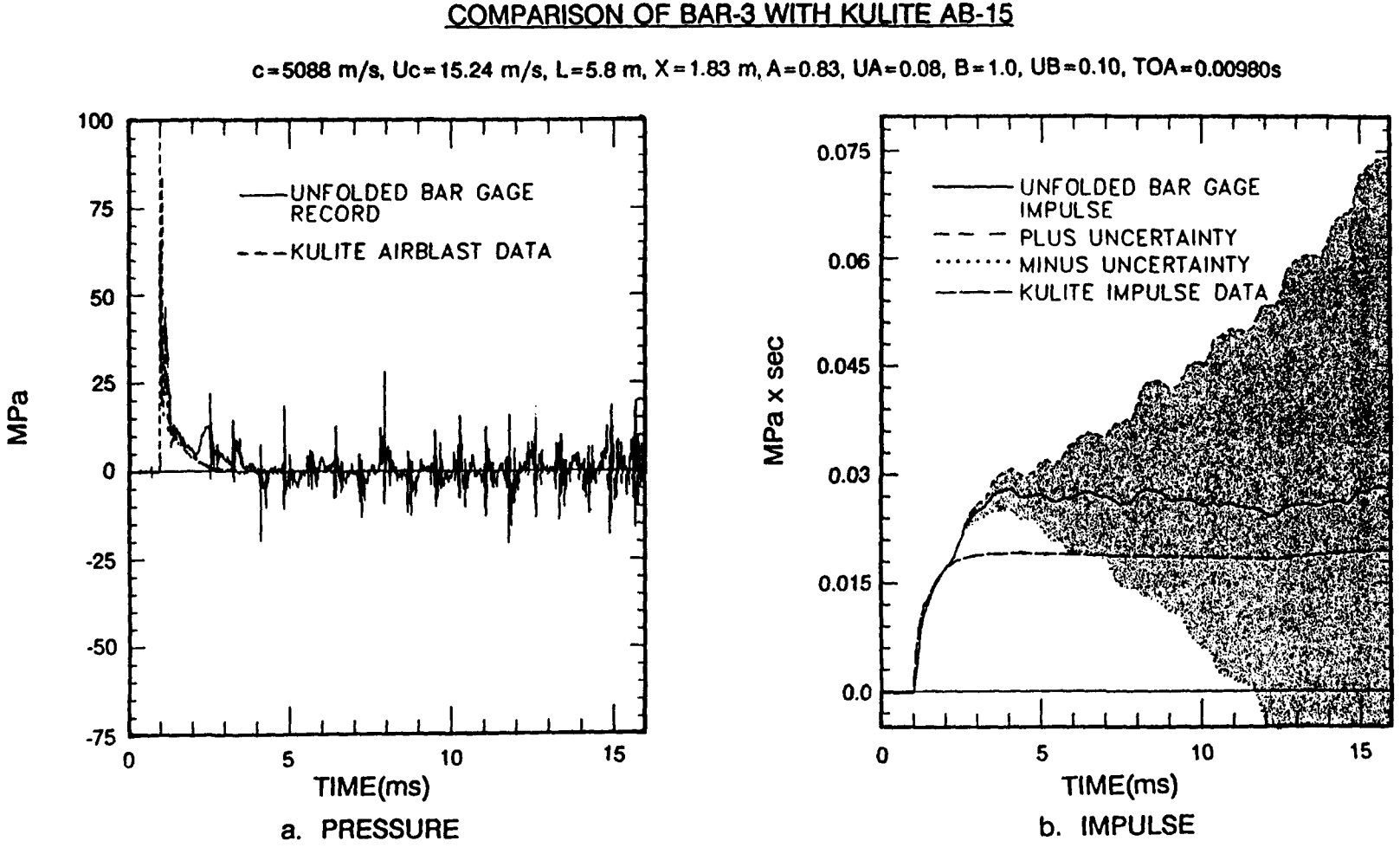

Figure 29. Comparison of the unfolded wave form of Bar-3 with the wave form recorded by the Kulite airblast gage AB-15.

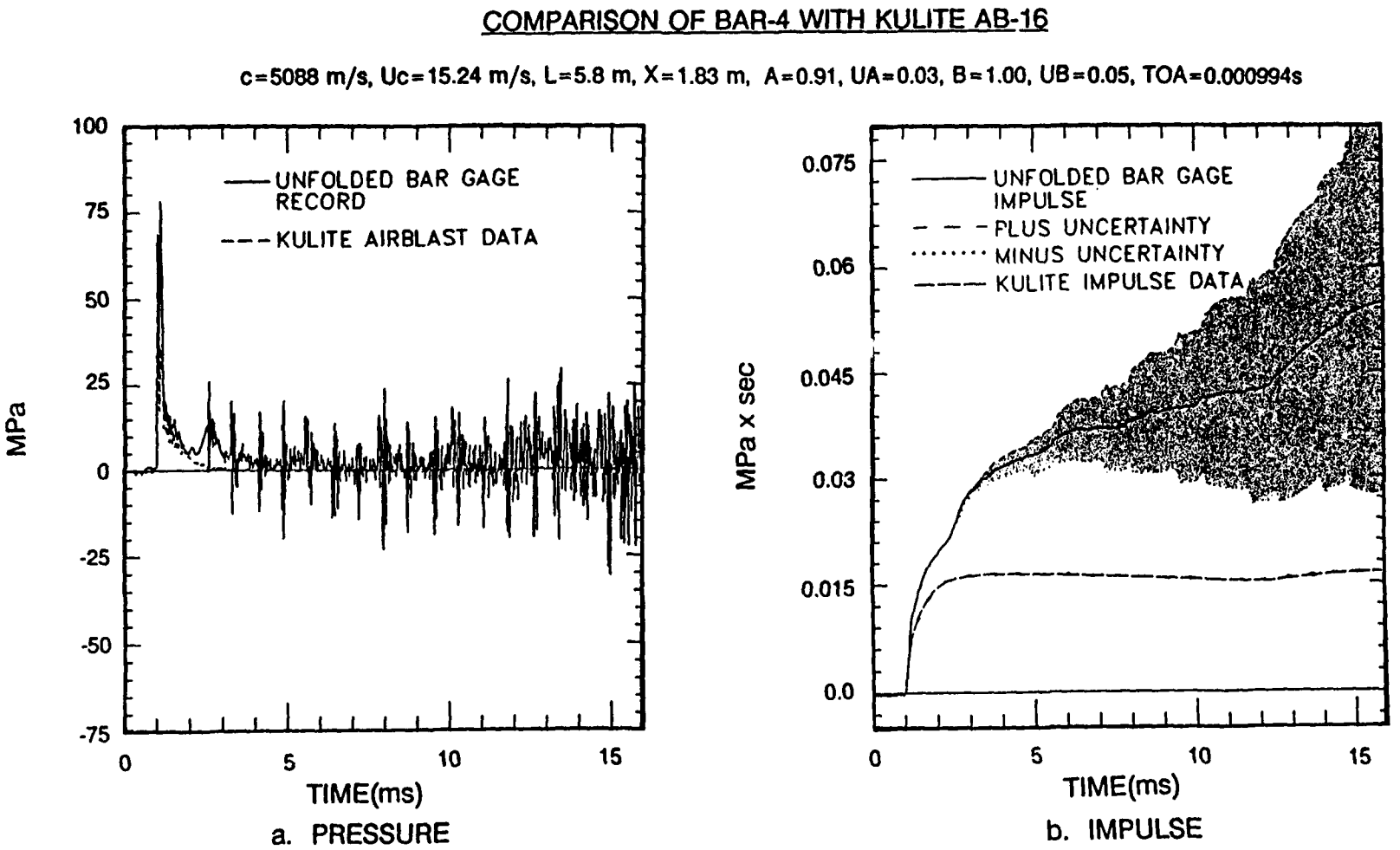

Figure 30. Comparison of the unfolded wave form of Bar-4 with the wave form recorded by the Kulite airblast gage AB-16.

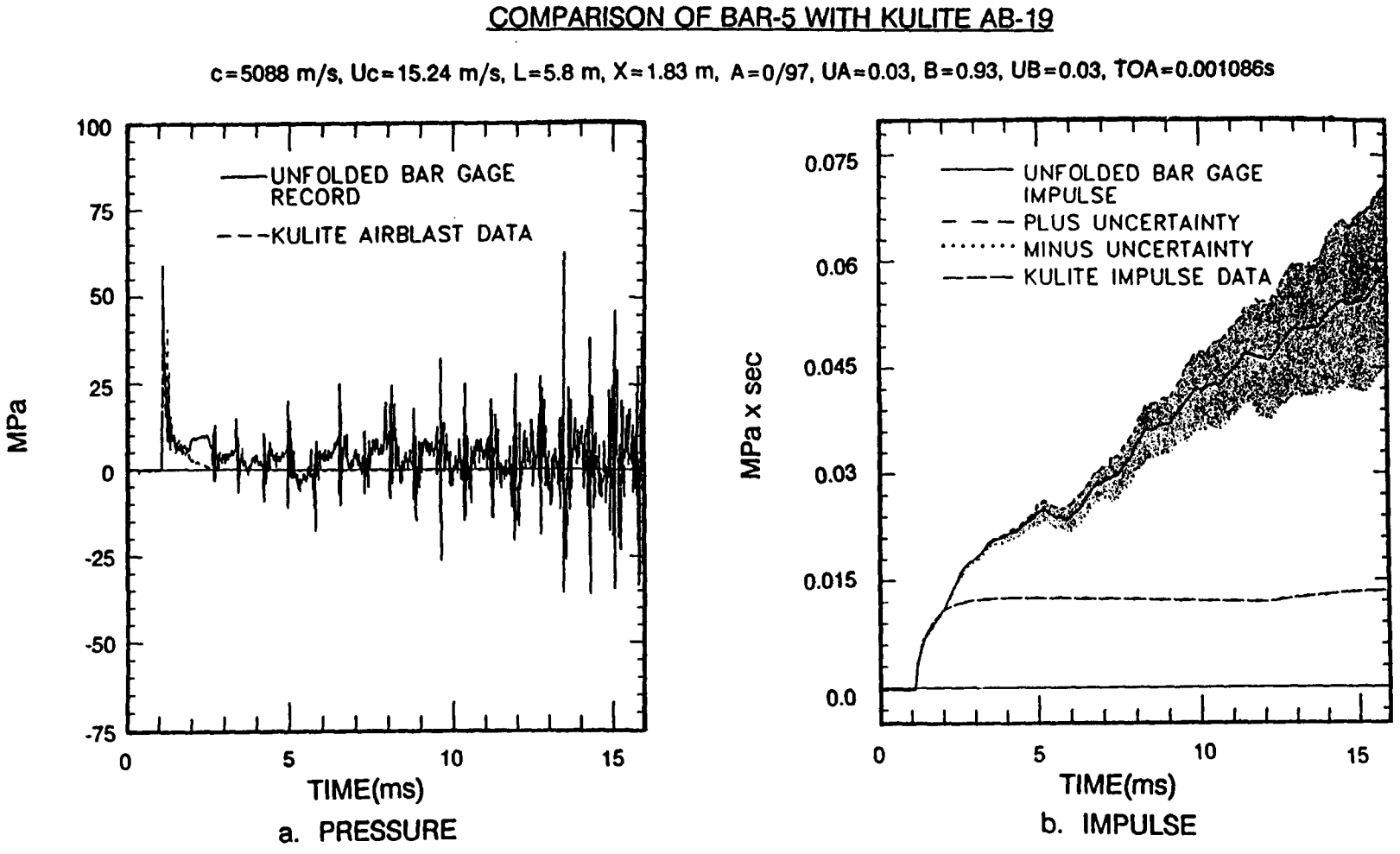

Figure 31. Comparison of the unfolded wave form of Bar-5 with the wave form recorded by the Kulite airblast gage AB-19.

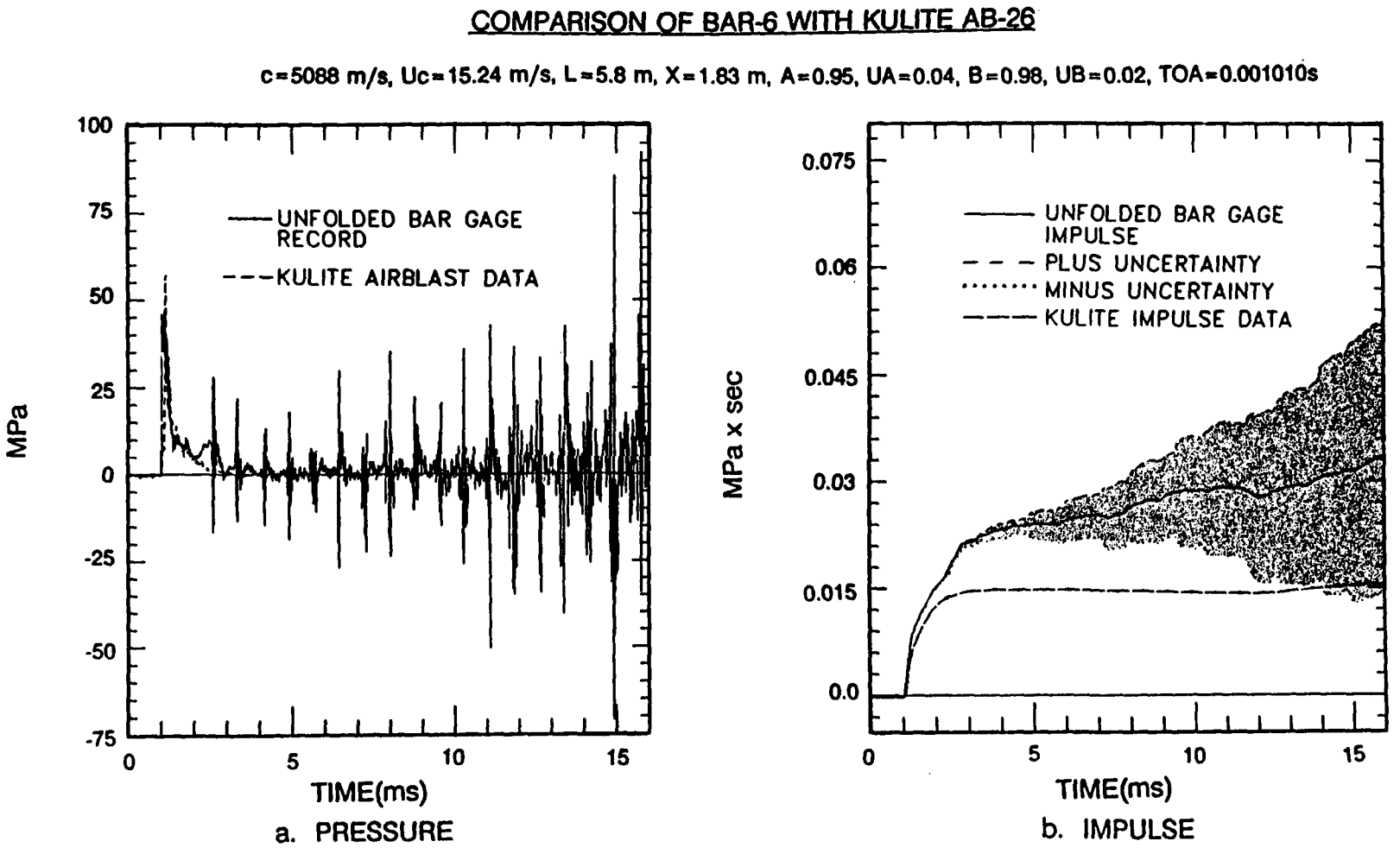

Figure 32. Comparison of the unfolded wave form of Bar-6 with the wave form recorded by the Kulite airblast gage AB-28.

pulse lengths. It was determined that 16-ms plots would be adequate to display all of the useful data. Since the Kulite airblast gage trace returns to the baseline (zero pressure) and stays there, the dashed trace is difficult to see on the pressure plots.

Impulses from the unfolded bar gage records range from 40 to 100 percent higher than the impulses measured by the Kulite airblast gages. With differences this extreme, the impulses measured by the Kulite airblast gages remain well below the minus uncertainty in the unfolded wave forms. Recall that numerical unfolding leaves the portion of the wave form prior to the first tensile reflection untouched. In each of Figures 27 through 32 the impulse measured by the bar gage exceeds the impulse measured by the Kulite airblast gage well before the first reflection is unfolded. Hence, the discrepancy between the two gage types is established before numerical unfolding can contribute. For these reasons, numerical unfolding could not have caused the discrepancies between the two gage types.

Because the bar gages were located close to their companion Kulite airblast gage, it is highly unlikely that the pressure field generated by the symmetric charge caused the systematic differences observed by the two gage types. These differences appear to fall well outside of data scatter (see, for example the Kulite and bar gage measurements along Radial A). Therefore, one can conclude that the discrepancies between gage types are not due to position in the test bed, or just excessive scatter in the data.

The likely cause for differences between gage types is some fundamental difference in the measurement techniques. Observe the

pressure plots. The bar gage recoreds indicate a second pressure pulse arriving about 0.5 to 1.2-msec after the arrival of the primary pressure pulse. This second pulse is not evident on the wave forms measured by the Kulite airblast gages. Since this second pulse on the bar gage records has substantial amplitude and duration, it affects the impulse significantly. This second pulse accounts for the difference in impulse measured by the two gage types.

Recent analysis of the data indicate that the bar gages are in error, i.e., the second pulse is not representative of the actual pressure environment at the end of the bar gage (Reference 12). It has been hypothesized that ground shock loadings, water jacket effects, or shear loads induced by relative motion between the bar and the surrounding jacket, might cause the peculiar bar gage output.

For completeness, it should be pointed out that there is no guarantee that the unfolding routine will correctly unfold data that is input to the lateral surfaces of the bar gage. Hence, from a purist point of view, errors due to poor bar gage performance can also be unfolded incorrectly and contribute to further unfolding errors. Future research and development will likely lead to bar gage designs which minimize influences from lateral loadings. In the absence of lateral loading induced errors, the uncertainties due to wave speed and reflection coefficients are the primary sources of error in the unfolding routine.

While the numerical unfolding of the these bar gage records was not necessary to reveal the differences between the two types of airblast gages, this application demonstrates how numerical unfolding

can be used during data analysis. Had there been no grievous differences between the gage types, more profound conclusions might have been made. In general, numerical unfolding with the calculated uncertainties can be used for the following purposes during data analysis:

1. Determine for each individual wave form the length of unfolded bar gage record that can be used without incurring too much error.
2. Gain insight into the quality of the bar gage record. Bar gage records of good quality tend to produce predictable wave shapes when unfolded.
3. Allow comparisons with other airblast gages having longer duration records. If other wave forms lie outside of the error bounds of the numerical unfolding, the discrepancy is due to some source other than the numerical unfolding. If the wave forms lie inside the error bounds of the numerical unfolding, then it is possible that discrepancies are due to the unfolding and further explanations for the discrepancies must be presented carefully, or withheld all together.

CHAPTER VI

CONCLUSIONS

Review

Bar gages are frequently used to measure airblast on explosive tests. The unique design and configuration of a bar gage allows it to measure high peak pressure and impulse close to an explosive charge. Unfortunately, the arrival of reflections from the ends of the bar gage limit the length of time that the primary pressure pulse can be measured. In this thesis we investigated the errors associated with the use of D'Alembert unfolding to numerically remove the reflections from the bar gage record, thereby restoring the original pressure pulse.

D'Alembert unfolding is a numerical technique by which the tensile reflections from the bottom of the bar gage, and the compressive reflections from the top of the bar gage, are added and subtracted from the measured wave form in such a way as to restore the original pressure pulse. The numerical technique makes the same assumptions as D'Alembert did in formulating his classical wave propagation equation. The most notable assumption being that the pulse propagates up and down the bar at a constant wave speed without changing shape. By further assuming that accurate and constant reflection coefficients can be identified for the ends of the bar gage while it makes the measurement,

the reflections can be subtracted from the measured wave form. In 1983, computer programs were written to perform this numerical technique on actual bar gage records.

Although D'Alembert unfolding often yielded reasonable results, critics pointed out potential flaws in the technique. Dispersion in high-frequency data is contrary to the principle assumptions on D'Alembert unfolding; namely, the wave speed varies with frequency content, and hence the pulse changes shape as it propagates down the bar. Also, reflection coefficients seem to vary throughout the record slightly. By assuming a constant reflection coefficient for each end of the bar, considerable error could be introduced into the numerical result. It was argued that this error could cause large errors in specific impulse (first integral of pressure), a very important quantity for explosive testing. Alternatively, proponents of unfolding indicated that if even one reflection could be unfolded with acceptable error, it would greatly increase the value of the bar gage measurement. This thesis sought to quantify the errors inherent to D'Alembert unfolding, permitting a sound judgement to be made regarding the credibility of the numerical technique.

The governing equation for D'Alembert unfolding was examined and three error sources were chosen for study. These error sources (listed below) comprise most of the error in the unfolding technique:

1. Specifying incorrect low frequency wave speed, c_o.

2. Choosing incorrect reflection coefficients, or assuming constant reflection coefficients when in reality, reflection coefficients were changing.
3. Dispersion and incorrect bar gage dimensions.

The first two errors were addressed analytically and numerically to arrive at the uncertainty in the unfolded wave form. The last errors were merely discussed to qualitatively assess their significance.

Recent experiments, suggest that bar gage output may be influenced by lateral loading during high expl sive tests. The purpose of the bar gage and the unfolding routine are to deduce the pressure loading at the end of the bar. Lateral loads originate at places other than the end of the bar and propagate away hence forth. The unfolding routine is not designed to correct for these sorts of input. It is conceivable that the unfolding routine could generate further errors when used on bar gage records generated by multiple loading sites. Determination or treatment of errors induced by lateral loading are beyond the scope of this thesis. In the absence of such lateral loading errors, the uncertainty analysis presented in this thesis has addressed the primary error sources.

Errors in the unfolded wave form due to uncertainty in the wave speed were identified numerically. Upper and lower bounds were placed on the wave speed, and the wave form unfolded for each case. The uncertainty in the unfolded wave form due to uncertainty in wave speed was then simply the difference between the wave forms.

Errors in the unfolded wave form due to uncertainty in the reflection coefficients were determined analytically by applying classical uncertainty analysis to the mathematical expression for the unfolded wave form. This yielded exact expressions for the uncertainty due to reflection coefficients, which could then be applied to specific wave forms.

The effect of these errors was then examined by unfolding candidate wave forms and calculating the uncertainty due to both error sources individually. Two types of wave forms were used. The first type, was a record from a ball drop calibration on a specially made bar gage where all of the dimensions were precisely known. The ball drop calibration is a controlled laboratory test. The input to the bar gage from a ball drop calibration is well known and is complete before the first tensile reflection arrives. Consequently, it was a good choice for evaluating the effect of unfolding errors. Ball drop calibrations also have lower frequency content, so dispersion is not prevalent.

The second type of wave form was a typical high explosive test record, specifically the WLB-1 record. Unfolding this wave form revealed the effect of the individual uncertainties on a wave form which contained considerable high frequency content. The wave form from the high explosive test also had larger uncertainties in reflection coefficients, which is typical of most explosive test data. Therefore, this wave form was representative of practical applications.

The proper method for combining these two errors; i.e., that due to uncertainty in wave speed, and that due to uncertainty in reflection coefficients, was then studied. It was determined that adding the

uncertainty due to incorrect wave speed to the RSS combination (square root of the sum of the squares) of the uncertainties due to the reflection coefficients was the best method of arriving at the total uncertainty of the unfolded wave form. This was incorporated into a computer program that calculated the uncertainties for the specific wave form of interest. In this way, upper and lower bounds on the true unfolded wave form could be established for the data analyst.

This error analysis was applied to airblast data from a candidate high explosive test. This test allowed for the comparison of unfolded bar gage records with another reputable type of airblast gage, the Kulite HKS airblast gage. All of the bar gage records were unfolded and then compared to their Kulite airblast gage counterpart. This analysis demonstrated the D'Alembert unfolding technique upon actual field test data and revealed systematic differences between bar gage measurements and the Kulite HKS airblast gage.

Conclusions

Several conclusions are drawn from this study. They are:

1. An uncertainty analysis method was developed which treats the uncertainties inherent in the D'Alembert unfolding technique as applied to strain-gaged Hopkinson bar gage records. A modified unfolding program was written which provides the analyst with the useful upper and lower bounds of uncertainty for a particular wave

form. The magnitude of the uncertainty is wave form specific, i.e., dependent on the character of the particular wave form being analyzed.

2. Errors in the reflection coefficients may yield large errors in unfolded impulse. These errors are the primary factor limiting the usefulness of D'Alembert unfolding. With the unfolding of subsequent reflections, the error in impulse from these sources increases geometrically.

3. Errors in wave speed produce spikes on the unfolded pressure wave form, but do not yield large errors in impulse. In general, with higher frequency content airblast data, and with larger uncertainty in wave speed, the spiky, noise-like behavior will be more prevalent.

4. Dispersion, uncertainties in bar gage dimensions, and other errors are less significant, and manifest themselves in a manner similar to errors in wave speed.

5. The differences between the unfolded bar gage measurements and Kulite airblast measurements are not due to errors in the D'Alembert unfolding technique. Evidence suggests that bar gage measurements were influenced by phenomena other than airblast (e.g., lateral loading), and that

the Kulite airblast gages were not affected by these phenomena.

6. Unfolding bar gage records can aid the data analyst in assessing the quality of the bar gage measurement. Peculiar behavior that is "hidden" in the reflections sometimes is revealed by D'Alembert unfolding.

These conclusions assume that the analyst has made reasonable choices of wave speed and reflection coefficients, and the uncertainties associated with these parameters. Performing D'Alembert unfolding with grossly incorrect parameters or very large uncertainties can lead to results which are contrary to the above conclusions.

Recommendations

The objective of this thesis was to ascertain the credibility of D'Alembert unfolding as a data reduction technique for bar gage records. The error analysis of the D'Alembert unfolding method accomplished that objective by quantifying the errors due to unfolding a particular wave form. This error analysis included only the effects of uncertainty in wave speed, reflection coefficients, and dispersion. If other significant sources of error are found, effort should be made to incorporate these errors into the uncertainty calculations.

The most important recommendation from this work is to apply the modified D'Alembert unfolding program to more field data. As was eluded to in earlier chapters, bar gages exhibit phenomena which are not fully understood. By unfolding the bar gage records and comparing

them to other airblast measurements, bar gage performance might be better understood. Having the upper and lower bounds on the numerical unfolding errors, the analyst can confidently choose the length of unfolded record to use and assess the validity of its comparison to other measurements or predictions.

APPENDIX

This appendix contains the computer program listings for the unfolding programs used in this thesis. Refer to Chapter 3 for a description of the basic organization of these codes. A flow chart of the basic workings of these programs is shown in Figure 8 of Chapter 3.

The computer program UNFOLD is essentially the same program developed by Welch and White for operation on Tektronics and VAX computer systems. This program was modified to run on IBM personal computers and compatibles for this thesis, and named UNFOLD. UNFOLD1 uses the first program as its core, but also calculates a plus and minus uncertainty in the unfolded wave form due to uncertainty in wave speed. UNFOLD2 uses the first program as its core, but calculates plus and minus uncertainty in the unfolded wave form due uncertainties in both reflection coefficients. UNFOLD4 is the final program developed for this thesis. UNFOLD4 combines the uncertainties in the unfolded wave form due to wave speed and reflection coefficients.

The computer program UNFOLD3 is conspicuously missing from this appendix. UNFOLD3 was written to identify the differences between two different schemes of combining the uncertainties in the unfolded wave form due to both wave speed and reflection coefficients. UNFOLD3 was subsequently used to generate the data for Figure 18 (Chapter 4). One of those schemes was deemed inappropriate. Accordingly, the listing of

UNFOLD3 is not included in this thesis to avoid confusion.

The listings of UNFOLD, UNFOLD1, UNFOLD2, and UNFOLD4 follow this narrative in their respective order.

```
      PROGRAM UNFOLD
C*****REVISED ON 10-13-90 TO MAKE THE PROGRAM MORE EFFICIENT***
C*****ROUTINE NOW DISCERNS WHICH REFLECTION POINT "I" IS IN****
C*****AND ONLY RUNS LOOP THAT MANY TIMES.  OTHER THINGS ARE****
C*****TO MAKE PROGRAM M ORE LOGICAL AND EFFICIENT.  MORE********
C*****COMMENTS STATEMENTS ARE ADDED FOR CLARITY****************

C*****INITIALIZE AND DEFINE SOME VARIABLES AND ARRAYS**********

      CHARACTER*30 BARFILE1,BARUNFOLD
      PARAMETER (NN=17000)
      DIMENSION A(NN), F(NN)
      NFIRST=4.

C*****INPUT BAR GAGE PARAMETERS AND OTHER INFORMATION**********

      PRINT*,'INPUT WAVE SPEED OF BAR (FT/S)  '
      READ(*,*) C
      PRINT*,'INPUT LENGTH OF BAR (FT)  '
      READ(*,*) BARLEN
      PRINT*,'INPUT DISTANCE BETWEEN TOP OF BAR AND GAGE (FT)  '
      READ(*,*) X
      PRINT*,'INPUT REFLECTION COEFFICIENT FOR DUMP END OF BAR  '
      READ(*,*) GAMMA1
      PRINT*,'INPUT REFLECTION COEFFICIENT FOR INPUT END OF BAR  '
      READ(*,*) GAMMA2
```

```
      PRINT*,'INPUT TIME OF ARRIVAL (SEC)  '
      READ(*,*) TOA
      PRINT*,'WHAT IS NAME OF BAR GAGE DATA FILE TO UNFOLD?  '
      READ(*,1000) BARFILE1
      PRINT*,'WHAT IS NAME OF FILE FOR UNFOLDED DATA?  '
      READ(*,1000) BARUNFOLD
      PRINT*,'HOW MANY TENSILE REFLECTIONS ARE THERE?  '
      READ(*,*) NREFL

C*****OPEN FILES, READ HEADER INFORMATION**********************

      OPEN(15,FILE=BARFILE1,STATUS='OLD',FORM='FORMATTED')
      OPEN(16,FILE=BARUNFOLD,FORM='FORMATTED')

      READ(15,2000) TFIRST,TINC,FKOUNT
      WRITE(16,2000) TFIRST,TINC,FKOUNT
      KOUNT=IFIX(FKOUNT)

C*****UNFOLD WAVEFORM*********************************************

      TWOC=2./C

      DO 100 I=NFIRST,KOUNT
        G1=0.0
        G2=0.0
```

```
      DO 200 N=1,NREFL
        TEMP=TWOC*(FLOAT(N)*BARLEN-X)
        VAL1=TIME-TEMP-TOA
        IF(VAL1.GT.0) THEN
         J=IFIX(TEMP/TINC)
         J=I-J
         IF(J.GT.0) THEN
          IF(J.GE.NFIRST) THEN
            G1=G1+(GAMMA1**N)*(GAMMA2**(N-1))*F(J)
            TEMP=TWOC*FLOAT(N)*BARLEN
            VAL2=TIME-TEMP-TOA
              IF(VAL2.GT.0) THEN
                J=IFIX(TEMP/TINC)
                J=I-J
                IF(J.GT.0) THEN
                    IF(J.GE.NFIRST) THEN
                      G2=G2+(GAMMA1**N)*(GAMMA2**N)*F(J)
                    END IF
                END IF
              END IF
            END IF
          END IF
        END IF
  200 CONTINUE
```

```
      READ(15,*) TIME, A(I)
      F(I)=A(I)+G1-G2
      WRITE(16,4000) TIME, F(I)

100   CONTINUE

50    CLOSE (UNIT=15)
      CLOSE (UNIT=16)

C*****FORMAT STATEMENTS*********************************************

1000  FORMAT(A30)
2000  FORMAT(E12.4,/,E12.4,/,E12.4)
3000  FORMAT(E12.4)
4000  FORMAT(F10.8,1X,F12.5)
      END
```

```
      PROGRAM UNFOLD1
C*****THIS PROGRAM CALCULATES UPPER AND LOWER BOUND ***********
C*****UNFOLDED WAVEFORMS FOR SPECIFIED CHANGES IN WAVE ********
C*****SPEED.  THREE WAVEFORMS ARE OUTPUT, UNFOLDED *************
C*****WAVEFORM, PLUS AND MINUS UNCERTAINTY**********************

C*****REVISED ON 11-26-90 TO MAKE THE PROGRAM MORE EFFICIENT***
C*****ROUTINE NOW DISCERNS WHICH REFLECTION POINT "I" IS IN****
C*****AND ONLY RUNS LOOP THAT MANY TIMES.  OTHER THINGS ARE****
C*****TO MAKE PROGRAM MORE LOGICAL AND EFFICIENT.  MORE********
C*****COMMENTS STATEMENTS ARE ADDED FOR CLARITY****************

C*****INITIALIZE AND DEFINE SOME VARIABLES AND ARRAYS**********

      CHARACTER*30 BARFILE1,BARUNFOLD,MINUSUNC,PLUSUNC
      PARAMETER (NN=16000)
      DIMENSION A(NN), F(NN)
      DIMENSION G1(3), G2(3)
      NFIRST=4.

C*****INPUT BAR GAGE PARAMETERS**********************************

      PRINT*,'INPUT WAVE SPEED OF BAR (FT/S)  '
      READ(*,*) C
      PRINT*,'INPUT UNCERTAINTY OF WAVE SPEED (+/- "X" FT/S)  '
      READ(*,*) UC
```

```
      PRINT*,'INPUT LENGTH OF BAR (FT)  '
      READ(*,*) BARLEN
      PRINT*,'INPUT DISTANCE BETWEEN TOP OF BAR AND GAGE (FT)  '
      READ(*,*) X
      PRINT*,'INPUT REFLECTION COEFFICIENT FOR DUMP END OF BAR  '
      READ(*,*) GAMMA1
      PRINT*,'INPUT REFLECTION COEFFICIENT FOR INPUT END OF BAR '
      READ(*,*) GAMMA2
      PRINT*,'INPUT TIME OF ARRIVAL (SEC)  '
      READ(*,*) TOA
      PRINT*,'WHAT IS NAME OF BAR GAGE DATA FILE TO UNFOLD?  '
      READ(*,1000) BARFILE1
      PRINT*,'WHAT IS NAME OF FILE FOR UNFOLDED DATA?  '
      READ(*,1000) BARUNFOLD
      PRINT*,'WHAT IS NAME OF FILE FOR MINUS UNCERTAINTY?  '
      READ(*,1000) MINUSUNC
      PRINT*,'WHAT IS NAME OF FILE FOR PLUS UNCERTAINTY?  '
      READ(*,1000) PLUSUNC

C*****OPEN FILES, READ HEADER INFORMATION**********************

      OPEN(15,FILE=BARFILE1,STATUS='OLD',FORM='FORMATTED')
      OPEN(16,FILE=BARUNFOLD,FORM='FORMATTED')
      OPEN(17,FILE=MINUSUNC, FORM='FORMATTED')
      OPEN(18,FILE=PLUSUNC, FORM='FORMATTED')
```

```
      READ(15,2000) TFIRST,TINC,FKOUNT
      WRITE(16,2000) TFIRST,TINC,FKOUNT
      KOUNT=IFIX(FKOUNT)

C*****UNFOLD WAVEFORM*********************************************

      DO 100 I=NFIRST,KOUNT
         READ(15,*,END=50) TIME, A(I)

      DO 125 L=1,3
       G1(L)=0.0
       G2(L)=0.0
125   CONTINUE

      DO 150 K1=1,3
      IF (K1.EQ.1) THEN
          C1=C-UC
      ELSE IF (K1.EQ.2) THEN
          C1=C
      ELSE IF (K1.EQ.3) THEN
          C1=C+UC
      ENDIF

C*****IF "I" LIES PRIOR TO FIRST TENSILE REFLECTION, WRITE******
C***** POINT DIRECTLY TO OUTPUT FILE*****************************
```

```
      TWOC=2./C1
      IF (TIME.LT.(TOA+TWOC*(BARLEN-X))) THEN
       GO TO 5
      ELSE

C*****IF "I" LIES AFTER FIRST TENSILE REFLECTION, FIND**********
C*****OUT WHICH REFLECTION IT LIES IN, AND SET VARIABLE "N"*****
C*****TO THAT NUMBER************************************************

       DIF=(TIME-(TOA+TWOC*(BARLEN-X)))/(TWOC*BARLEN)
       WNUM=AINT(DIF)
       DEC=DIF-WNUM
        IF (DEC.LT.0.50) THEN
         DIF=DIF+0.50
        ENDIF
       N=NINT(DIF)
      ENDIF

C*****PERFORM SUMMATIONS OF SECOND TERM**************************

      DO 200 K=1,N
       TEMP=(2./C1)*(FLOAT(K)*BARLEN-X)
       J=IFIX(TEMP/TINC)
       J=I-J
         G1(K1)=G1(K1)+(GAMMA1**K)*(GAMMA2**(K-1))*F(J)
```

```
C*****DETERMINE IF SUMMATIONS OF THIRD TERM ARE NECESSARY, *****
C*****AND IF SO, PERFORM THEM**********************************

            TEMP=(2./C1)*FLOAT(K)*BARLEN
          VAL2=TIME-TEMP-TOA
           IF(VAL2.GT.0) THEN
             J=IFIX(TEMP/TINC)
             J=I-J
               G2(K1)=G2(K1)+(GAMMA1**K)*(GAMMA2**K)*F(J)
             END IF
200   CONTINUE
150   CONTINUE

C*****COMPUTE AMPLITUDE OF UNFOLDED VALUE OF POINT "I" AND *****
C*****WRITE IT TO THE OUTPUT FILE*******************************

5     F(I)=A(I)+G1(2)-G2(2)
      FMINUS=A(I)+G1(1)-G2(1)
      FPLUS=A(I)+G1(3)-G2(3)
      WRITE(16,4000) TIME, F(I)
      WRITE(17,4000) TIME, FMINUS
      WRITE(18,4000) TIME, FPLUS
100   CONTINUE
```

```
50    CLOSE (UNIT=15)
      CLOSE (UNIT=16)
      CLOSE (UNIT=17)
      CLOSE (UNIT=18)

C*****FORMAT STATEMENTS*********************************************

1000  FORMAT(A30)
2000  FORMAT(E12.4,/,E12.4,/,E12.4)
3000  FORMAT(E12.4)
4000  FORMAT(F10.8,1X,F12.5)
      END
```

```
      PROGRAM UNFOLD2

C*****PROGRAM IS THE SAME AS UNFOLD EXCEPT THAT IT ALSO*****
C*****CALCULATES THE UNCERTAINTY IN THE UNFOLDED WAVEFORM***
C*****DUE TO THE UNCERTAINTY IN THE REFLECTION COEFFICIENTS*

C*****REVISED ON 11-12-90 TO INCORPORATE CHANGES WHICH MAKE*
C*****PROGRAM MORE LOGICAL AND EFFICIENT.******************

C*****INITIALIZE AND DEFINE SOME VARIABLES

      CHARACTER*30 BARFILE1,BARUNFOLD,UNCFILEP,UNCFILEM
      PARAMETER (NN=17000)
      DIMENSION A(NN), F(NN)
      NFIRST=4.

C*****INPUT BAR GAGE PARAMETERS**********************************

      PRINT*,'INPUT WAVE SPEED OF BAR (FT/S)  '
      READ(*,*) C
      PRINT*,'INPUT LENGTH OF BAR (FT)  '
      READ(*,*) BARLEN
      PRINT*,'INPUT DISTANCE BETWEEN TOP OF BAR AND GAGE (FT)  '
      READ(*,*) X
      PRINT*,'INPUT REFLECTION COEFFICIENT FOR DUMP END OF BAR  '
      READ(*,*) GAMMA1
```

```
      PRINT*,'UNCERTAINTY OF THE DUMP END REFL. COEFFICIENT  '
      READ(*,*) UA
      PRINT*,'INPUT REFLECTION COEFFICIENT FOR INPUT END OF BAR '       READ(*,*)
GAMMA2
      PRINT*,'UNCERTAINTY OF THE INPUT END REFL. COEFFICIENT  '
      READ(*,*) UB
      PRINT*,'INPUT TIME OF ARRIVAL (SEC)  '
      READ(*,*) TOA
      PRINT*,'WHAT IS NAME OF BAR GAGE DATA FILE TO UNFOLD?  '
      READ(*,1000) BARFILE1
      PRINT*,'WHAT IS NAME OF FILE FOR UNFOLDED DATA?  '
      READ(*,1000) BARUNFOLD
      PRINT*,'GIVE A FILENAME FOR THE PLUS UNCERTAINTY VALUES  '
      READ(*,1000) UNCFILEP
      PRINT*,'GIVE A FILENAME FOR THE MINUS UNCERTAINTY VALUES  '
      READ(*,1000) UNCFILEM

C*****OPEN FILES, READ HEADER INFORMATION**********************

      OPEN(15,FILE=BARFILE1,STATUS='OLD',FORM='FORMATTED')
      OPEN(16,FILE=BARUNFOLD,FORM='FORMATTED')
      OPEN(17,FILE=UNCFILEP,FORM='FORMATTED')
      OPEN(18,FILE=UNCFILEM,FORM='FORMATTED')
```

```
      READ(15,2000) TFIRST,TINC,FKOUNT
      WRITE(16,2000) TFIRST,TINC,FKOUNT
      WRITE(17,2000) TFIRST,TINC,FKOUNT
      WRITE(18,2000) TFIRST,TINC,FKOUNT
      KOUNT=IFIX(FKOUNT)

C*****UNFOLD WAVEFORM*********************************************

      TWOC=2./C

      DO 100 I=NFIRST,KOUNT
         READ(15,*,END=50) TIME, A(I)
         G1=0.0
      G2=0.0
         A1=0.0
      A2=0.0
      B1=0.0
      B2=0.0

C*****IF "I" LIES PRIOR TO FIRST TENSILE REFLECTION, WRITE******
C***** POINT DIRECTLY TO OUTPUT FILE*****************************

         IF (TIME.LT.(TOA+TWOC*(BARLEN-X))) THEN
          GO TO 5
```

```
      ELSE

C*****IF "I" LIES AFTER FIRST TENSILE REFLECTION, FIND**********
C*****OUT WHICH REFLECTION IT LIES IN, AND SET VARIABLE "N"******
C*****TO THAT NUMBER**********************************************

        DIF=(TIME-(TOA+TWOC*(BARLEN-X)))/(TWOC*BARLEN)
        WNUM=AINT(DIF)
        DEC=DIF-WNUM
         IF (DEC.LT.0.50) THEN
          DIF=DIF+0.50
         ENDIF
        N=NINT(DIF)
      ENDIF

C*****PERFORM SUMMATIONS OF SECOND TERM**************************

      DO 200 K=1,N
        TEMP=TWOC*(FLOAT(K)*BARLEN-X)
        J=IFIX(TEMP/TINC)
        J=I-J
        G1=G1+(GAMMA1**K)*(GAMMA2**(K-1))*F(J)
        A1=A1+K*(GAMMA1**(K-1))*(GAMMA2**(K-1))*F(J)
        B1=B1+(K-1)*(GAMMA1**K)*(GAMMA2**(K-2))*F(J)
```

```
C*****DETERMINE IF SUMMATIONS OF THIRD TERM ARE NECESSARY, *****
C*****AND IF SO, PERFORM THEM************************************

                TEMP=TWOC*FLOAT(K)*BARLEN
                VAL2=TIME-TEMP-TOA
              IF(VAL2.GT.0) THEN
                J=IFIX(TEMP/TINC)
                J=I-J
                    G2=G2+(GAMMA1**K)*(GAMMA2**K)*F(J)
                    A2=A2+K*(GAMMA1**(K-1))*(GAMMA2**K)*F(J)
                    B2=B2+K*(GAMMA1**K)*(GAMMA2**(K-1))*F(J)
                  END IF
200   CONTINUE

C*****COMPUTE AMPLITUDE OF UNFOLDED VALUE OF POINT "I" AND *****
C*****WRITE IT TO THE OUTPUT FILE********************************

5     F(I)=A(I)+G1-G2
      UNCA=((A1-A2)/F(I))*UA
      UNCB=((B1-B2)/F(I))*UB
      U=((UNCA**2)+(UNCB**2))**0.5
      UP=F(I)+(U*ABS(F(I)))
      UM=F(I)-(U*ABS(F(I)))
```

```
      WRITE(16,4000) TIME, F(I)
      WRITE(17,4000) TIME, UP
      WRITE(18,4000) TIME, UM

100   CONTINUE

50    CLOSE (UNIT=15)
      CLOSE (UNIT=16)
      CLOSE (UNIT=17)
      CLOSE (UNIT=18)

C*****FORMAT STATEMENTS*****************************************

1000  FORMAT(A30)
2000  FORMAT(E12.4,/,E12.4,/,E12.4)
3000  FORMAT(11X,E12.4)
4000  FORMAT(F10.8,1X,F12.5)
      END
```

```
      PROGRAM UNFOLD4

C*****THIS PROGRAM CALCULATES UNCERTAINTY DUE TO C, A, AND B,****
C*****AND WRITES THE PLUS AND MINUS UNCERTAINTIES TO A FILE.*****

C*****REVISED ON 11-26-90 TO MAKE THE PROGRAM MORE EFFICIENT***
C*****ROUTINE NOW DISCERNS WHICH REFLECTION POINT "I" IS IN****
C*****AND ONLY RUNS LOOP THAT MANY TIMES.  OTHER THINGS ARE****
C*****TO MAKE PROGRAM MORE LOGICAL AND EFFICIENT.  MORE********
C*****COMMENTS STATEMENTS ARE ADDED FOR CLARITY****************

C*****INITIALIZE AND DEFINE SOME VARIABLES AND ARRAYS**********

      CHARACTER*30 BARFILE1,BARUNFOLD,MINUSUNC,PLUSUNC
      PARAMETER (NN=16000)
      DIMENSION A(NN), F(NN)
      DIMENSION G1(3), G2(3)
      NFIRST=4.

C*****INPUT BAR GAGE PARAMETERS**********************************

      PRINT*,'INPUT WAVE SPEED OF BAR (FT/S)  '
      READ(*,*) C
      PRINT*,'INPUT UNCERTAINTY OF WAVE SPEED (+/- "X" FT/S)  '
      READ(*,*) UC
      PRINT*,'INPUT LENGTH OF BAR (FT)  '
```

```
      READ(*,*) BARLEN
      PRINT*,'INPUT DISTANCE BETWEEN TOP OF BAR AND GAGE (FT)  '
      READ(*,*) X
      PRINT*,'INPUT REFLECTION COEFFICIENT FOR DUMP END OF BAR '
      READ(*,*) GAMMA1
      PRINT*,'UNCERTAINTY OF THE DUMP END REFL. COEFFICIENT  '
      READ(*,*) UA
      PRINT*,'INPUT REFLECTION COEFFICIENT FOR INPUT END OF BAR '
      READ(*,*) GAMMA2
      PRINT*,'UNCERTAINTY OF THE INPUT END REFL. COEFFICIENT  '
      READ(*,*) UB
      PRINT*,'INPUT TIME OF ARRIVAL (SEC)  '
      READ(*,*) TOA
      PRINT*,'WHAT IS NAME OF BAR GAGE DATA FILE TO UNFOLD?  '
      READ(*,1000) BARFILE1
      PRINT*,'WHAT IS NAME OF FILE FOR UNFOLDED DATA? '
      READ(*,1000) BARUNFOLD
      PRINT*,'WHAT IS NAME OF FILE FOR MINUS UNCERTAINTY? '
      READ(*,1000) MINUSUNC
      PRINT*,'WHAT IS NAME OF FILE FOR PLUS UNCERTAINTY? '
      READ(*,1000) PLUSUNC

C*****OPEN FILES, READ HEADER INFORMATION**********************
```

```
      OPEN(15,FILE=BARFILE1,STATUS='OLD',FORM='FORMATTED')
      OPEN(16,FILE=BARUNFOLD,FORM='FORMATTED')
      OPEN(17,FILE=MINUSUNC, FORM='FORMATTED')
      OPEN(18,FILE=PLUSUNC, FORM='FORMATTED')

      READ(15,2000) TFIRST,TINC,FKOUNT
      WRITE(16,2000) TFIRST,TINC,FKOUNT
      KOUNT=IFIX(FKOUNT)

C*****UNFOLD WAVEFORM*********************************************

      DO 100 I=NFIRST,KOUNT
         READ(15,*,END=50) TIME, A(I)

         A1=0.0
        A2=0.0
        B1=0.0
        B2=0.0

      DO 125 L=1,3
        G1(L)=0.0
        G2(L)=0.0
125   CONTINUE
```

```
      DO 150 K1=1,3
       IF (K1.EQ.1) THEN
           C1=C-UC
       ELSE IF (K1.EQ.2) THEN
           C1=C
       ELSE IF (K1.EQ.3) THEN
           C1=C+UC
       ENDIF

C*****IF "I" LIES PRIOR TO FIRST TENSILE REFLECTION, WRITE******
C***** POINT DIRECTLY TO OUTPUT FILE*****************************

          TWOC=2./C1
          IF (TIME.LT.(TOA+TWOC*(BARLEN-X))) THEN

            GO TO 5
          ELSE

C*****IF "I" LIES AFTER FIRST TENSILE REFLECTION, FIND**********
C*****OUT WHICH REFLECTION IT LIES IN, AND SET VARIABLE "N"******
C*****TO THAT NUMBER*********************************************

            DIF=(TIME-(TOA+TWOC*(BARLEN-X)))/(TWOC*BARLEN)
            WNUM=AINT(DIF)
            DEC=DIF-WNUM
             IF (DEC.LT.0.50) THEN
```

```
          DIF=DIF+0.50
         ENDIF
        N=NINT(DIF)
       ENDIF

C*****PERFORM SUMMATIONS OF SECOND TERM**************************

       DO 200 K=1,N
        TEMP=(2./C1)*(FLOAT(K)*BARLEN-X)
        J=IFIX(TEMP/TINC)
        J=I-J
         G1(K1)=G1(K1)+(GAMMA1**K)*(GAMMA2**(K-1))*F(J)
           IF(K1.EQ.2) THEN
            A1=A1+K*(GAMMA1**(K-1))*(GAMMA2**(K-1))*F(J)
            B1=B1+(K-1)*(GAMMA1**K)*(GAMMA2**(K-2))*F(J)
           ENDIF

C*****DETERMINE IF SUMMATIONS OF THIRD TERM ARE NECESSARY, *****
C*****AND IF SO, PERFORM THEM************************************

           TEMP=(2./C1)*FLOAT(K)*BARLEN
           VAL2=TIME-TEMP-TOA
            IF(VAL2.GT.0) THEN
              J=IFIX(TEMP/TINC)
              J=I-J
              G2(K1)=G2(K1)+(GAMMA1**K)*(GAMMA2**K)*F(J)
```

```
                IF(K1.EQ.2) THEN
                    A2=A2+K*(GAMMA1**(K-1))*(GAMMA2**K)*F(J)
                    B2=B2+K*(GAMMA1**K)*(GAMMA2**(K-1))*F(J)
                END IF
            END IF
200   CONTINUE
150   CONTINUE

C*****COMPUTE AMPLITUDE OF UNFOLDED VALUE OF POINT "I" AND *****
C*****WRITE IT TO THE OUTPUT FILE*********************************

5     F(I)=A(I)+G1(2)-G2(2)
      FMINUS=F(I)-(A(I)+G1(1)-G2(1))
      FPLUS=F(I)-(A(I)+G1(3)-G2(3))
      UNCA=(A1-A2)*UA
      UNCB=(B1-B2)*UB
      UP=F(I)-FPLUS+((UNCA**2)+(UNCB**2))**0.5
      UM=F(I)-FMINUS-((UNCA**2)+(UNCB**2))**0.5
      WRITE(16,4000) TIME, F(I)
      WRITE(17,4000) TIME, UM
      WRITE(18,4000) TIME, UP
100   CONTINUE

50    CLOSE (UNIT=15)
      CLOSE (UNIT=16)
      CLOSE (UNIT=17)
```

```
      CLOSE (UNIT=18)



C*****FORMAT STATEMENTS*****************************************

1000  FORMAT(A30)

2000  FORMAT(E12.4,/,E12.4,/,E12.4)

3000  FORMAT(E12.4)

4000  FORMAT(F10.8,1X,F12.5)

      END
```

REFERENCES

1. Welch, Charles R., (1983). Unpublished notes on the D'Alembert unfolding technique.

2. White, Howard G., & Welch, Charles R., "D'Alembert Unfolding of Hopkinson Bar Airblast Data"; June 1985; Published in the Proceedings of the 55th Shock and Vibration Symposium.

3. Hopkinson, B. (1914). Phil. Transactions of the Royal Society of London; A 213, 437

4. Davies, R. M. (1948). "A Critical Study of the Hopkinson Pressure Bar; Phil. Transactions of the Royal Society of London; A 240, 375;

5. Fox, G., & Curtis, C. W. (1957). "Elastic Strain Produced by Sudden Application of Pressure to One End of a Cylindrical Bar Part II. Experiment Observant". Journal of Applied Mechanics 24, 2, 240.

6. Miklowitz, J., & Nisewanger, C. R. (1957) "The Propagation of Compressional Waves in a Dispersive Elastic Rod Part I". Journal of Applied Mechanics. 24, 2, 240.

7. Baum, N., & Simmons, K. (1987). "The SIMBA Bar and Acoustic Filtering of Piezoresistive Pressure Transducers"; AFWL-TR-87-51, Kirtland AFB, N.M.

8. Wilson, P. S. (1986). "Development of a Damped Bar Gage for Long-Duration Stress Pulse Recording"; DNA-TR-86-70;

9. Coleman, H., & Steele G., (1988). Pre-published copy of Experimentation and Uncertainty Analysis for Engineers; John Wiley & Sons.

10. Graff, Karl F. (1975). Wave Motion in Elastic Solids; Ohio State University Press.

11. Kulite Semiconductor Products. (1981) Kulite Miniature Metal Diaphragm Pressure Transducers, Bulletin KM-1000B.

12. Welch, Charles R. (1990). Private communication regarding data analysis of explosive test.

DISTRIBUTION LIST

Defense Nuclear Agency
6801 Telegraph Road
Alexandria, VA 22310-3398
ATTN: TDTR M. Flohr
ATTN: SPWE K. Peterson

Commander
Field Command
Defense Nuclear Agency
Test Operations Directorate
Kirtland AFB, NM 87115-5000
ATTN: TTST, E. Rinehart

U.S. Army Engineer Waterways
Experiment Station
3909 Halls Ferry Road
Vicksburg, MS 39180-6199
ATTN: (CEWES-SE-R)
J.K. Ingram
H.G. White
C.R. Welch

Applied Research Associates
Aberdeen Research Center
P.O. Box 548
Aberdeen, MD 21001
ATTN: N. Ethridge

California Research & Technology
5117 Johnson Drive
Pleasanton, CA 94588
ATTN: J. Thomsen

Carpenter Research Corp.
P.O. Box 2490
Rolling Hills Estates, CA 90274
ATTN: H.J. Carpenter

Fluid Physics Inc.
4265 Manchester Ave.
Encinitas, CA 92024
ATTN: R. Traci

Geo Centers, Inc.
P.O. Box 428
Newton Upper Falls, MA 02164
ATTN: B. Nelson

Ktech Corporation
901 Pennsylvania Ave. N.E.
Albuquerque, N.M. 87110
ATTN: E. Gaffney

Logicon R & D Associates
6940 S. Kings Hwy
Suite 210
Alexandria, VA 22310
ATTN: J. Webster

Logicon R & D Associates
P.O. Box 9377
Albuquerque, NM 87119-9377
ATTN: G. Ganong

Logicon R & D Associates
P.O. Box 92500
Los Angeles, CA 90009
ATTN: C.K.B. Lee

New Mexico Engineering Research
Institute
University of New Mexico
Albuquerque, NM 87131
ATTN: N. Baum

S-Cubed
A Division of Maxwell Labs, Inc.
P.O. Box 1620
La Jolla, CA 92038-1620
ATTN: C. Peterson
ATTN: P. Coleman

Science Applications Intl. Corp.
10260 Campus Point Drive
San Diego, CA 92121
ATTN: C. Hsiao

SRI International
333 Ravenswood Avenue
Menlo Park, CA 94025-3434
ATTN: D. Keough

Waterways Experiment Station Cataloging-in-Publication Data

Ohrt, Alan Paul.
Analysis of D'Alembert unfolding technique for Hopkinson bar gage records / by Alan Paul Ohrt ; prepared for Defense Nuclear Agency.
136 p. : ill. ; 28 cm. — (Technical report ; SL-92-12)
Includes bibliographic references.
1. Stress waves — Measurement. 2. Physical measurements. 3. Strain gages. I. Title. II. United States. Defense Nuclear Agency. III. U.S. Army Engineer Waterways Experiment Station. IV. Series: Technical report (U.S. Army Engineer Waterways Experiment Station) ; SL-92-12.
TA7 W34 no.SL-92-12